Application of Combined Power and Thrust Capping to Tidal Turbine Farms

Tuo Wang
St. Edmund Hall
University of Oxford

A thesis submitted for the degree of
Master of Science by Research
Trinity 2017

Acknowledgements

I would first like to express my gratitude to my supervisor, Prof. Thomas Adcock for his invaluable advice and guidance throughout this project. Despite his busy schedule, Tom has always found the time for our frequent meetings and to help and advise me on my work. This thesis would not have been possible without his continuing support.

I would also like to thank my colleagues and friends in Oxford for their help and support. They have made my life in Oxford so much more enjoyable.

Finally, thanks to my family, who have always been there for me. Your trust and encouragement will always be my strength.

Abstract

As an important form of renewable energy, tidal energy is challenged by many factors including its high cost and potential environmental concerns. This thesis is aimed to contribute to the development of tidal energy by introducing an operation strategy that is able to reduce the capital cost and environmental impacts of extracting tidal energy. This thesis considers the optimal strategy for the design and operation of tidal stream turbine farms. Such operation strategy aims to reduce the capital cost of tidal turbine farms by reducing the maximum power and thrust loading. In addition, this strategy can potentially reduce the environmental impacts with the cost of reducing a certain amount of overall power production.

Because of the advantages in computation time and ease in interpreting results, an idealised 0D model is used first to explore the effectiveness of implicating power and thrust capping (i.e. limiting the peak power and peak thrust of the turbines) to a tidal turbine farms. In addition, the impact brought by tidal turbine support structures to the tidal energy farm and the local flow field is considered by this idealised 0D model.

The power and thrust capping strategy is further explored by using a 2D Shallow Water Equations (SWEs) model based on one real candidate tidal energy site locating at North Scotland, the Pentland Firth. The impact of power and thrust capping on power production and on the environmental impacts are further evaluated in detail. Different combination of power capping and thrust capping are also evaluated. The effects of combined power and thrust capping are believed to be representative. However, the detailed setting (i.e. choice of capping ratio) are very likely to be site specific and thus more specific analysis would be required for the capping strategy to be applied to other potential tidal energy sites.

The results suggest that a combined power and thrust capping strategy is beneficial to a tidal turbine farms in terms of optimising power production, reducing capital cost and reducing environmental impacts, and therefore should be adopted in the design of tidal stream turbine farms.

Contents

List of Figures

Nomenclature

Symbols

A	**cross-sectional area of channel,** m^2
b	**breadth of the channel,** m
B	**blockage ratio: the ratio of turbine swept area to the cross-section of channel**
C_d	**channel bed drag coefficient**
$C_{d,s}$	**support structure drag coefficient**
C_p	**power coefficient**
C_t	**thrust coefficient**
D	**support structure diameter,** m
F	**force,** N
F_{nat}	**channel bed friction (per unit mass),** m/s^2
$F_{turbine}$	**total turbine thrust (per unit mass),** m/s^2

$F_{support}$	**total support structure drag (per unit mass),** m/s^2
g	**gravitational constant,** m/s^2
h	**depth of channel,** m
L	**length of channel,** m
L_s	**support structure length,** m
M_2	**principal lunar semi-diurnal tide**
M_z	**bending moment,** $N \cdot m$
n	**number of turbine rows**
N_t	**number of turbines**
P	**power,** W
P^*_{cap}	**power capping ratio: the ratio of threshold power to be capped to the maximum power**
P_{cap}	**power capping value: the threshold power to be capped per unit turbine swept area,** kW/m^2
Q	**volumetric flowrate,** m^3/s

S_2	**principal solar semi-diurnal tide**
t	**time,** s
T	**turbine thrust**
T^*_{cap}	**thrust capping ratio: the ratio of threshold thrust to be capped to the maximum thrust**
T_{cap}	**thrust capping value: the threshold thrust to be capped per unit turbine swept area,** kN/m^2
u	**water velocity,** m/s
Z_e	**section modulus,** m^3
α_4	**wake induction factor: ratio of velocity in the turbine wake to the upstream undisturbed velocity**
ζ	**free surface elevation,** m
η	**elevation head difference between two ends of the channel,** m
ρ	**density of water,** kg/m^3

σ_{max}	**maximum stress in the structure,** Pa
δ_0	**natural friction term,** m^{-4}
δ_1	**turbine thrust term,** m^{-4}
δ_2	**turbine support structure drag term,** m^{-4}

Terms

Available power	**power that can be transformed into other forms of energy such as electricity**
Extractable power	**total power removed from a tidal channel**

Acronyms

0D	**zero-dimensional: simplified case that does not consider parameters' variation in any of the 3 dimensions**
1D/2D	**one- /two-dimensional**
ADCIRC	**Advanced Circulation Model**
BEM	**Blade Element Momentum Theory**

CFD	**Computational Fluid Dynamics**
DG/DG-ADCIRC	**Discontinuous Galerkin version of ADCIRC**
LMADT	**Linear Momentum Actuator Disc Theory**
PC	**Power Capping**
TC	**Thrust Capping**
PTC	**Combined Power and Thrust Capping**
THAWT	**Transversal Horizontal Axis Water Turbine**

Chapter 1

Introduction

The growing concerns about climate change caused by the emission of carbon dioxide from the use of fossil fuel has led to a substantial increase in the demand for renewable energy (MacKay 2009). The limitation of non-sustainable resources and the concern of energy security also promotes the development of renewable energy. For example the EU had set a target for UK in 2009 to have 15% of the overall energy consumption from renewable sources in 2020(European Parliament 2009). Because of its advantages in geological position and climate, the UK has significant resources of wind and marine energy. Marine energy in particular has the potential to play a significant role in UK's electricity production (Jeffrey et al. 2013). These have been marked in the Renewable Energy Roadmap (DECC 2011) as a target for renewable energy development.

Tidal energy is the energy obtained from the tidal waves mainly driven by the gravitational force of the moon and the sun. Recent technology can successfully convert it into useful forms of power, mainly electricity. Tidal energy as a clean and renewable energy has long been viewed as a potential alternative energy source. Its

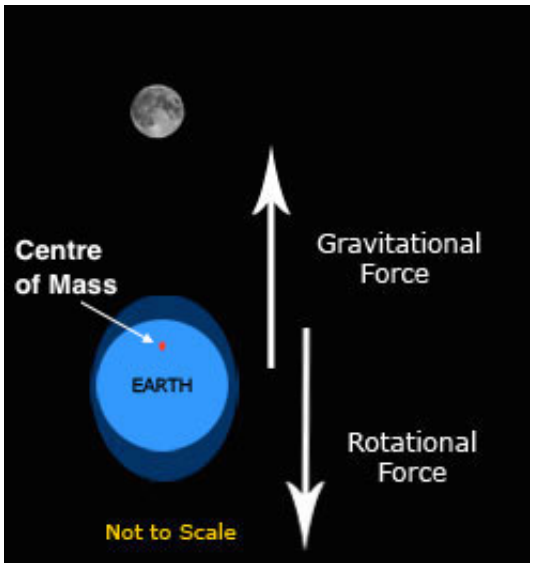

Figure 1.1: A sketch of the earth-moon system (Figure based on Boyle 2017)

renewability and predictability has gained the attention of a number of researchers and the use of tidal energy has been widely discussed (MacKay 2009).

1.1 Background

1.1.1 Formation of tides

Tides are formed by the gravitational pull of other celestial bodies (e.g. the sun and moon). A key to the physical understanding of the dynamics of tides are the Newton's laws of motion, of which the first conclude that a body will remain steady or at a uniform speed unless acted upon by a force. Consider the earth-moon system, the moon applies additional force on the water on earth surface. In order to balance with this force the water deforms and those parts facing the moon rises above the average sea level to reach a new steady state (as shown in 1.1 as the gravitational force).

The rise of water level on the other side of the earth can be understood in two

ways. The first explanation is that instead of only the moon rotating about the earth, unlike how it is normally described, both the earth and moon are rotating about their common centre of mass, which is inside but away from the centre of earth (as indicated in Figure 1.1). The water on the side of the earth that is far from the moon receives less gravitational force from the moon, but stronger rotational force to the opposite direction of the moon because of a longer radius of rotation of the earth. The second way to understand this is to consider the motion of the earth-moon system as a free fall, to which a uniform circular motion is physically equivalent, towards each other. The part of earth surface that is closer to the moon receives a stronger gravitational force than the earth centre, while the part to the opposite direction receives weaker force. According to the Newton's second law, the difference in force results in variance of acceleration, which "pull" the two parts of surface water away from the earth centre.

In summery the gravitational force of the moon causes the water level on both sides of earth surface to rise. As the earth is spinning on its own axis once every 24hrs, assuming the moon stand still, both "high water surface" will move around the earth once a day, causing 2 high tides and 2 low tides a day. But as the moon is also orbiting in the same direction as the earth's self spin, it takes 24hr and 50mins for the moon to be in the same position again. This semidiurnal tide caused by the moon is named as the M_2 tide.

1.1.2 The spring-neap cycle

Similar to the earth-moon system above. If we consider the earth-sun system without the presence of the moon, it will result a similar but weaker semidiurnal tide (named as the S_2 tide). It is weaker because of the much longer distance between the sun and earth compared to the moon and earth, although the mass of the sun is much greater. A more detailed calculation of the tidal forces caused by the moon and the sun is given by Pugh (1996).

The real tides are the combination of the M_2 tide and S_2 tide (in fact there are many other tidal constituents but they are neglected for simplification here). The earth spins at different angular velocity relative to the moon and the sun, which causes the difference in periods of M_2 and S_2 tides. As shown in Figure 1.2, when M_2 and S_2 tides are in phase (the moon, sun and earth are in the same line) these two tides sum up and forms the highest (and lowest) tide called the spring tide. When they are 90° out of phase (the moon and sun are in a perpendicular direction to the earth) they partially cancel out and forms the lowest high tide (and highest low tide) called the neap tide. The cycle of a spring and neap tides is named the spring-neap cycle, which has a length of around 28 days. A modelled example of current speed in the centre of the Pentland Firth is shown in Figure 1.3. The left most part of this figure is during neap tide and the right part is spring tide.

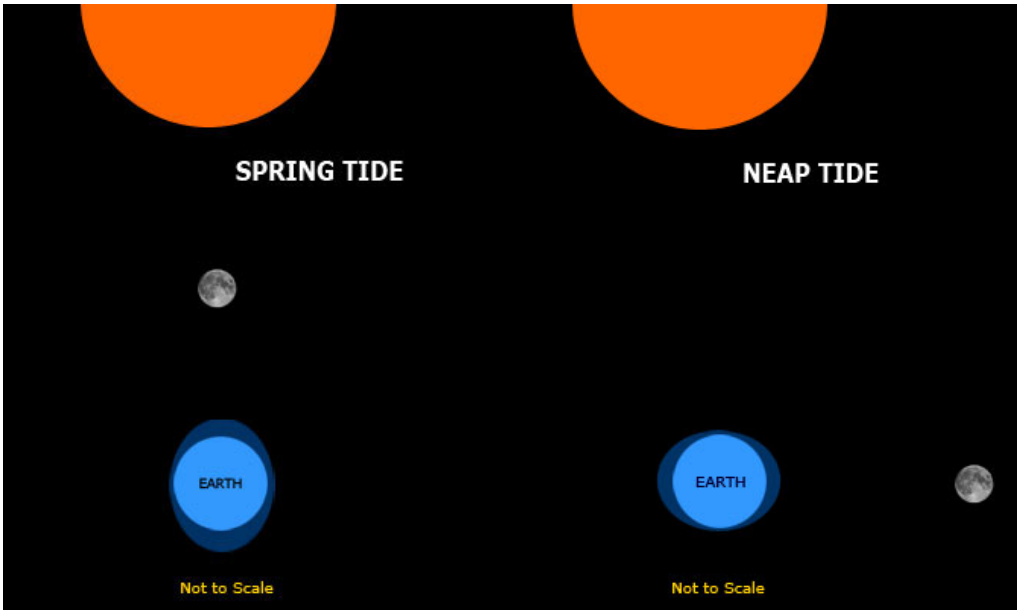

Figure 1.2: Formation of the spring and neap tide (Figure taken from Boyle 2017)

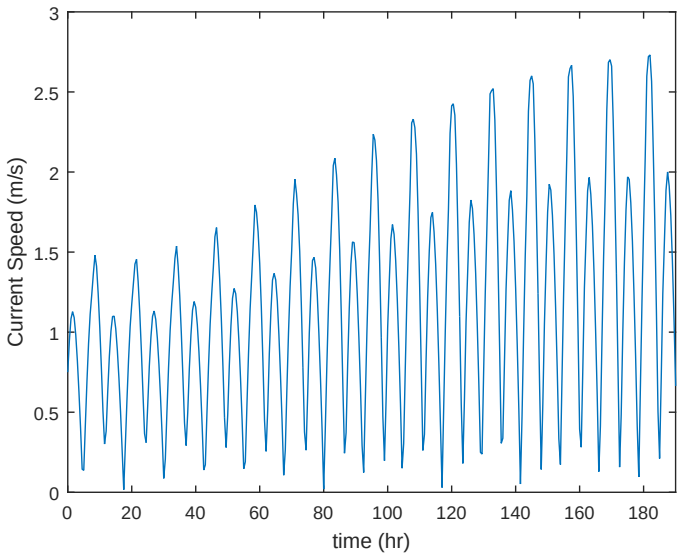

Figure 1.3: Modelled current speed in the Pentland Firth

1.1.3 The dynamic theory of tides

Tides in the real world oceans behave differently to the idealised ocean-covered earth (as explained in the previous sections) because of the existence of landmasses, variation of water depth, rotation of the earth and the Coriolis Effect.

Ocean depth Tidal waves are considered as shallow water waves, because tides have a much longer wavelength than the depth of ocean, the ocean is considerably shallow in the scale of wavelength of tidal waves. For a shallow water wave the wave speed is directly proportional to the square root of the water depth ($speed = \sqrt{gh}$ where g is gravitational acceleration and h is water depth). Therefore in shallower water the tidal waves propagate at a much slower velocity, which causes the waves to be more concentrated at certain locations (Figure 1.4).

Phase lag In the previous sections where a smooth earth is assumed, ocean water is assumed to be always in line with the sun and moon, which requires the waves to move at a similar speed to the rotation of the earth. However, if we do an estimation of the wave speed (as shallow water waves) by the depth of ocean, the maximum wave speed estimated is slightly slower. This means that the rise of water caused by the gravitational pulls and rotational force is lagged behind the position of the moon and sun. Therefore the high tide at a certain location does not necessarily happen when the moon is directly overhead. However, because the rotational velocity of the earth decreases with latitude, at higher latitudes the waves experience much less, or even no lag at some locations.

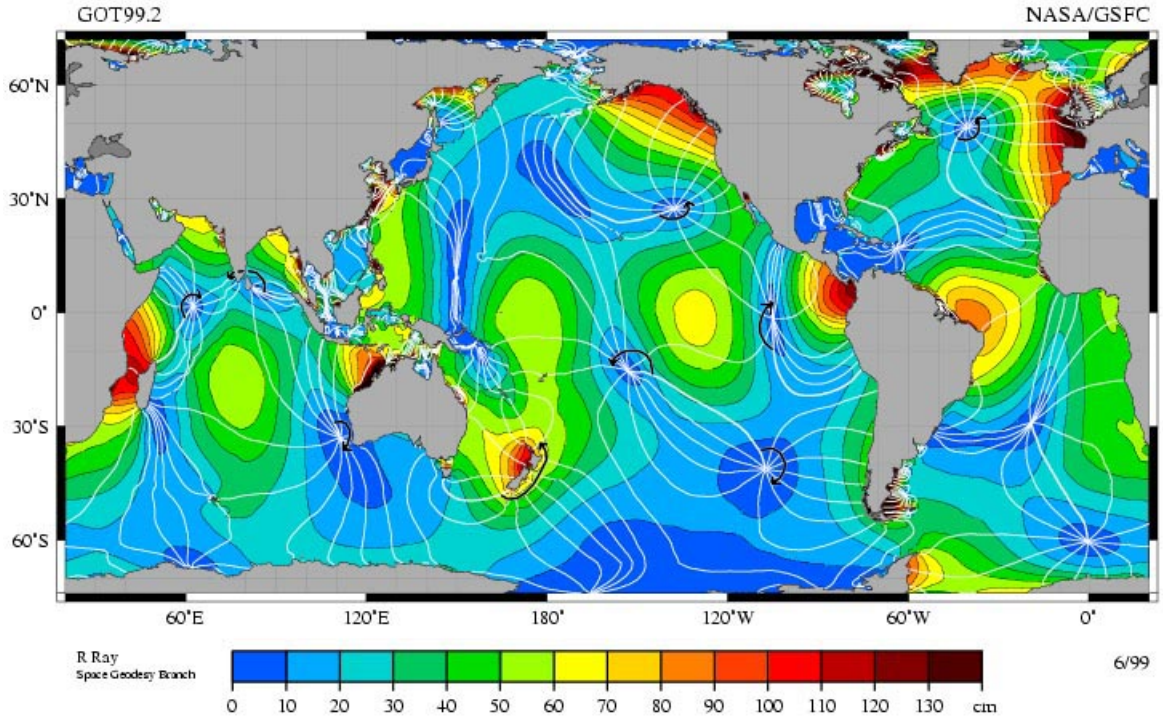

Figure 1.4: M_2 tidal constituent amplitude map (Figure taken from NASA Scientific Visualization Studio)

Continents and the Coriolis Effect Landmasses on the earth surface prevent the wave from propagating freely. As the wave hits the land boundary, it's weakened and reflected back to the ocean basin. This reflected wave resonates with the original wave and causes its amplitude to be enhanced or reduced depending on the local geographical condition. This reinforce of tidal wave by reflections is called tidal resonance (Platzman 1991). The reflection also, along with the Coriolis Effect, causes waves to rotate around an ocean basin.

1.2 Tidal Energy Resource

As tidal waves propagate around the ocean, the waves are concentrated at certain part due to the variance in costal geometries. Energy is concentrated and tidal wave amplitudes are enhanced where flows are constricted (Bonar 2017), such as headlands (Draper 2011) and narrow channels (Blanchfield et al. 2008, Vennell 2011, Adcock et al. 2013). As shown in Figure 1.4 the amplitude of M_2 tidal constituent is enhanced at some specific location. This concentrated energy can be used as a alternative energy resource as it is low-carbon, renewable and reliable. The UK is focusing on many renewable energy resources including offshore wind, biomass, geothermal energy, wave and tidal energy DECC (2011). Tidal energy in particular is of significant importance because it is highly predictable and reliable due to the nature of tides, and that there are a number of sites around the UK having a high tidal current speed (Serhadlıoğlu 2014), which is a critical advantage for tidal power extraction.

The use of tidal energy, as a low-carbon and renewable energy source, has been widely discussed by a number of researchers (MacKay 2009, O'Rourke et al. 2010). Vennell et al. (2015) stated "Power generated from tidal currents could make a significant contribution to the global demand for renewable energy". Although it is commonly accepted that extracting tidal energy is a relatively expensive source of renewable energy, a key advantage of tidal energy stated by Adcock et al. (2015) is the high predictability – it can be predicted by the relative positions of the moon and sun to the earth. This is beneficial because for the replanning of power supply. This is unlike wind power which depends much on the weather and prediction of power

can only be made a few days ahead. Tidal energy is more stable and predictable and this makes it more reliable in terms of energy usage management.

The development of tidal energy is restricted by the uncertainties regarding the environmental impacts of implementation of tidal turbines on the marine ecosystems (Copping et al. 2013). As the tidal turbine applies force to the flow, it changes the flow pattern and hence the tidal regime. This can in turn affect the power available and the design and arrangement of turbines. The change in flow may affect the marine ecosystem and local pollutants transport. For example the suspended sediment concentrations as well as bacteria concentrations may decrease upstream and downstream of a turbine array, while increasing along the side of arrays, as found by Ahmadian and Falconer (2012). Such environmental impacts must be clearly identified before the sustainability of tidal energy to be evaluated in detail. The aim of this project is to identify the environmental impacts of extracting tidal energy by evaluating the alteration of the tidal current flow within the tidal channel. This study can provide an understanding of the sustainability of tidal energy, and provide possible solutions to eliminate or reduce the resulted impacts on the flow.

1.3 Aim, Objectives and Outline

Much research have been done on evaluating the maximum extractable power for real sites (Draper et al. 2014). However, due to the fluctuating nature of tidal stream, sometimes extracting all the extractable power may not be an economical option. A high maximum power will result in high demand in power generator and cabling. Also

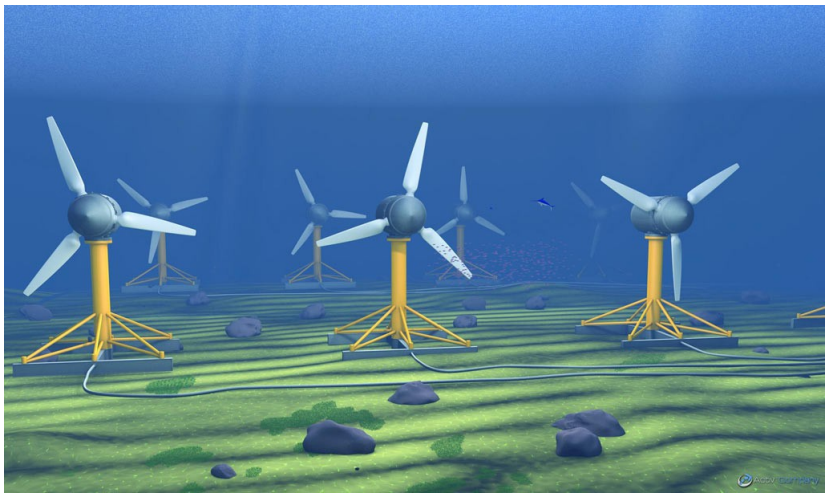

Figure 1.5: Tidal turbines under water (Figure credit to Bureau Veritas)

high generator capacity would spend much of its lifetime operating at a power that is significantly lower than its designed value, and would be operating less efficient at a low flow speed due to the large inertia of the devices (Vogel 2014). In addition, the alteration of flow and the consequent environmental issues brought by extracting tidal energy can not be ignored. Therefore it would be advantageous to use a smaller tidal turbine and power generator although it may not be able to maximise the power production during a full tidal cycle. To serve this purpose a method called power capping is introduced to limit the power during peak tide. This work introduced another capping method similar to power capping, thrust capping which limits turbine thrust instead. It has been stated by many researchers (Blanchfield et al. 2008, Vennell 2011, Adcock et al. 2013) that tidal channels are ideal sites for tidal turbine farm. Therefore the focus of this project is tidal channel based turbine farm.

Aim

One typical disadvantage of extracting tidal energy is that it is much more expensive than other forms of renewable energy like wind power. The combined power and thrust capping would be able to reduce the capital cost of tidal turbine farms as well as optimise the efficiency of tidal turbines. The aim of this thesis is to evaluate the effectiveness of combined power and thrust capping in a tidal turbine farm. It is also proposed to reduce the environmental impacts brought by alteration of tidal stream flow. The effects on power production, turbine thrust and environmental impacts are evaluated by a 2D Shallow Water Equations (SWEs) real site model.

Objectives

- To review the scientific literature and identify the key models and potential sites for tidal power extraction.
- To develop a simplified model for general evaluation and faster computation of capping problem.
- To develop a real site-based model for site specific evaluation of tidal power extraction.
- To evaluate the benefits of applying power and thrust capping in a tidal turbine farm.
- To develop an operation strategy that can effectively limit both maximum power and turbine thrust, with little cost of overall power production.

Outline

Chapter 2 presents a review of relevant models that have been used to simulate tidal channels and power extraction by tidal turbines, as well as the environmental impacts brought by extracting tidal energy and proposing a capping strategy. Chapter 3 introduces a simplified 0D model that evaluates the power extraction by an array of turbines from an idealised tidal channel. A power and thrust capping algorithm is included to limit the maximum power and thrust when required. Chapter 4 develops a real site model based on the Pentland Firth using finite element method. This model is to be solved by a DG-ADCIRC SWEs solver. A more developed power and thrust capping method is introduced in this chapter. Although there are some differences in the methods of capping in the models using in Chapters 3 and 4, a comparison of both model is included in Chapter 5. The conclusions of this thesis are presented in Chapter 6, along with recommendations for future work.

Chapter 2

Literature Review

2.1 Introduction

This literature review will discuss a few most common type of tidal energy devices, and the following chapters will be focusing on one of them, tidal stream turbines. It has been pointed out by Adcock et al. (2015) that the most practical way of extracting power from strong current flow is passing the water through a turbine (Figure 1.5). Tidal stream turbines have been claimed to have the advantages of lower capital costs and lower environmental impacts (Xia et al. 2010). Although this is not necessarily true when considering an array of tidal stream turbines and other tidal energy devices producing the same amount of power, tidal stream turbines are more flexible because the power production and resulted environmental impacts can be controlled by the size and number of turbines. In this work tidal energy being extracted by tidal turbines is to be evaluated.

The literature review will start with a brief introduction to the suitable sites and

devices for tidal energy extraction. Then one of the key models that is commonly used in the research of tidal energy, the actuator disc theory, will be introduced. Then a few extensions to actuator disc theory will be reviewed. The discussion of turbine models will be followed by a channel model used in this work. 2D Shallow Water Equations (SWE) model will be discussed later. Then the review will be finished with a few further explorations about tidal energy included in this project, including power capping, support structures and environmental impacts.

2.2 Extracting Tidal Energy

Adcock et al. (2015) have pointed out that the most practical way of extracting power from strong current flow is passing the water through a turbine. Generally, there are three different ways of extracting tidal energy:

1) Constrained (water level controlled): A tidal barrage is built to constrain the water to build up significant head difference, and force all the flow to pass through the turbine for power generation. This is as shown in Figure 2.1 (a).

2) Constrained (water level uncontrolled): A barrier is built to constrain part of the current to build up the head difference across the channel. The current can bypass the barrier and so the resulted head difference will be lower than using a tidal barrage (Mei, 2012). This is as shown in Figure 2.1 (b).

3) Unconstrained: No barrier is used and turbines are placed as an array in the water. This is as shown in Figure 2.1 (c).

Each of these methods requires different turbine design and arrangement. The first two designs have barrages that can block all the local flow and force it to pass through the turbine, both of them generate power from the head difference built up. The third one has different turbine design that the flow can pass around it, it generates power from the current flow. The third approach is expected to have a smaller change to the local environment (Adcock et al. 2015). Although to generate the same amount of power the unconstrained approach may need to introduce even more environmental impacts, it has less restriction to the selection of potential site because most of the sites would not allow significant changes to the marine environment. Therefore the third approach would be focused on in this report. However the lack of barrage limits the head difference across the turbines and results in a lower power production. Therefore these turbines must be placed in site that has strong current. Blanchfield et al. (2008), Vennell (2011), Adcock et al. (2013) stated that tidal channels are ideal sites for tidal turbine farm. Because of the advantage of power resources in tidal channels, this project will focus on the case that power is extracted from a tidal channel by the implementation of tidal turbines.

There are three main categories of tidal energy devices: axial-flow turbines, cross-flow turbines and oscillating hydrofoils (as shown in Figure 2.2). The axial-flow turbine is the most commonly used design for both wind and tidal power extraction. Turbine rotates about a horizontal axis along the flow direction. The incoming flow

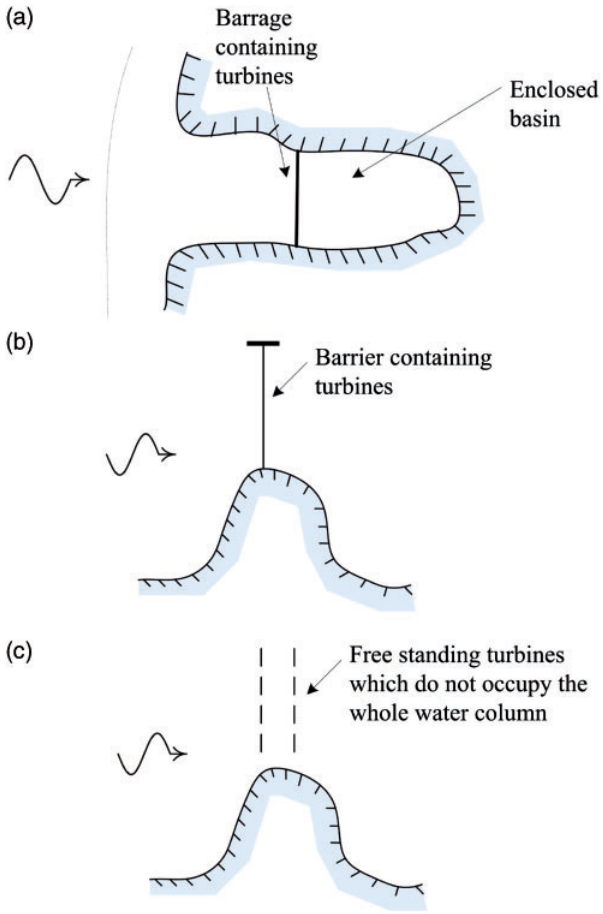

Figure 2.1: Schematic of different ways of installing turbines (top view) (Figure taken from Adcock et al. 2015)

is required to be parallel or has little angle to the axis of rotation for the turbine to be efficient (Schluntz 2014).

Cross-flow tidal turbines can be vertical (Figure 2.2(b)) or horizontal (Figure 2.2(c)). Both have a rotation axis perpendicular to the direction of flow. Unlike axial-flow turbines, cross-flow turbines allow a wider range of direction of flow to extract energy from (Schluntz 2014). Therefore this type of design is attractive to those sites where the flow direction changes significantly during a tidal cycle. Another advantage of the cross-flow turbines, especially horizontal-flow turbines, is that it can be deployed across the entire cross section of a channel (McAdam et al. 2009),

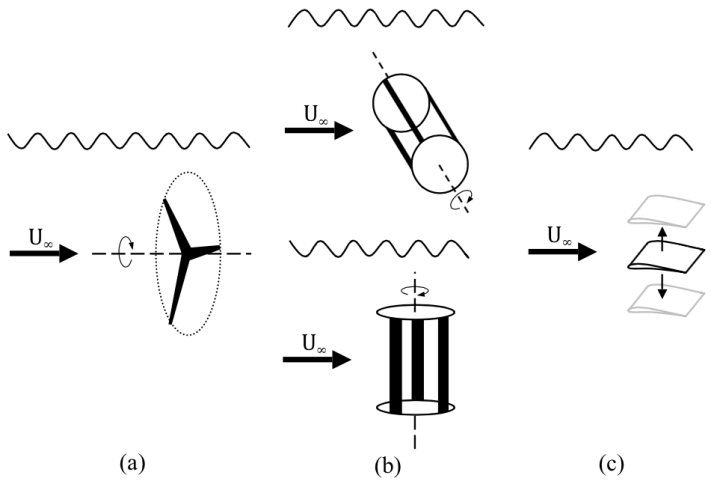

Figure 2.2: Different design of tidal turbines: (a) Axial-flow turbine, (b) Horizontal-axis (top) and vertical-axis (bottom) cross-flow turbine, (c) Oscillating hydrofoil. (Figure taken from Schluntz 2014)

therefore they are ideal for those sites where a very high blockage ratio is desired.

Oscillating hydrofoil devices (as shown in Figure 2.2(d)) extract energy from the oscillating motion of hydrofoil caused by the passing tidal current. Schluntz (2014) has pointed out that oscillating hydrofoils have low hydrodynamic efficiency because the variance in angle of the hydrofoil casing it to be at off-optimal angle of attack most of the time. The substantial loading on this type of devices also increase the requirement in support structures.

2.3 Resource Assessment

Tidal energy has been commonly considered similar to wind energy, while being constrained by the higher cost and immaturity of techniques and thus has not been widely used (Adcock et al. 2013). As a result, there is little knowledge about the optimal design or the cost of building and maintaining tidal devices, and the resource of a

candidate sites cannot be accurately quantified (Adcock and Draper 2014b). Adcock and Draper (2014b) and Hou et al. (2015) have highlighted the importance of quantifying the magnitude of the resource in advance in order to evaluate the potential sites for tidal energy development. Recently a number of resource assessments (Adcock and Draper 2014a, Draper et al. 2014, Vennell 2011, Hau and Renouard 2006, Hou et al. 2015, Zhang et al. 2014) have been done for candidate sites for tidal power farm to evaluate their feasibility of extracting tidal energy.

The power that can be extracted from the channel is directly related to the phase and amplitude of the tidal current flow through the channel. GC05 have stated that the extractable power in a channel is limited by its tidal dynamics. The Pentland Firth is well known because of its remarkably fast tidal currents, and hence has became a focal point for tidal energy extraction (Adcock et al. 2013). It connects the Atlantic Ocean to the North Sea and concentrates great amount of tidal energy. It is proposed to explore a case study of this site in the later chapter.

Recent research on the Pentland Firth suggest that theoretically an average power of up to approximately 4 GW could be extracted from this site (Draper et al. 2014). Considering the upper limit of power that is available from a candidate site is an important method of estimating the power resource (Adcock and Draper 2014b) that has been used by many researchers (Garrett and Cummins 2005, Adcock and Draper 2014a, Vennell and Adcock 2014, Zhang et al. 2014, Hou et al. 2015). This estimation gives an understanding of the magnitude of the power resource. However this estimation is only a theoretical upper limit of the tidal powers for this site, it is not feasible to generate that much power because of environmental concerns, turbine inefficiency

and other channel usage (i.e. local transport and marine life). Adcock and Draper (2014b) demonstrate that for a small array of tidal turbines the resource assessment can be done by multiplying the magnitude of the tidal currents' kinetic energy flux by the power coefficient of turbines. However, for a large scale of turbine arrays that is going to generate significant amount of power, a significant change to the flow will take place. In this case the kinetic flux method is no longer applicable (Adcock and Draper 2014b). Therefore a more site specific model is required in order to take into account the complex interaction between turbine arrays and the flow. In this thesis a simplified channel model is used first, followed by a 2D SWEs model built based on the Pentland Firth.

2.4 Turbine Models

Design of a tidal turbine farm is complicated because of the complex dynamics of tidal current. In addition the current will also be modified by the implementation of tidal devices (Bonar 2017). Thus numerical models are essential to the design of tidal turbine farm as well as resource assessment. However, the performance of numerical models are limited by computational requirements (Bonar 2017). Therefore certain degree of simplifications are often made in a model.

A common simplification made to the turbine is the actuator disc theory which simplifies the turbine as a disc applying uniform forces to the fluid (refer to the next section for more details). Figure 2.3 shows the cross-section of a simplified channel with four turbines (represented by actuator disc theory as circles). The depth of

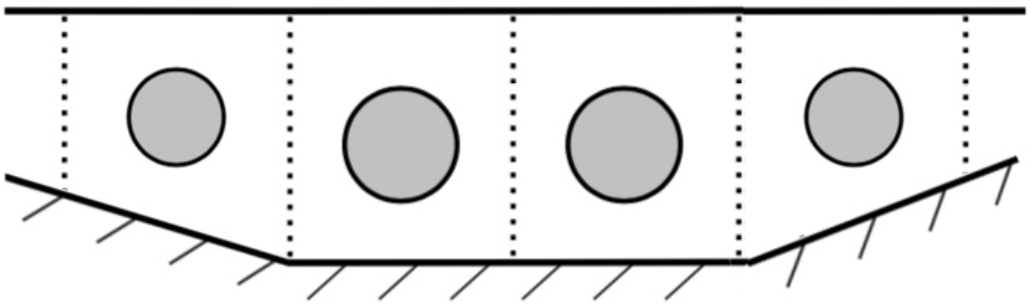

Figure 2.3: Sketch of cross-section of a simplified tidal channel

water may vary across and/or along the channel. The size of turbines may change according to the channel depth.

When modelling tidal turbine farms there are a few key parameters that need to be considered as shown in Figure 2.4:

1. Turbine thrust: as the water flow through the turbine, it receives a thrust from the turbine and this thrust is used to generate power.

2. Channel bed drag: drag force applied by the channel bed and wall due to natural friction.

3. Blockage ratio B: the ratio of total swept area to the channel cross-sectional area

4. Wake induction factor α_4: ratio of velocity in the turbine wake to the upstream undisturbed velocity.

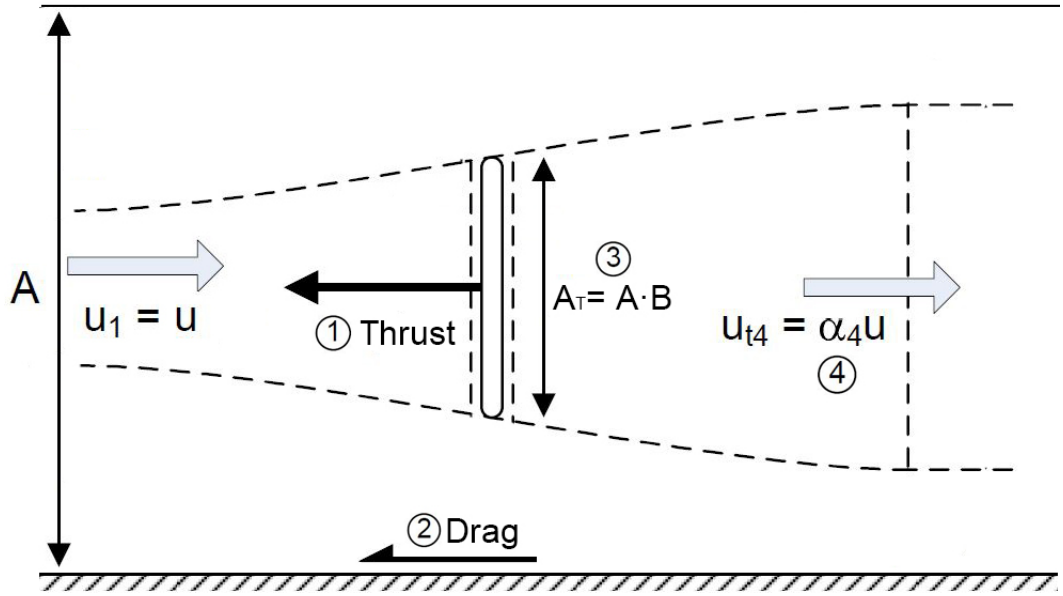

Figure 2.4: Sketch of cross-section of a simplified tidal channel

2.4.1 Actuator disc theory used in wind turbines

Tidal turbines and wind turbines are often considered together because both of them consist of extracting energy from flowing fluid through turbines. The most simplified representation of the complex behaviour of a real turbine is actuator disc theory. The actuator disc theory was first developed by Rankine (1865) to describe the flow field around a driving ship propeller, and has been adopted by Betz (1920) and Joukowsky (1920) to approximate the performance of an idealised wind turbine. The turbine is represented by a uniform circular disc having the same area as the swept area of the turbine (as shown in Figure 2.5). The streamtube is assumed to be irrotational and incompressible. Actuator disc applies uniform thrust T to the passing flow (between stations 2 and 3) so that the pressure just upstream and downstream the turbine are both uniform across the turbine plate (Garrett and Cummins 2007). This thrust applied by the turbine causes the flow to decelerate and the streamtube to

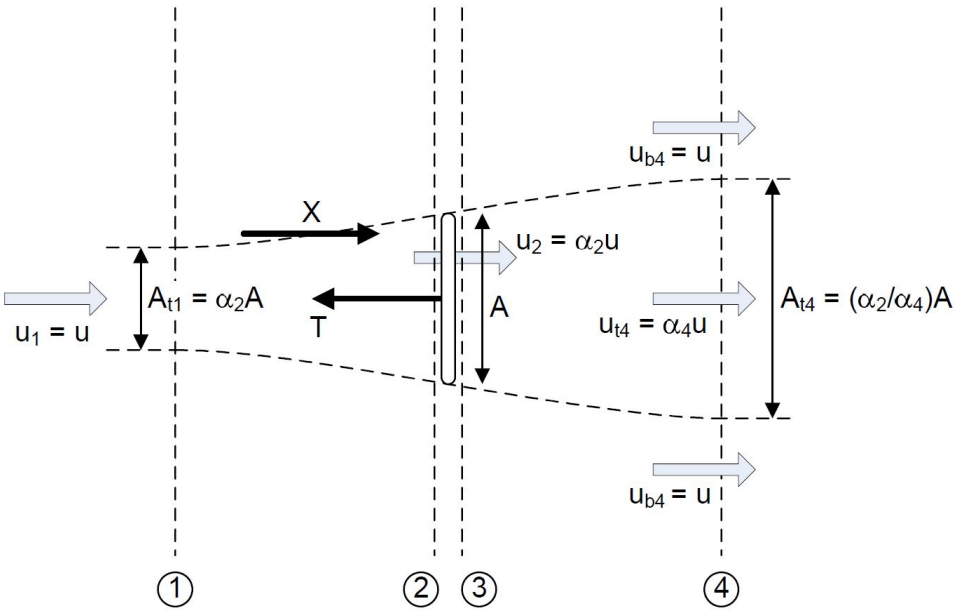

Figure 2.5: Actuator disc model of an unconstrained turbine

be expanded as the steam passing through the turbine. An opposite thrust equal to T is applied to the turbine by the stream and this force is used to extract power. This model allows the complicated dynamics of flow to be approximated by a much simpler technique. This model assumes that the fluid around the turbine is not constrained by its boundaries.

A most well known result deduced from analysis of this simplified model is that the power extracted by the actuator disc cannot exceed $\frac{16}{27}$ of the kinetic flux the disc (i.e. power coefficient $C_p < \frac{16}{27}$ where $C_p = \frac{Power}{\frac{1}{2}\rho u^3 A_{disc}}$), this is known as the Lanchester-Betz limit (Lanchester 1915, Betz 1920). Draper (2011) gave a qualitative explanation of this limit that the power extracted is low when the porosity of the disc is high because little thrust was applied on the turbine. As the porosity of the disc decreasing, it applies a larger force to the flow, resulting in a lower flowrate and ultimately lower power to be extracted (where power is equal to the force applied multiply by the

velocity of fluid passing through). The Lanchester-Betz limit is an ideal solution where the optimal thrust is applied and the power extracted is maximised. The Lanchester-Betz limit and the actuator disc theory have proven to be very useful as a guide to wind turbine design as a power potential estimate (Burton et al. 2001). However reaching the Lanchester-Betz limit is not applicable because of certain simplification in the actuator disc approximation. For example, actuator disc theory assumes the flow to be irrotational. However, rotating turbine blades will introduce tangential velocity into the flow wakes (Draper 2011). The rotational energy in the wakes is counted as part of the energy lost due to the turbine, therefore the actual available power to the turbine will be lowered (Burton et al. 2001).

2.4.2 Extensions to actuator disc theory for tidal turbines

It is reasonable to expect that the actuator disc theory will be effective for tidal turbines because a similar principle applies: they remove momentum from the flow in the axial direction. (Draper 2011). However, the application of actuator disc theory to tidal turbines is not straightforward. The unconstrained case is applicable to wind turbine because there is little change caused by the turbine to the surrounding atmosphere and little constraint by the boundary of atmosphere. The application of actuator disc theory to open tidal channel flow has been attempted by many researchers (Whelan et al. 2007, 2009, Houlsby et al. 2008, Garrett and Cummins 2007). The basic idea is the momentum, mass and energy conservation of the fluid under the thrust by actuator discs.

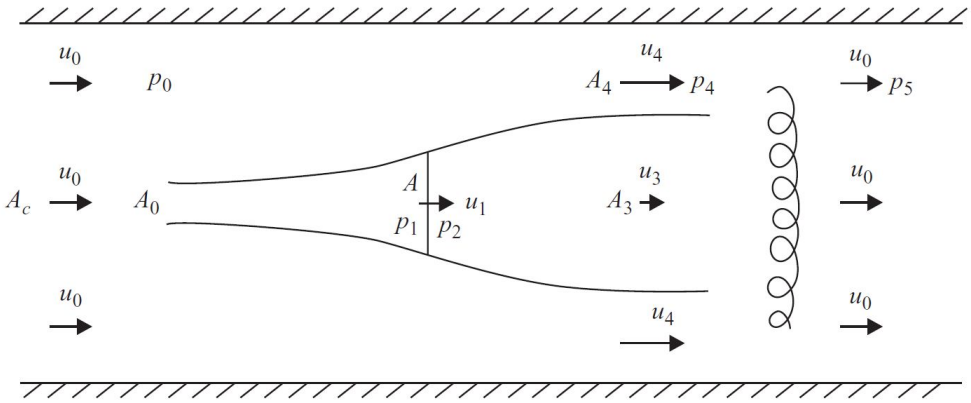

Figure 2.6: Definition sketch for a single turbine in a channel (Figure taken from Garrett and Cummins 2007)

Tidal current constrained in a channel has very different dynamics to the flow of air in the unconstrained atmosphere (Bryden et al. 2007). In most of the cases, tidal turbines are subject to shallow water flow (Whelan et al. 2007) where the turbines are constrained significantly by the channel bed and free water surface. As a result of that, tidal turbines can in turn change the flow and affect the power available from a tidal channel (Whelan et al. 2007). As pointed out by Fraenkel (2002), the application of unconstrained actuator disc model would only apply to tidal turbines if the flow boundaries are far from the turbine. When the flow boundaries are sufficiently close to the turbine, which applies to most of the cases for tidal turbines, the assumptions made in unconstrained actuator disc model are no longer applicable (Bryden et al. 2007).

Garrett and Cummins (2007) extended the actuator disc theory to a tidal turbine in a narrow channel at low Froude number where the change in the free surface is negligible. They started with the analysis of a single turbine in a channel (Figure 2.6) formed by two parallel walls, channel bed and an assumed fixed free surface.

They found that the power coefficient is maximised at $\alpha_4 = \frac{1}{3}$ – the same as the Lanchester-Betz limit. They also found that the power coefficient of a turbine in a channel would increase as the blockage ratio B (the ratio of total swept area of turbine to the channel cross sectional area) increases. The Lanchester-Betz limit of $C_p < \frac{16}{27}$ for a turbine would be increased by a factor of $(1-B)^{-2}$. However, a large C_p does not necessarily mean higher power production because extracting power from the channel decelerate the flow throughout the channel and reduce the maximum available power of all turbines within the array (Garrett and Cummins 2005, Vennell 2010). However, Garrett and Cummins (2007) also concluded that in the case of a evenly distributed row of turbines (Figure 2.7) with a low B, the maximum energy produced by turbines will be 2/3 of the case where a single turbine occupying the entire cross-section of a channel, and if B is large (i.e. close to 1), this fraction will decrease to 1/3. However the actual power still increases as the blockage ratio increases. This is again confirmed by Vennell (2013) that tidal turbines in a channel would be more efficient due to the accelerated duct, which is caused by the constrain of channel sides and proximity of other turbines (see Figure 2.7), formed around turbines. Garrett and Cummins (2007) also concluded that given the turbine is operating with the optimum setting, some energy will be dissipated in the mixing of the downstream wake and accelerated bypassing flow. As a result of this wake dissipation, as well as some other loss of energy like blade frictions, the power available for electricity production (defined as the available power) would be much lower than the power extracted from the flow due to the installation of turbines (defined as the extracted power). Their model assumed that turbulent mixing downstream occur only after where the pressure across the

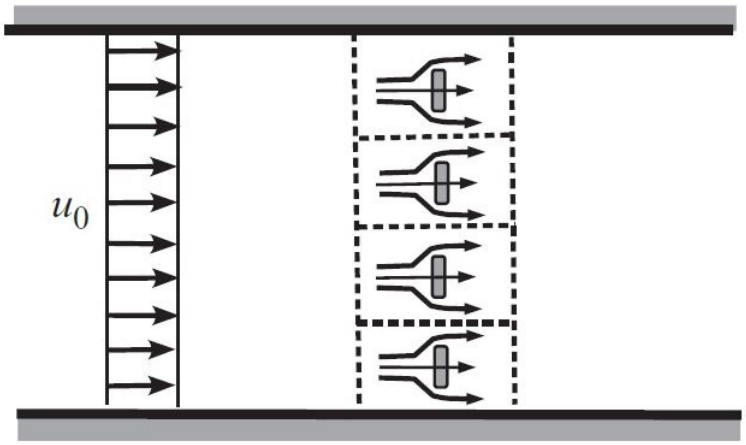

Figure 2.7: Schematic of a row of turbines in a tidal channel (Figure taken from Vennell 2013)

channel cross section has reached equilibrium.

Vennell (2010) claims that Garrett and Cummins' assumption of no change in free stream flowrate is impractical due to the additional drag brought by implementing tidal turbines (Garrett and Cummins 2005). Therefore the result of exceeding the Lanchester-Betz limit of $C_p < \frac{16}{27}$ do not apply to array of turbines in a tidal channel. Considering the flowrate change caused by applying tidal turbines, maximizing the power output would require the turbines to be tuned and arranged specifically according to the site (Vennell 2010, 2011). Therefore Vennell (2013) states a stricter definition for exceeding the Lanchester-Betz limit that a turbine in a channel with a reduced flowrate would produce more power than an isolated Betz turbine operating at the same undisturbed flowrate. According to this definition, for a large channel (much wider than the size of a turbine) exceeding the Lanchester-Betz limit is equivalent to having turbines produce more power than the first turbine installed (Vennell 2013). It is important to note that a large array does not always have a large number

of turbines. For example, a few turbines in a small channel can be a large array, while a large number of turbines in a large channel can be a small array. Vennell et al. (2015) have defined a large array as "one which is able to influence channel scale dynamics or one where the channel alters turbine performance".

An important assumption made by Garrett and Cummins (2007) is that the free water surface change across the turbine row can be ignored. However Houlsby et al. (2008) have pointed out that this assumption is formally incorrect since it assumes the water level to be constant along the channel while allowing the pressure to vary. The free water surface is subjected to hydro-static pressure. In the case of a non-zero flow Froude number, the change in pressure would result in changes in free surface. This change becomes significant when B is high (Whelan et al. 2009). Based on Garrett and Cummins' (2007) model that considers turbine flows constrained between two channel walls, Whelan et al. (2009) extended the work to allow the change in free water surface level caused by the pressure changes across the turbine. This change removes the restriction on Froude number. They have taken both the proximity of the free water surface and the channel bed into account in their model for a constrained tidal turbine array. Whelan et al. (2009) have derived an expression of the power coefficient as a function of the blockage ratio, Froude number and α_4 of the turbines. Their work has also shown that the optimal power coefficient may exceed the Lanchester-Betz limit with a finite blockage ratio. However, the results produced by Whelan et al. (2009) shows a discontinuous solution in cases with $B \geqq 0.3$ because the bypass flow reaches hydraulically supercritical, this is further explained in Draper (2011). Also Whelan et al. (2009) did not include downstream wake mixing in their model, which is

necessary to understand the efficiency of a turbine in a channel with non-zero Froude number (Draper 2011).

Houlsby et al. (2008) extended the works done by Garrett and Cummins (2007) and Whelan et al. (2009), to explore the performance of a turbine in an open channel flow (with a variable free surface). Houlsby et al. (2008) solved the open channel model by assuming a constant pressure boundary and a constant volume boundary. The model built by Houlsby et al. (2008) (named the open channel model, Figure 2.8) considers the reduction in water depth and the associated increase in downstream velocity caused by the extraction of power (White 2009). The reduction in water depth is represented by a discontinuous change in depth after the turbine. The increase in the downstream kinetic flux is consistent with open channel theory (Draper 2011, White 2009), but in contrast to the assumption made by Garrett and Cummins (2007) that the kinetic flux does not change. In addition to the flow field considered by Whelan et al. (2009), an additional station (station 5 in Figure 2.8) has been included to account for the analysis of flow field after the wake mixing.

Three additional assumptions were made for the open channel mode: 1. hydrostatic pressure at stations 1, 4 and 5; 2. negligible seabed friction and 3. seabed and channel walls remain straight and parallel to the tidal stream (Draper 2011). Houlsby et al. (2008) derived a relation between the turbine parameters (B, α_4, etc.) and the change in upstream and downstream flow velocities and depths. The results given by Houlsby et al. (2008) describing the change in free surface has been used as the basis of the momentum sink method in a depth-averaged model to represent the power removal by the turbine (Draper et al. 2010, Draper 2011, Serhadlıoğlu 2014). The

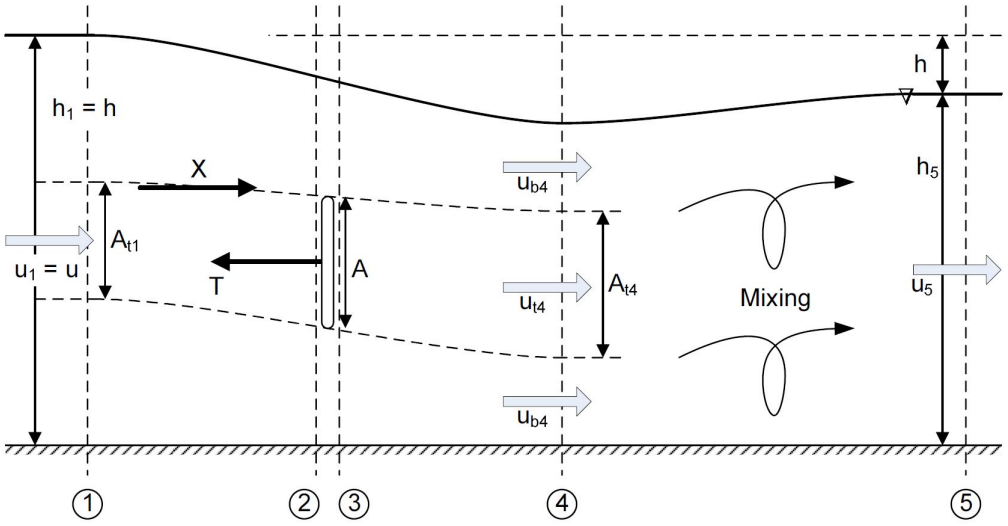

Figure 2.8: Actuator disc model of a turbine in open channel flow (Figure taken from Houlsby et al. 2008)

inclusion of the momentum sink will be described in the later section of 2D SWEs model.

Nishino and Willden (2012) has extended Garrett and Cummins (2007)'s model in a different direction from the model built by Vennell (2010), while the general conservation of momentum, mass and energy remain unchanged. Their model considered the case of a partial tidal fence that only occupies part of the channel's cross section instead of the entire cross section in Garrett and Cummins (2007). This model has explored the effects of channel dimensions and spacing between turbines on the total power efficiency. Their model proved that C_p depends on B due to the "blockage effect" that accelerated bypassing flow would increase power efficiency – at $B = 0.40$ the efficiency can reach a maximum of $C_p = 0.798$ for an infinitely wide channel. Their model for a shallow channel suggests that when B is low, there is an optimal inter-turbine spacing for the overall power efficiency to be maximised for a given chan-

nel dimension. As the inter-turbine spacing is reduced, the power efficiency increases due to the local "blockage effect", but when the spacing is further reduced the effect of array-scale choking (i.e. the total flow through the turbine is reduced) causes the power efficiency to decrease.

2.4.3 Constrained Blade Element Momentum Theory

Actuator Disc Theory has been used often as an approximation to a real turbine. However the actuator disc theory is a highly simplified model of turbine plates that ignores vertical and radial variations of flow, which will bias the estimated power. Blade Element Momentum Theory (BEM) is often considered as a more advanced model over actuator disc theory because of its capability in considering radial variation of flow. The unconstrained version of BEM model has been used for modelling wind turbines (Hau and Renouard 2006). Vogel (2014) has adopted BEM and developed a constrained BEM model for tidal turbines in a constrained channel. The BEM model divides the stream into concentric annular stream tubes as shown in Figure 2.9. The core theory of this model is again the conservation of momentum, mass and energy. The BEM model assumes no momentum transfer between adjacent stream tubes. The model is able to consider the effects of lift and drag force of the turbine blades separately, it also takes the pressure gradient upstream and downstream the turbine into account.

BEM model generally assumes an infinite number of blades in a turbine to ensure that all fluid particles suffer the same change in momentum when they flow through

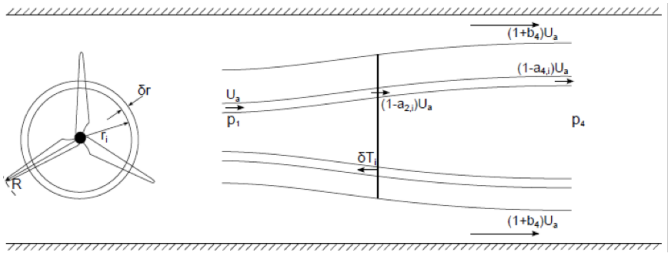

Figure 2.9: Schematic diagram of constrained BEM theory (Figure taken from Vogel 2014)

the turbine plate. However a practical turbine would only have a few blades and hence cannot provide such uniform change in momentum. Therefore a correction method is required to better define the change in fluid momentum. Prandtl's tip loss model has been used to correct wind turbines (Leishman 2006). Vogel (2014) has adopt this tip loss correction in his constrained BEM model to take into account the reduction in momentum changing at the tip of turbine blades. The resulted model has a good agreement to the Reynolds-Averaged Navier-Stokes numerical simulations by Schluntz (2014).

2.5 Basin Scale Hydrodynamics

2.5.1 Simplified channel

Garrett and Cummins (2005) developed a simple analytical model to explore the extraction of tidal energy by turbines from a tidal channel. They used a simple 0D channel model that modelled the power extraction by considering the momentum balance across the entire channel. The channel is considered to be short compared with the wavelength of the tide, with variable cross-section area and connecting two

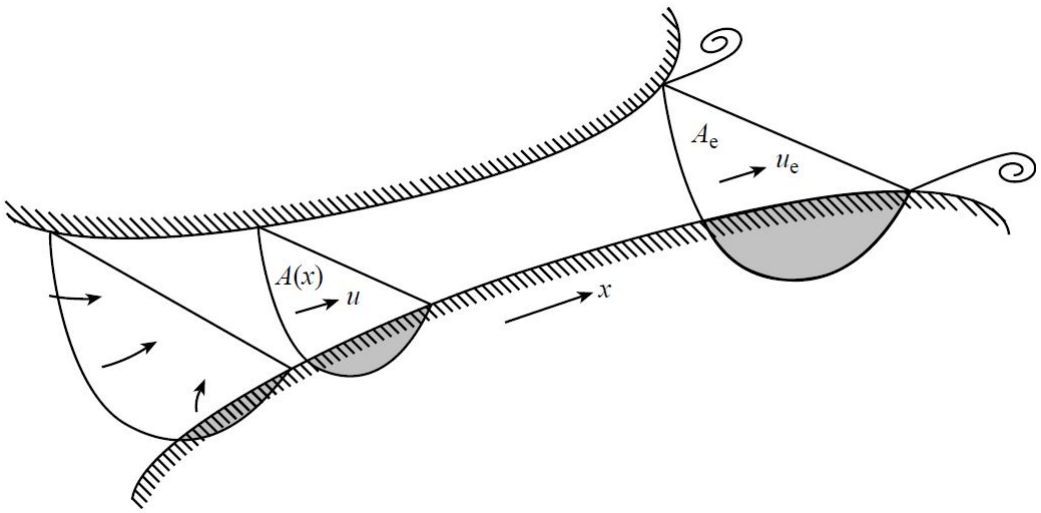

Figure 2.10: A channel connects two basins with different tidal elevations (Figure taken from Garrett and Cummins 2005)

large water bodies with a difference in water elevation (see Figure 2.10). Their work considers the thrust applied by tidal turbines as a increase in the seabed friction. This model assumes that the turbines are deployed uniformly across the channel cross section so that the additional friction force associated with the turbines is independent of the position in the channel. This model is able to consider how extracting power from a channel increases the drag coefficient and hence slow down the flow. One important results given by Garrett and Cummins (2005) is that the maximum time-averaged power can be approximated by $0.22\rho gaQ_{max}$ to within 10% (where ρ is the fluid density, g gravity acceleration, a the height of a sinusoidal tidal wave and Q_{max} the peak undisturbed volume flux). However, such representation of turbines as additional seabed friction cannot make a distinction between available power and extractable power.

This simplified model provides a basis to the idealised 0D model used in this study (Chapter 3). Vennell (2010) provided an approximated analytical solution to

the model by Garrett and Cummins (2005), for a idealised rectangular channel. This analytical solution has been used as a first approximation, and a numerical method was used for solving the idealised 0D model in this study.

2.5.2 Shallow Water Equations (SWEs) model

The simplified channel model discussed previously can produce a good estimate of tidal power extraction in a channel. However a simplified model can only provide an estimation for an idealised channel, and it cannot model the complex dynamics in a real site (Adcock et al. 2013). Therefore when it comes to the real site investigation, a more advanced model that is able to handle a more complex geometry with a higher accuracy is required. The Shallow Water Equations (SWEs) model is such a model that has been used by many researchers (Serhadlıoğlu et al. 2013, Draper 2011) as a way of modelling tides.

The 2D SWEs are used to describe flow in a water body where the depth is much smaller than the scale of wavelength. The SWEs assumes a hydrostatic pressure and uniform velocities along the depth. The SWEs can be derived by integrating the Navier-Stokes equations (Falconer 1993) along the depth of the fluid body and hence reduces the 3D free boundary problem to a 2D fixed boundary problem (Tan 1992). It has been used to study many physical phenomena including tidal waves, tsunami waves, storm surges, off-shore structure forces and can be coupled to transport equations to evaluate the movement of chemical species (Aizinger and Dawson 2002).

The fundamental limitations of the SWEs model is raised from the nearly horizontal flow assumption, in another word the vertical component of velocity is neglected in comparison to the horizontal components (Falconer 1993). In SWEs models the vertical velocity profile is approximated by a fixed log profile which is related to the bed friction coefficient used in the model (Draper 2011). However, velocity profile in real world may vary significantly due to, for example, steep bathymetry. Although the application of tidal devices, as evaluated in this project, would indeed introduce significant variation of the vertical velocity profile, we assume the use of SWEs models to be applicable because of two reasons: first, tidal devices would only affect relatively small area comparing to the entire site; second, the use of 3D modelling is too computationally expensive to evaluate the problems in this project.

Various methods exist to find numerical solutions to the SWEs. The approach used in this thesis is the discontinuous Galerkin (DG) version of ADCIRC 2D SWE solver (Kubatko et al. 2006), which is based on the Godunov method (Chippada et al. 1998) in several ways. Instead of calculating higher order polynomials by some post-processing procedure, they are naturally built into the method (Aizinger and Dawson 2002). This method can also incorporate diffusive terms into it, while the Godunov method cannot handle the mechanism for second order derivatives. Additionally, the DG method is capable for the use of non-conforming grids, which will be helpful when working with very complex geometries and adaptive meshes. Instead of representing tidal turbines as additional bed friction as done by Garrett and Cummins (2005), the DG version of ADCIRC has been modified to consider the head loss across the turbines as a discontinuous change in velocity and water depth. (Draper 2011). Such

discontinuous change is presented by a line of momentum sink, which can be modelled by the turbine models mentioned earlier such as the actuator disc theory. A DG-ADCIRC model using the open channel model to calculate the line of momentum sink has been used in this study (Chapter 4).

2.6 Environmental Impacts and Solutions

2.6.1 Environmental impacts

Although tidal energy is is normally regarded as a low-carbon energy (WaveNet 2003), marine energy is not without environmental impact. Less research has focused on the environmental and ecological impacts of tidal energy than on power production, as the majority of tidal energy farm are still undergoing theoretical evaluation (Bonar et al. 2015). Although renewable energy has been widely discussed and supported (Warren et al. 2005), Bonar et al. (2015) emphasised that the development of tidal energy is limited not only by the natural and technical condition, but also by the uncertainties regarding the environmental impacts of extracting tidal energy on marine ecosystems. Adcock et al. (2015) have mentioned that one major environmental concern about tidal energy is that energy extraction from a tidal channel will cause changes in the current flow. For example Garrett and Cummins (2005) showed that when the extracted power is maximised, the current flow in an idealised tidal channel would reduce to 58% of that without the presence of turbines. Although in actual application it would not be possible to reach the maximum power, this indicates that a significant

change in flowrate would occur when turbines are implemented. The implementation of tidal devices are limited by the concern of several environmental impacts, such as changes to the marine ecosystem, damage to fish and marine mammals by the turbine blades, and changes in sediment transport (Neill et al. 2009, Ahmadian et al. 2012). However, those impacts on the marine ecosystem and animals are hard to qualify with a numerical model. Some ecological analysis would be required to perform such evaluation. Therefore this thesis would only focus on those environmental impacts that are related to changes in flowrate which is more sensible to evaluate with a numerical model.

For tidal energy to be truly sustainable, the potential environmental impacts must be identified and evaluated so that the adverse effects of extracting tidal energy can be minimised before the devices are applied in larger arrays (Bonar et al. 2015). It is suggested that environmental impacts are likely to be site specific and can also vary with season (Bonar et al. 2015), because of the variation of design of turbines and scale of arrays. The impacts may also be cumulative, in time or with increasing number of turbines (Shields et al. 2009, Witt et al. 2012).

Tidal turbines can partly block or decelerate the tidal current flow, meanwhile accelerate the bypass flow around the turbine and create mixing in the far wakes (Garrett and Cummins 2007). These blockage and mixing effects alter the local flow patterns. Waves and tides play a significant role in marine ecosystems, the alteration of these natural fluxes many greatly affect the maintenance of ecosystems (Copping et al. 2013, Shields et al. 2011). Shields et al. (2009) stated that the implementation of tidal turbines may change the local sedimentation patterns and

hence affect deep ocean ecology. Erosion may occur around turbines where the current flow is accelerated and deposition can happen upstream or downstream the turbines where flow is decelerated (Shields et al. 2011). Modification of sedimentation patterns can alter the local nutrient levels, total metal and bacteria concentrations (Bonar et al. 2015, Shields et al. 2009). The changes in sedimentation patterns may also affect the pollutant dispersal around some sites where there are ocean disposal nearby.

2.6.2 Support structures

Although most of the models discussed above have neglected the impact of it, the support structure is an important element of tidal farm that has been discussed by many researchers (Adcock et al. 2015, Muchal and Willden 2014). Adcock et al. (2015) have considered the impact of support structures in the discussion of power capping although no detailed analysis has been done. Muchal and Willden (2014) have evaluated the turbine support structures in their model. The model considers the drag force of support structures as an external term of thrust. Thus in their model there are three components of forces including thrust applied by the turbines, drag from the support structures and channel bed friction. The work suggests that the support structures can have significant impact on a turbine farm's total power output. Muchal and Willden (2014) concluded that the efficiency as well as power output of a turbine drops due to the presence of support structure, and the drop is even higher for higher flow velocities. Their results also showed that drag coefficient of support structure has significant impact on the total power efficiency.

This project has considered the drag force caused by the presence of turbine support structures using a simplified 0D model. The size of support structure is evaluated by a bending beam model and the drag is calculated in a similar way as Muchal and Willden (2014) did that the drag force is taken as an external term of thrust. Muchal and Willden (2014) have also evaluated the impact of flow rate reduction constraints which limits the changes to the tidal current flowrate by the installation of turbines to a certain percentage of the peak flowrate. Although limiting the changes to the flowrate will eventually reduce the power available, it is worth considering when there is a concern about the environmental impact.

2.6.3 Power Capping

Tidal energy is a predictable and renewable source of energy. The technology is still at an early stage of development, with the first large scale development currently being installed in the Inner Sound of the Pentland Firth. A key challenge in developing the technology is optimisation of the design of tidal farms so as to maximise the power produced whilst limiting cost and environmental impacts. This is a complex, interdisciplinary problem. In this work we consider the leading order physics of one aspect of this problem — the impact of limiting the maximum power and, in particular, thrust, on the tidal stream resource and environmental impact.

Although extracting all the available energy by tidal turbines can be ideal for maximising power production, it requires the turbines to be able to hold the maximum thrust which results in turbine inefficiency in power generation during low tides. Also

it will require power generators and electric cables to have a capacity of generating and proceeding the maximum power during peak tide. Generators make up a significant part – 37.6% of tidal turbine capital costs as estimated by Peterson (2008). Reducing peak power can effectively save turbine costs. In order to balance the size of power generator with economically reduced power production, a strategy known as power capping, which can reduce the requirement in generator capacity, have been discussed by a few researchers (Vogel 2014, Adcock et al. 2014). Power capping is a method that limits the power production when it exceeds a predetermined threshold point during peak tide. Such capping can reduce the peak power and thus reduce the requirement of power generator and cable capacity as well as increasing the capacity factor of turbines. Figure 2.11 shows the relation between capped power and stream velocity. In addition, power capping can also reduce the thrust loads on the turbines (Adcock et al. 2014). This will in turn reduce the force applied to the flow and hence reduce the change in flowrate. Therefore power capping can be considered as a potential solution to the environmental impacts brought by implementing tidal turbines.

A practical way to implement power capping stated by Adcock et al. (2014) is to modify the tip speed ratio when needed to change the power coefficient. Running the turbine at a lower tip speed ratio during peak tide can effectively reduce the power and can keep the power production constant. This can also reduce the thrust coefficient. An alternative way is to increase the tip speed ratio which will also reduce the power coefficient, but meanwhile thrust coefficient will be increased Adcock et al. (2014). Decreasing tip speed ratio is generally preferred as it would reduce the loads on turbines. Therefore this method will be used in the power capping analysis in this

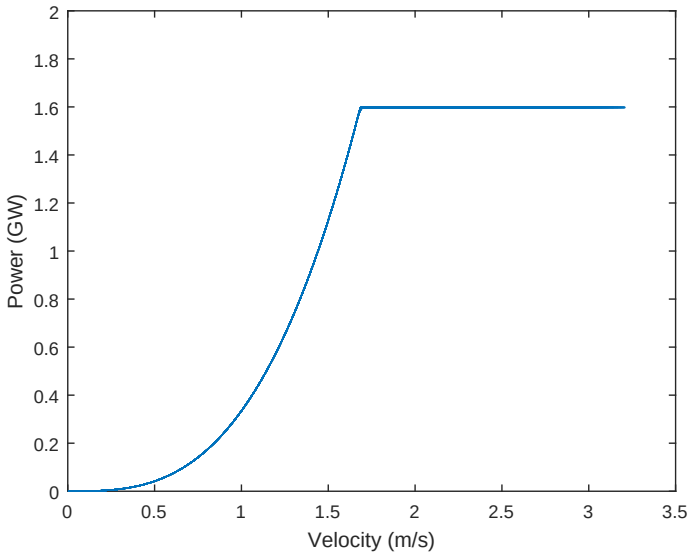

Figure 2.11: An example of power capping

work. The capping can reduce the thrust coefficient of turbines, however the drag by the support structure, which might be significant, cannot be reduced Adcock et al. (2014). The reduction in turbine thrust can be further reached by doing a similar capping to the turbine thrust, however not much work has been done on such thrust capping. This work will carry out a brief evaluation of the effectiveness of such thrust capping.

2.6.4 Thrust Capping

The thrust applied by the turbine, and the force on the foundations, are periodic as well as the power. It is the thrust load that determines the design of turbine blade and supporting structures. As McAdam (2011) pointed out that fatigue is a significant effect that may affect the life time of tidal devices, and it is mainly dependent on the thrust load. In addition, high thrust can result in significant changes in tidal stream

flow that may have potential environmental impact on the local submarine eco-system. In this work we consider limiting not only the peak power but also introduce the idea of operating tidal stream turbines so as not to exceed a given thrust — or thrust capping (TC). This has the benefit of reducing the size of the support structure and the peak loads on the turbine and foundations. It also has the benefit of reducing the peak force applied to the tidal flow, which, although a complicated relationship, would be expected to reduce the change to the naturally occurring current. Of course, the power and thrust capping strategies are inter-related — but we show in this work that both should be adopted, to some degree, in the design of tidal turbine farms.

Chapter 3

Combined Power and Thrust Capping in Idealised 0D Model

3.1 Introduction

It is commonly accepted that a power capping (PC) strategy will be adopted in the design of wind turbines Vogel (2014). Because of the similarity in mechanism and design of wind turbine and tidal turbine, we believe a similar strategy will be equally beneficial for tidal turbine farms. In this work the implementation of PC in tidal turbine farms will be discussed. Figure (3.1) shows the difference in the power profile under fully exploited and PC conditions. This example shows PC in a tidal channel that is dominated only by M_2 tidal constituent. In this example the peak power is reduced to 80% of its original value while total power production does not decrease significantly. Instead of sizing the generator based on the fastest current at a site, which only occurs for a short period of time, a generator with a lower power rating is

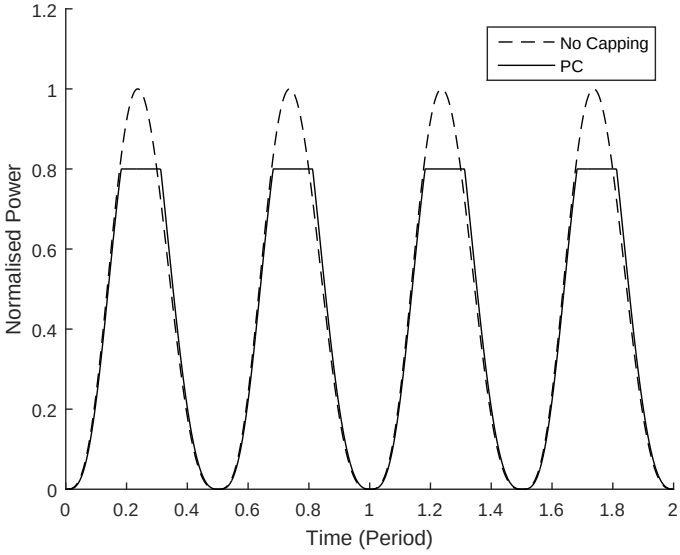

Figure 3.1: An example of PC

used with appropriate changes to the hydrodynamics of the turbine to produce this lower power. The strategy generally only makes a small reduction to the total power produced but is expected to have significant cost savings in generators and cables. A number of studies (Adcock et al. 2014, 2015, Vogel et al. 2014) have considered the implications of such a strategy on the magnitude of the resource.

In this chapter we seek to examine the leading-order effects of PC. Thrust capping (TC) and the combination of power and thrust capping (PTC) are also evaluated. A rather simplified 0D model was used to produced the results in this chapter due to the much faster computational time comparing to the 2D SWE model used in the later chapter. The model was modified from Adcock and Draper (2014a) by introducing an additional force applied by the turbine support structures. Due to the fact that support structure size and force load are dependent on each other, and similarly support structure and the channel flow, the model was solved using two iterations

process – more detail about the algorithm will be introduced in the Algorithm section. Due to the limitation of time and computational power, such iteration processes would be too expensive to run on a 2D model. Therefore the evaluation of support structures has only been done in this chapter.

All three capping strategy sacrifice part of the power production when the load is high. Practical engineering design will face trade-offs between the peak thrust on a structure, the generated power, and the total power available in the undisturbed tidal resource. We use a simple idealised tidal channel model and analyse power and thrust capping for different scenarios. The models were firstly tested when the flow is formed by a single tidal constituent and then evaluations over a sping-neap cycle in M_2 and S_2 channels which are more realistic of behaviour at a real tidal site. We demonstrate how the available power varies as a function of different capping for an idealised channel.

3.2 Model

A simple 0D model for an idealised tidal channel has been used to evaluate the effectiveness of capping as well as gaining an initial idea of the impact of different capping strategy. The model was built following the works done by Garrett and Cummins (2005) and Adcock and Draper (2014a). This model has been used by numerous researchers (Vennell 2010, 2012, Adcock and Draper 2014a) to explore the leading order characteristics of tidal stream energy extraction. The model has been compared with more complex 2-D models (Blanchfield et al. 2008, Adcock et al. 2013)

and has been shown to give good qualitative representation of the behaviour of a real channel. In this chapter this model is used to emulate an idealised channel instead of a real one. Only two main tide components, the M_2 and S_2 tides are considered in this model.

The simplified model considers the tidal channel to be a rectangular and uniform channel, although it has the potential to be modified to represent more complex shapes. Although the model does not account for the complex nature of the flow in a real channel, it provides a conceptual model that is able to make a qualitative analysis of power and turbine thrust profiles. In addition, a simplified model would have much less complex physics going on and hence would be much easier to interpret the results. Thus we can investigate PC, TC, PTC strategies without substantial computational effort.

3.2.1 Background

The model is derived from the 1D shallow water equations in a narrow tidal channel, which has a stream velocity $u(x)$ varying along the channel's length due to variation of channel geometry. The 1D shallow water continuity equation and momentum balance in the channel is given by Adcock and Draper (2014a) as:

$$\frac{\partial \zeta}{\partial t} + \frac{1}{b}\frac{\partial Q}{\partial x} = 0 \tag{3.1}$$

and

$$\frac{\partial}{\partial t}u + u\frac{\partial}{\partial x}u + g\frac{\partial \zeta}{\partial x} = -F_{nat} - F_{turbine} \tag{3.2}$$

It is important to note that the forces to the right hand side of equation 3.2 is force per unit mass. In this work an additional drag force by the support structures of turbines is introduced, therefore equation 3.2 becomes:

$$\frac{\partial}{\partial t}\frac{Q}{A} + (\frac{Q}{A})\frac{\partial}{\partial x}(\frac{Q}{A}) + g\frac{\partial \zeta}{\partial x} = -F_{nat} - F_{turbine} - F_{support} \tag{3.3}$$

In the simplified case of a rectangular channel that the geometry of channel and B do not change along the length and assuming all turbines and their support structures are identical. The forces (per unit mass) applied by the channel bed to the right hand side of equation 3.3 are given by Adcock and Draper (2014a) as:

$$F_{nat} = \frac{C_d Q|Q|}{2A^2 h} \tag{3.4}$$

Thrust applied by a single row of turbine is given as:

$$Thrust = \frac{1}{2}BC_t A\rho u|u| \tag{3.5}$$

Hence the total thrust per unit mass is calculated as:

$$F_{turbine} = \sum \frac{\frac{1}{2}BC_t A\rho u|u|}{\rho AL} = \frac{nBC_t Q|Q|}{2A^2 L} \tag{3.6}$$

We include a simplistic representation of the turbine support structure in this

model. Following Muchal and Willden (2014), the drag from a cylinder support structure can be calculated using equation 3.7

$$Drag = \frac{1}{2} C_{d,s} \rho u |u| L_s D \tag{3.7}$$

The force applied by support structures per unit mass is then calculated as:

$$F_{support} = \frac{\frac{1}{2} N_t C_{d,s} \rho u |u| L_s D}{\rho A L} = \frac{N_t C_{d,s} L_s D Q |Q|}{2 A^3 L} \tag{3.8}$$

where the drag coefficient is taken as $C_{d,s} = 1$

The support structure is assumed to be a hollow cylinder and the drag is modelled using Morison's equation (Morison et al., 1950). The size of cylinder required is calculated according to the thrust and material strength to evaluate the benefit of TC. And the support structure diameter is calculated by

$$\sigma_{max} = \frac{M_z}{Z_e} \tag{3.9}$$

M_z is the bending moment applied to the beam given by $M_z = Force \times Length$, in this model the turbine and support thrust is assumed to be acting on the top end of beam and perpendicular to it.

For hollow cylinder with outer and inner radius $= r_o, r_i$ respectively we have

$$Z_e = \frac{\pi (r_o^4 - r_i^4)}{4 r_o} \tag{3.10}$$

Given the peak thrust calculated by the given tidal channel model, length of

supporting column unit and σ_{max}, Z_e can be calculated by equation (3.8), hence the radius can be calculated by equation (3.10). To size the support column we assume a maximum allowable stress of 250 MPa (a rough estimation of the tensile strength of steel). We assume the support structure is a column of thickness 5% of the column diameter. The size of support structures is calculated using an iteration algorithm which will be explained in detail in the Algorithm section.

Integrating equation 3.3 over the length of channel (L) is justified if the channel is "short" – a short channel defined by Vennell (1998) as one where the channel length is much smaller than the wavelength – which is reasonable for most candidate sites for tidal stream energy. This integration, and further simplifying by assuming the cross-section is rectangular gives equation (3.11)

$$\frac{L}{A}\frac{dQ}{dt} = g\eta - (\delta_0 + \delta_1 + \delta_2)Q|Q| \tag{3.11}$$

where δ_0, δ_1 and δ_2 are three terms of force that we considered in this model: turbine thrust, support structure thrust and channel bed friction, respectively, defined by equations (3.12), (3.13) and (3.14).

$$\delta_0 = \int_0^L \frac{C_d}{2hA^2}dx = \frac{C_d L}{2hA^2} \tag{3.12}$$

$$\delta_1 = \int_0^L \frac{nBC_t}{2A^2 L}dx = \frac{nBC_t}{2A^2} \tag{3.13}$$

$$\delta_2 = \int_0^L \frac{N_t C_{d,s} L_s D}{2A^3 L} dx = \frac{N_t C_{d,s} L_s D}{2A^3} \tag{3.14}$$

The time series of flowrate is calculated by solving equation 3.11 with 4th order Runge-Kutta method. Then the generated power (P) and turbine thrust (T) are calculated by equations (3.15) and (3.16),

$$P = \frac{1}{2} n B C_p A \rho |u^3| \tag{3.15}$$

$$T = \frac{1}{2} n B C_t A \rho u^2 \tag{3.16}$$

C_p and C_t are power and thrust coefficients given by Garrett and Cummins' (2007) model as

$$C_p = \alpha_2 C_t \tag{3.17}$$

$$C_t = \beta_4^2 - \alpha_4^2 \tag{3.18}$$

where α_2 and β_4 are given as

$$\alpha_2 = \frac{1 + \alpha_4}{(1 + B) + \sqrt{(1 - B)^2 + B(1 - \frac{1}{\alpha_4})^2}} \tag{3.19}$$

and

$$\beta_4 = \frac{1 - B\alpha_2}{1 - \frac{B\alpha_2}{\alpha_4}} \tag{3.20}$$

3.2.2 Turbine model

Following Vennell (2010) we represent tidal turbines using the actuator disc theory based on Garrett and Cummins (2007). Actuator disc theory provides a simple and convenient approximation to the behaviour of a real tidal stream turbine although greatly simplifying real turbine characteristics. Actuator disc theory assumes the turbine can be modelled as a simple area resisting the flow in a uniform current. The model in Garrett and Cummins (2007) captures the dominant behaviour in flows of finite Froude number and shear flow (Draper et al. 2016). Real turbines will have rather different performance characteristics which will be important in determining the power and thrust capping strategies of real deployments. Such characteristics are turbine dependent and will be neglected here.

The actuator disc model has two parameters: the wake velocity coefficient, alpha4, and the channel blockage, B. Although peak power coefficient occurs at $\alpha_4 = 1/3$, in a tidal channel there is a trade off between peak power and the drag imposed on the flow in the channel. For example, at $\alpha_4 = 1/3$ the C_p is maximised but flowrate is low, while at a higher α_4, C_p will be lower but flowrate is high. This requires the flow to be "tuned" (Vennell 2010).

3.2.3 Algorithm

The model includes two set of parameters that are determined by each other: support structure size and drag applied on it are calculated based on each other (i.e. introducing support structure introduce additional drag, which in turn increase requirement

for support structure), and a similar relationship between the support structure drag and flow in the channel. Therefore a iteration algorithm is used to calculate this two sets of parameters.

The algorithm can be summarised as below:

1. Initial conditions from a linear approximated solution.
2. Run a dimensional model, which solves Equation 3.11, without considering any capping and support structure for reference data of flowrate, power and thrust.
3. Calculate the threshold values for capping based on the peak power and thrust from reference data.
4. 1st Iteration (as described in Figure 3.2) process based on the reference data for an initial guess of support structure diameter.
5. Input the diameter and other variables into the main part of model.
6. Run for a selected length of time until the steady state.
7. PC state: set α_4 according to Equation (3.15), (3.17) and (3.18) to reduce power generated to the capping value once it exceeds that value.
8. TC state: same as power capping but the limiting value is turbine thrust.
9. Extract the flowrate, power and thrust from step 4 to 7, calculate a new support structure diameter.

10. If the diameter converged, output all the results. If not, feed the new diameter back to step 4 and iterate again. This is defined as the 2nd Iteration, as shown in Figure 3.3.

The model will run for a few days longer than desired to allow for a spin-up before the results reach a steady state.

Detailed algorithm can be presented more clearly by flowcharts (Figure (3.2) to (4.3))

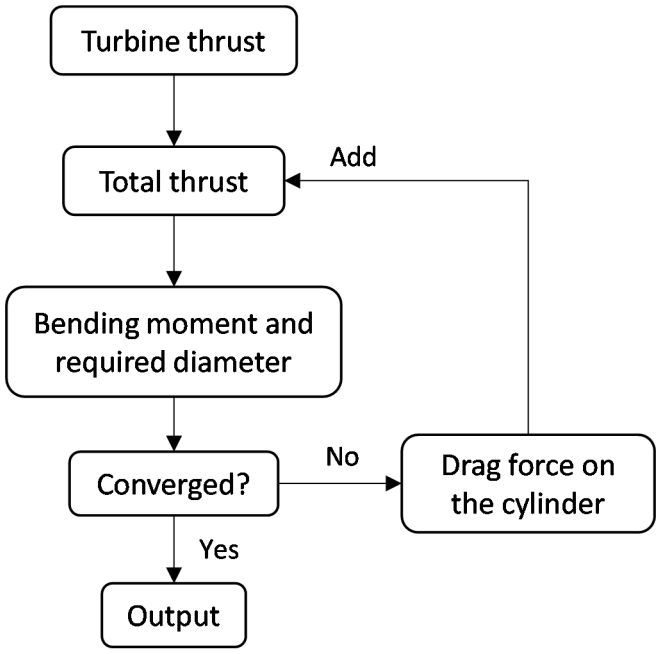

Figure 3.2: Flowchart of the 1st Iteration process for supporting structure diameter

Figure (3.2) shows the 1st Iteration process. This process includes the calculation of turbine thrust (Equation 3.16), support structure drag (Equation 3.8) and support structure diameter (Equation (3.10)). In the first step the support structure size is estimated by the total turbine thrust. Then in every iteration step the drag brought by the support structure will be added on to the total thrust, leading to a small increase

in support structure size. Finally when the increasement of support structure size is sufficiently low (i.e. lower than 0.001m) the iteration process is considered to be converged.

The 1st Iteration does not account for the changes due to the support structure on the tidal stream, for which another iterative process, including all the above calculations and the calculation of flowrate, power and thrust is needed to finally determine the diameter of support structure. This is the 2nd Iteration process (as shown in Figure (3.3)).

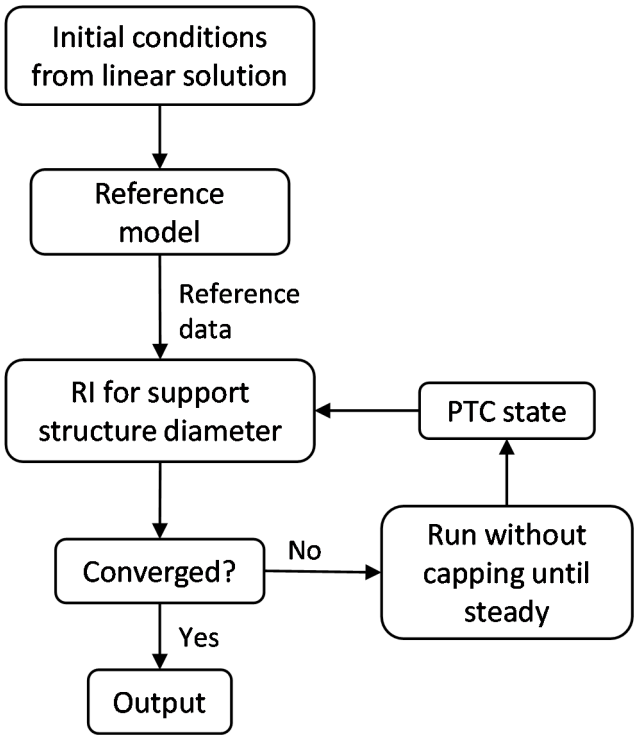

Figure 3.3: Flowchart of the 2nd Iteration process

The 2nd Iteration process includes a PTC state that is a combination of PC and TC. The algorithm for PTC state is as shown in Figure (4.3). A similar iteration to the 1st Iteration process is used here because the introduction of a support structure

will affect the channel flow in the same way it changes the total thrust. Similarly in every iteration step the channel flow is slightly reduced due to the small increasement in support structure drag (as calculated in the 1st Iteration). Finally when the change in flowrate between each iteration step is sufficiently small (i.e. lower than 0.1%) the iteration process is considered to be converged.

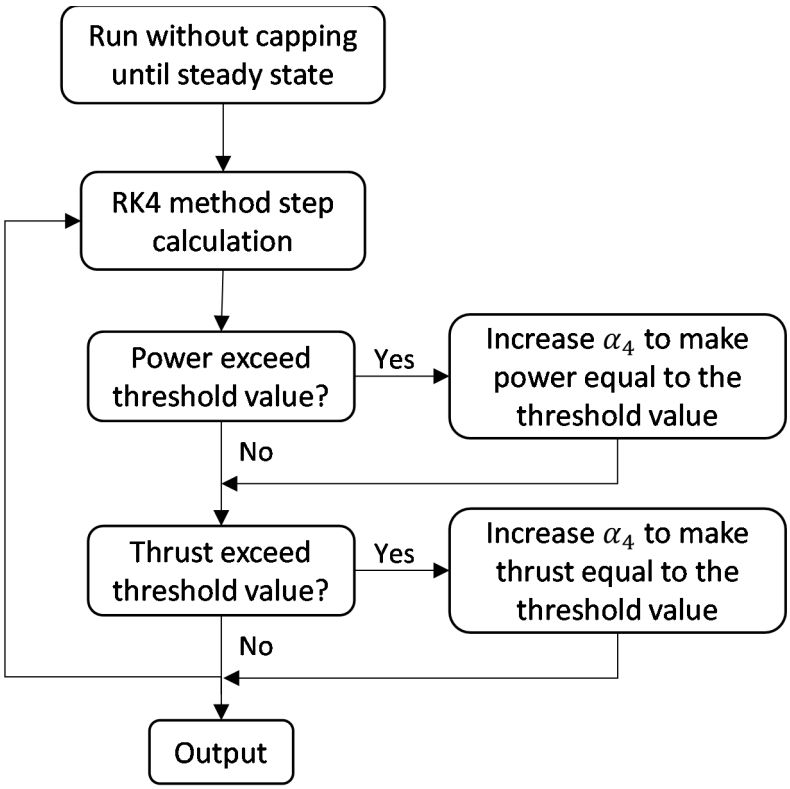

Figure 3.4: Flowchart of the PTC state algorithm

3.3 Results

3.3.1 Model verification

In order to quantitatively analyse the effectiveness of capping, a dimensional model based on Adcock and Draper (2014) has been built. It has been verified by reproducing

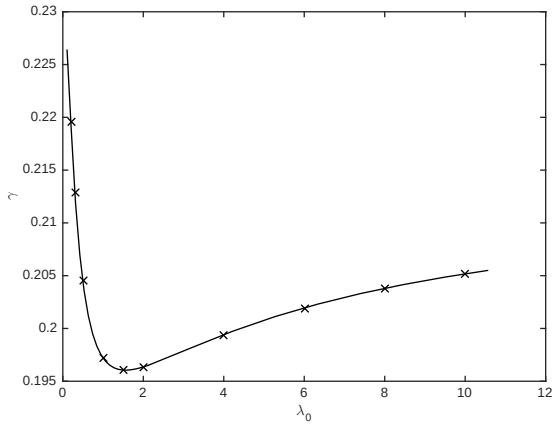

Figure 3.5: Comparison of parameter γ (solid line) with Garrett and Cummins (2005) (x read off from their Fig.4)

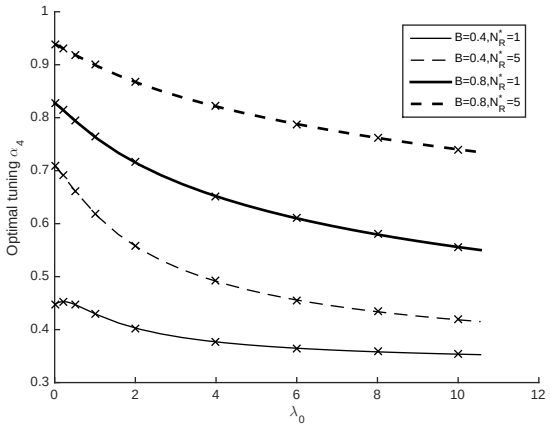

Figure 3.6: Comparison of optimal α_4 (solid and dashed lines) with Vennell (2010) (x read off from Fig.7(a))

the results from literatures (Garrett and Cummins 2005, Vennell 2010). Those data points from literatures are digitised from their figure.

An important work by Garrett and Cummins (2005) is representing the maximum average power as a form of $\gamma\rho gaQ_{max}$, a linear function of maximum neutrally occurring flowrate, where the factor γ is a function of the friction coefficient λ_0. Although the dimensional model uses channel bed drag coefficient C_d instead of λ_0 as the friction term, the corresponding λ_0 can still be calculated by C_d. Figure 3.5 shows the resulting γ and λ_0 curve calculated using the dimensional model. It has a good agreement with the work of Garrett and Cummins (2005).

Vennell (2010) has worked out the optimal tuning α_4 under different conditions. In this chapter the same tuning method has been repeated and the same results as Vennell (2010) has been reproduced as shown in Figure 3.6

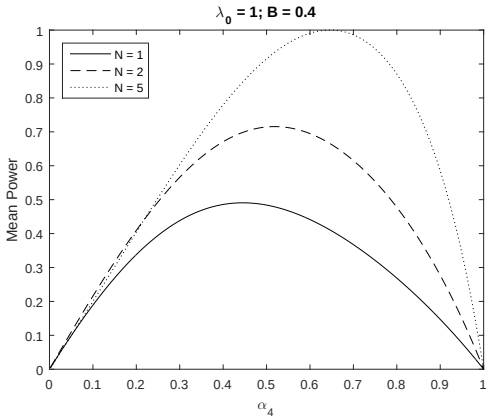

Figure 3.7: Mean power at different α_4 and N

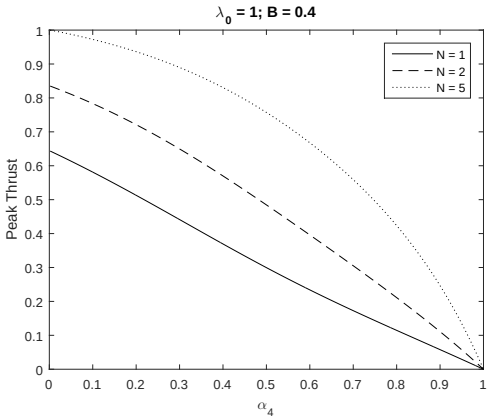

Figure 3.8: Peak thrust at different α_4 and N

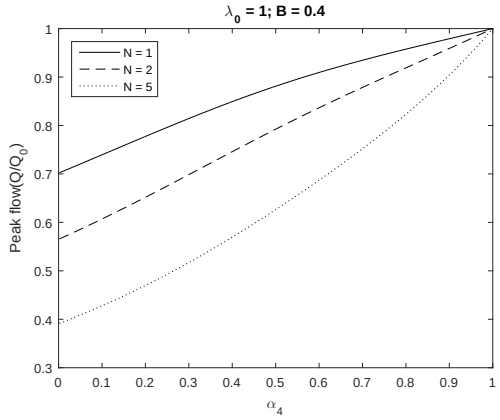

Figure 3.9: Peak flowrate at different α_4 and N

3.3.2 Analysis of variables

The study was started with analysis of the model's input variables to provide an overview of how they can affect model outputs. α_4 and N have been tested for the influences on power output, turbine thrust and tidal stream flow. The results have been normalised by the corresponding maximum value.

Figure 3.7 to 3.9 show that the power generation increases when more rows of turbines are used. However the additional power gained by each additional row diminishes. As a result of this, power generated per unit area of turbine decreases.

The power generation first increases along with α_4 increasing and then decreases as shown in Figure 3.7. In Figure 3.7 optimised α_4 , which maximise power generation, are all higher than 1/3, which Garrett and Cummins (2007) found maximised power output. This is because the 1/3 limit was based on the assumption that the flow is unaffected by power extraction by the turbines, which is not practical. Vennell (2010, 2011) showed that the optimal α_4 is not fixed, but always between 1/3 and 1, the exact value is site specific. With higher N the optimised α_4 increases, because large number of rows may block the tidal stream, and higher α_4 releases the blockage to the flow and hence the power generated by each row can be maximised.

Thrust is changing with the time and we are only interested in the peak value since it decides the requirement of supporting structure as well as changes to the flow. According to Figure 3.8 peak thrust drops significantly as α_4 increases. This is because the fact that higher α_4 introduces less resistance to the flow. This feature suggests that in TC we can cap the peak thrust by increasing α_4. Although in PC either increasing or decreasing α_4 can reduce the power production, decreasing α_4 may unnecessarily increase the turbine thrust. Therefore during PC α_4 is increased to reduce power generation in this model.

Figure 3.9 explains how α_4 will change the tidal stream flow. As stated before α_4 determines the ratio of downstream flowrate to the undisturbed flowrate. Lower α_4 will result in reduced flow, especially when N are large because more rows applies even higher thrust.

3.3.3 Temporal variations due to capping

Single tidal constituent We start by considering the influence of power capping on a single tidal constituent — nominally the M2 tide which dominates at most candidate sites for energy extraction. PC is a method that reduces power generation when it reaches the peak tides to avoid exceeding the capacity of power generator. TC is similar to PC while it limits turbine thrust, hence it can reduce the force on the foundations. To our knowledge, TC has not been explicitly considered in the literature. This work evaluates TC alone as well as combining it to power capping (PTC) to further evaluate their effectiveness.

We start by examining a few particular examples before we explore the parameter space. Figure 3.10 to 3.12 presents the variations in power, thrust and flow rate for models for a reference case with no capping, power capping only, thrust capping only, and combined power and thrust capping.

In the example shown in Figure 3.10 the power is capped at 80% of the uncapped value. The power production is extended slightly in time therefore power produced has only reduced slightly. In fact, in some cases, overall power production can increase compared to the reference case. These results are consistent with Vennell and Adcock (2014) who found that additional power was available by temporally varying the thrust of the tidal turbines over the tidal cycle. Thrust capping also reduces the peak power in this case. Figure 3.11 shows how the thrust on the support varies over time. Simply using a power capping strategy does reduce the peak thrust, but the peak is still considerably higher than when power and thrust capping are used (with, as

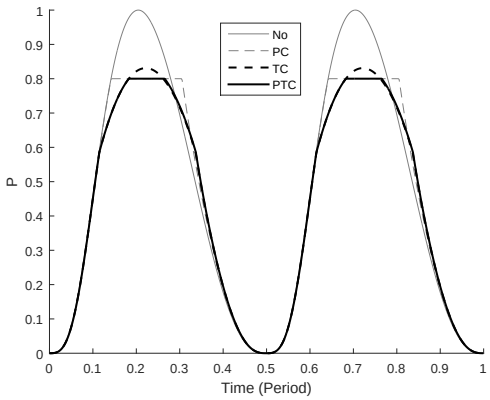

Figure 3.10: Normalised power with different capping strategies

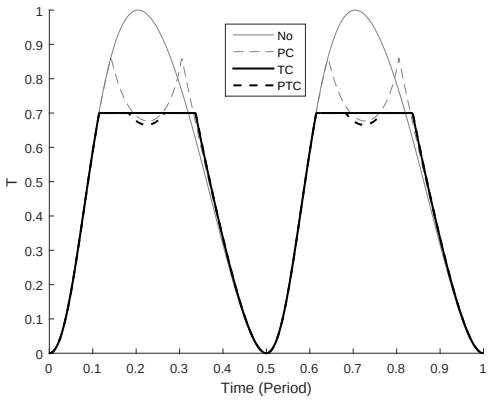

Figure 3.11: Normalised thrust with different capping strategies

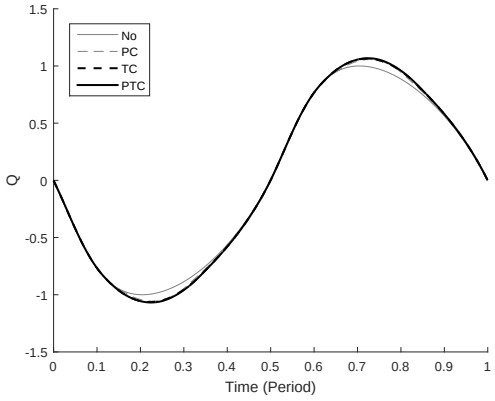

Figure 3.12: Normalised flowrate with different capping strategies
Normalised rated power $P^*_{cap} = 0.8$; Normalised rated thrust $T^*_{cap} = 0.7$, $N = 5$, $B = 0.4$; α_4 started with optimal value of 0.624.

already noted, minimal reduction in available power).

Figure 3.12 shows the flow in the channel over time. It can be seen that adopting capping strategy introduces a less reduction in flow rate through the channel than using constant turbine characteristics. This suggests that the changes in flow rate described in, for instance, Adcock et al. (2013) is overly pessimistic.

Spring/neap tidal channels Most candidate sites for tidal energy extraction exhibit a strong spring-neap tidal cycle as the two dominant semi-diurnal constituents

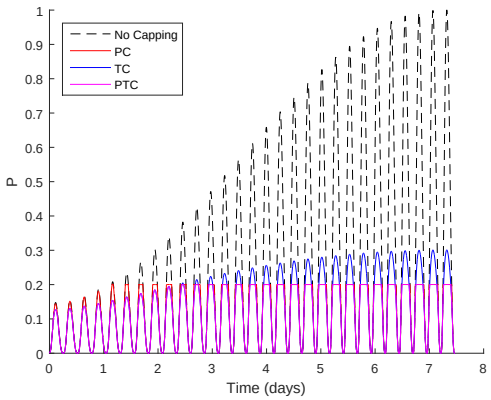

Figure 3.13: Normalised power with different capping strategies

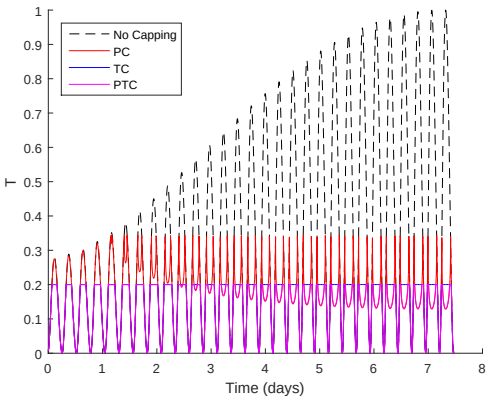

Figure 3.14: Normalised thrust with different capping strategies

move in an out of phase. Without some form of capping, tidal turbine farms will have an unreasonably low capacity factor where we define capacity factor (F_C) as the ratio of the mean power output to the peak power. F_C is an important parameter which indicates how long in a tidal cycle the generator is working at its designed power. A low F_C would be an indicator of device oversizing so that most of the time it is running at a rate much lower than its designed value. However a high F_C is not always a good thing because a generator running at full power most of the time can mean that the designed power is too low to catch most of the power. In order to reach a sensible F_C, the designed rated power must be much lower than the peak power which could be achieved at spring tide. Here we set Figure 3.13 shows an example with $P^*_{cap} = 0.2$ and $T^*_{cap} = 0.2$.

Vogel (2014) has introduced power factor F_P as the ratio of capped power production to the power extracted by non-capping tidal farm. Visually the power and thrust profiles are symmetric, therefore Figure (3.13) and (3.14) show only the power and thrust profile over half of a spring-neap cycle. However the F_C and F_P are calculated

over a complete cycle for accuracy. In this example PC increased the F_C from 0.24 to 0.59, with a F_P of 0.48. Similar to the case of an M_2 dominant channel, TC failed to cap the power as effective as PC – it resulted in a lower F_C of 0.41 with a similar F_P of 0.50. However taking TC as an improvement over the traditional PC effectively reduced the thrust loading, as shown in Figure (3.14), with only minor reduction in power during neap tide (F_C dropped to 0.56 and F_P to 0.45).

3.3.4 Exploration of different power and thrust capping approaches

Power production As the results above indicate, we consider operating both power and thrust capping is likely to be beneficial as it can increase the capacity factor to a sensible value (from 0.24 to 0.59) and reduce maximum thrust significantly. To some extent, the thrust capping can be considered as an add-on to power capping. As such, in the subsequent results we define the thrust factor (F_T) as the ratio of rated thrust to the maximum power capped thrust (rather than the maximum uncapped thrust). This will highlight if thrust capping is useful in addition to power capping.

Figure 3.15 and 3.16 show how the F_P and F_C would change when different PTC settings are used. The α_4 required when power or thrust is being capped is done by a linear approximated root finding method, which accelerates the computing and has a very low relative error, rather than normal root finding algorithm.

Here we point out an "optimal capping zone" on Figure 3.15 and 3.16 with a red circle. Within such optimal capping zone F_P would be sensitive to both F_T and P^*_{cap},

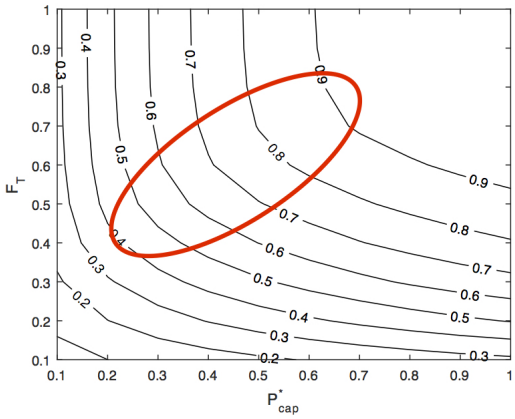

Figure 3.15: F_P with different F_T and P^*_{cap} combination

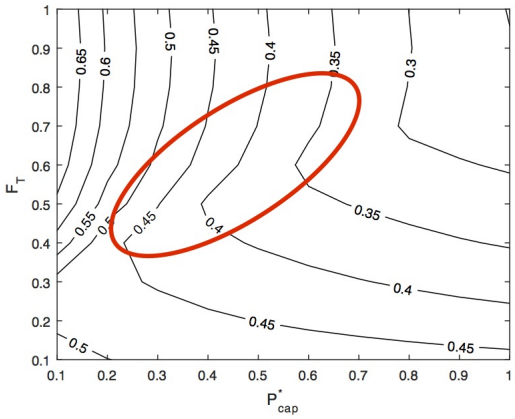

Figure 3.16: F_C with different F_T and P^*_{cap} combination

meaning that any further capping in power or thrust will lead to a sharp drop in F_P. Any point outside of optimal capping zone can be shifted in either direction (i.e. apply more PC or TC) without a sharp drop in F_P. In another word, given any fixed F_P, the setting in such zone can maximise both power and thrust capping. Therefore this optimal capping zone are considered as the potential optimal setting for power and thrust capping. This thesis has attempted Pentland Firth as one example site in the later chapter. However the choice of F_P may differ from site to site and would require a detailed economic analysis which is beyond the scope of this thesis.

Figure 3.15 shows that an optimal capping zone exist in the middle of the plot. The F_P drops almost linearly with rated power $<$0.4. Practical design of tidal farms will face the trade-off between F_C and F_P. Figure 3.16 shows that in order to get an $F_C > 0.4$, rated power would need to be less than 0.5. However the actuator disc model used can overestimate the power production so rated power less than 0.4 would be a viable option. A rated power between 0.2 to 0.4 would likely to be an optimal range to operate. Within this range F_T can be down to 0.5˜0.6, meaning a 40% to

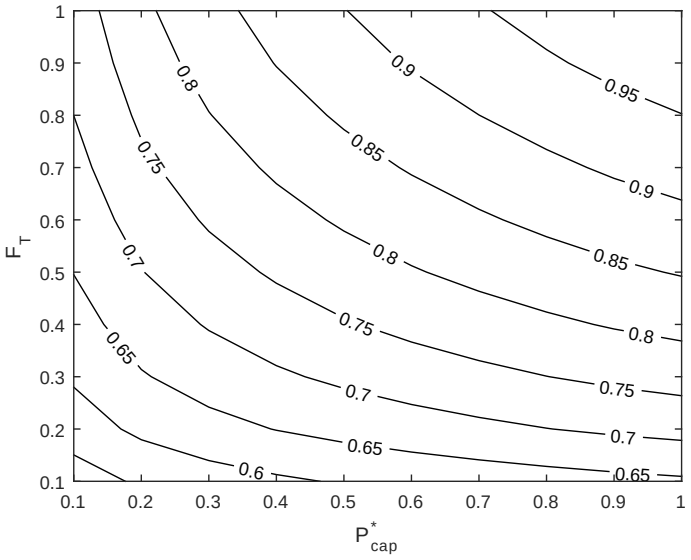

Figure 3.17: Normalised diameter with different F_T and P^*_{cap} combination

50% reduction in thrust loading. Further TC would result in significant drop in F_C as well as F_P.

Support structure size As discussed above, TC will reduce the peak load and therefore the size of the required support structure. This, in turn has the benefit of reducing the "parasitic" drag from support structure in the channel although the main benefit will probably be in reduced structure and foundation costs.

Figure 3.17 gives an ideal of how the diameter of supporting structures, which are assumed to be hollow cylinders, would change at different capping settings.

Figure 3.17 along with Figure 3.16 and 3.15 shown that doing PC or TC alone is not an optimal option. Because for any given PC ratio, rather than not capping thrust at all, introducing further TC would always reduce the supporting unit size while not changing the power output much. The optimal capping ratio observed from Figure 3.16 and 3.15

Table 3.1: Parameters used in this model

Channels	1	2	3
Channel length (km)	100	20	5
Channel width (km)	25	9	1
Channel depth (m)	150	50	20
H_{M2}(m)	1.6	1.0	0.26
H_{S2}(m)	0.67	0.42	0.11
Channel C_d	0.004	0.004	0.0043
λ_0	0.1	1.0	2.8

3.3.5 Example channels modelled results

Three idealised channels having the same dimensions as the example channels given by Vennell and Adcock (2014) were used to examine the effectiveness of PTC. The channel dimensions and other parameters used in this model are listed in Table 3.1,

Figure 3.16 and 3.15 show that a rated power between 0.2 to 0.4 would likely to be an optimal range, thus we select $P^*_{cap} = 0.3$ as the power capping setting for the three example channels, with varying F_T to evaluate the effectiveness of PTC. Figure 3.18 to 3.22 present the change of F_P, F_C, support diameter, normalised change of flow (ΔQ_{max}) during spring and neap tide according to F_T. We have considered each of the three channels under two different conditions, a lower blockage case where $N = 1$ and $B = 0.1$ and a higher blockage case where $N = 3$ and $B = 0.4$.

Figure 3.18 along with Figure 3.19 show that the optimal F_T when $P^*_{cap} = 0.3$ is around 0.5 to 0.6 before F_P or F_C start to drop significantly. Both F_P and F_C drop with F_T very slowly until F_T reaches its optimal value. However in Figure 3.19 F_C start to increase if F_T drops lower than 0.4, this is because a very low F_T can literally change the channel into a TC dominant so that the capping start to limit the peak power and hence changes F_C, rather than a PTC channel where it is PC that

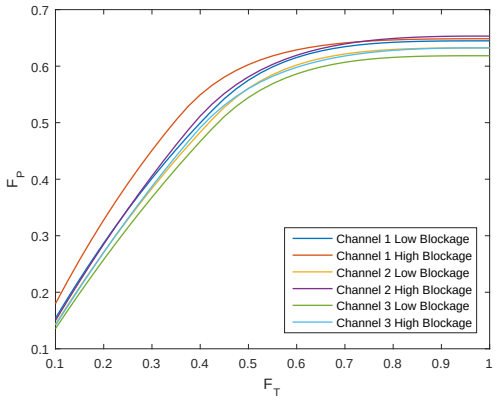

Figure 3.18: F_P change against F_T

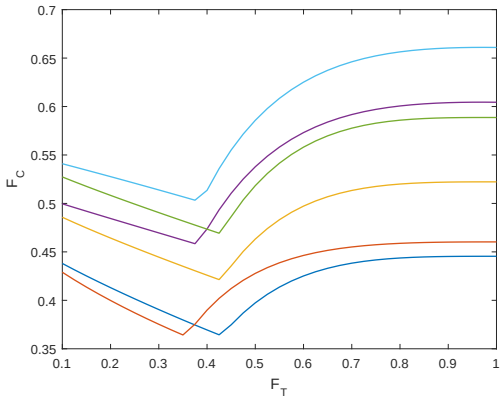

Figure 3.19: F_C change against F_T

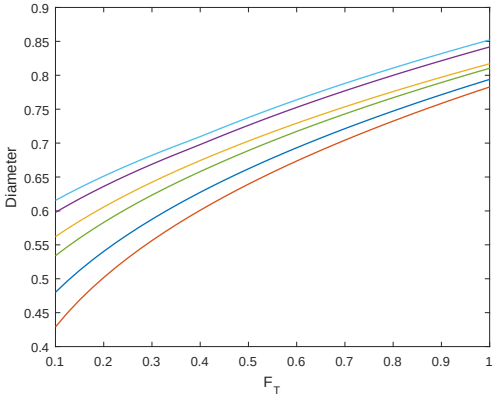

Figure 3.20: Support diameter change against F_T

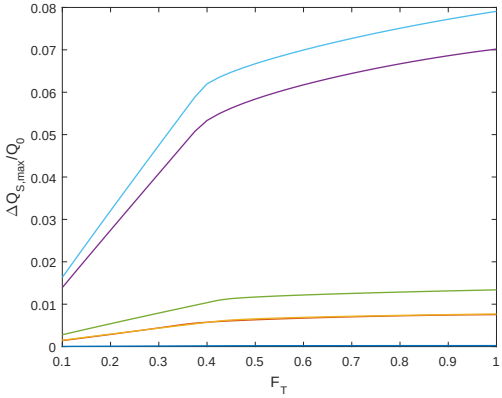

Figure 3.21: ΔQ_{max}at spring tide change against F_T

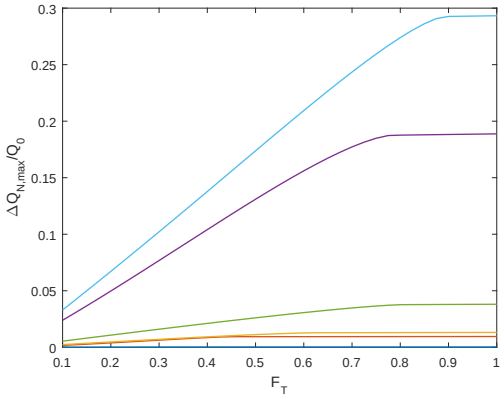

Figure 3.22: ΔQ_{max}at neap tide change against F_T

limits the peak power. Figure 3.20 shows that in all of the cases, the size of support structure decreases almost linearly as F_T drops. Figure 3.21 and 3.22 show how much less change to the flow we can reach by PTC. The figures show a good reduction in ΔQ_{max} for the higher blockage cases for channel 2 and 3, but not very viable change for the rest cases as PC at $P^*_{cap} = 0.3$ has already reduced ΔQ_{max} (as listed in Table 3.2).

Table 3.2: Modelled results

Case		F_C	F_P	$\bar{P}$/GW	T_m/GN	D/m	ΔQ_{max}
1	No	0.21	1	2.52	15.50	4.11	3.8%
	PC	0.46	0.65	1.63	6.95	3.22	0.76%
	PTC	0.45	0.63	1.59	4.17	2.78	0.68%
2	No	0.28	1	1.48	2.93	1.64	27.1%
	PC	0.60	0.65	0.97	1.31	1.39	7.03%
	PTC	0.58	0.62	0.92	0.79	1.24	6.20%
3	No	0.32	1	14.98	0.038	0.43	33.0%
	PC	0.66	0.63	9.47	0.017	0.37	7.92%
	PTC	0.63	0.60	8.96	0.010	0.33	7.02%

Table 3.2 concludes the F_C and F_P, mean power $\bar{P}$, support structure diameter effectively, maximum turbine thrust T_m and change of peak flowrate ΔQ_{max}, of doing PC, PTC, and No Capping for three different channels, with the optimal setting of $P^*_{cap} = 0.3$, $F_T = 0.6$ and higher blockage case. Both capping strategies have significantly increased F_C and lowered turbine thrust, while giving up 1/3 of the total power ($F_P =\sim 0.65$). And PTC, based on PC, has further reduced peak thrust with only minor reduction in F_C and F_P. This table only listed ΔQ_{max} during spring tide, this is because the capping mainly affects the flow profile at higher flowrate –

as shown in Figure 3.13 and 3.14 the flow during neap tide does not affect by the capping very much. It can be seen that for all three channels PC and PTC effectively reduced ΔQ_{max} by a factor of 4 or 5, although the differences between PC and PTC are not significant.

With that being said, PTC works well in terms of generator size saving, F_C optimising and force reduction. Although the difference between it and PC are small in power, the reduction in turbine thrust is significant. Considering that the turbine thrust can greatly affect the life time of turbines and support structures due to less fatigue, PTC is a viable method to use. In order to better quantify the benefits of PTC, further analysis of the impacts of fatigue on the devices and perhaps the environmental impacts caused by tidal energy extractions is needed.

3.4 Discussion

This chapter has analysed power capping and thrust capping strategies in the design of tidal stream turbine farms. We have shown that by adopting a strategy that prevents power or thrust exceeding a given value can be of significant benefit in several ways:

- Improved capacity factor. This can, simplistically, be considered as a proxy for the cost of electrical infrastructure. It will never be economic to size electrical infrastructure based on the peak currents at spring tide.

- Reduced environmental impact. Although this is complex, we have shown that adopting capping strategies mitigates the change to the naturally occurring

currents. This mitigates the changes in flushing, sediment transport and ecosystems.

- Reduced support structure. Limiting the thrust reduces the size of the support structure that needs to be used, reducing costs and the parasitic drag of support structure on the flow.

Thus we demonstrate that a combined power and thrust capping strategy should be applied in developing tidal stream turbine farms. The design of real farms will, of course, be far more complex than presented in this chapter. Even within the simplifications made by us in this work, it is not obvious where the best trade off is between different power capping strategies and total power production. Making this trade off will be a balance between financial considerations and environmental impact. The object of this work is to demonstrate the importance of both thrust and power capping in the development of a strategy for designing and operating tidal stream turbines.

Chapter 4

Combined Power and Thrust Capping at Pentland Firth by a 2D Model

4.1 Introduction

In the previous chapter, a capping algorithm has been developed in a 0D idealised channel model. In this chapter, a 2D power and thrust capping model, which is to be implemented at a real site (Pentland Firth), will be introduced. This 2D model is built based on the modification by Serhadlıoğlu (2014) of the DG-ADCIRC model.

The Pentland Firth is a well known candidate site for tidal energy extraction because of its remarkably fast tidal currents, and hence become one of the most focal point for tidal energy researchers (Adcock et al. 2013, Baston and Harris 2011, Easton et al. 2012, Martin-Short et al. 2015, Murray and Gallego 2017, Salter and Taylor 2007). The Pentland Firth is the channel which separates the Orkney Isles from Caithness in the north of mainland Scotland. It connects the Atlantic Ocean

to the North Sea and concentrates great amount of tidal energy from the current flow through. Recent research on the Pentland Firth suggest that theoretically an average power of up to approximately 4 GW could be extracted from this site (Draper et al. 2014). The Pentland Firth has two islands Swona and Stroma, by which it has been divided into three sub-channels where the simulated tidal turbine arrays will be placed at. For convenience, the sub-channels between Burwick and Swona, Swona and Stroma, Stroma and North Scotland are named as the Top Channel, Middle Channel and Bottom Channel respectively (As shown in Figure (4.1)).

Figure 4.1: Map showing the locations of the 3 sub-channels (from Google Map)

In this chapter we seek to examine the results from previous chapter of power and thrust capping in a more realistic model. The same principle of capping, which sacrifice part of the power production when the load is high, remains the same. The trade-offs between the peak thrust, the generated power, and the total power available

in the undisturbed tidal resource are still the focus of this study.

4.2 Model

In this chapter we use a 2D Shallow Water Equations (SWEs) model to simulate the tidal stream through three sub-channels at the Pentland Firth. A similar work (Adcock et al. 2013) has been done before simulating the tidal stream. However, that work has a rather poor mesh resolution so that the outline of the two islands were not accurately represented. Although this will not cause any major error in the qualitative analysis of the stream flow, it does affect the overall power extraction because of the narrowed channel width due to the enlarged island size. The mesh was built based on the well-known tidal energy candidate site Pentland Firth. The bathymetry data were obtained from Seazone. The offshore boundary conditions are taken from the model of Le Provost et al. (1998). The mesh used in this chapter has a minimum mesh size of around 100 metres which is able to closely match the outline of land and island edges. Higher resolution than this would lead to a mesh smaller than the water depth (where the water depth is around 80m) – spatial structure finer than the water depth generally is not well modelled in a depth-averaged simulation.

A similar capping algorithm to the 0D capping model has been used, with indeed some further consideration of the complex geometry and uneven distribution of flow and turbines in a 2D model. In the 0D model, only the overall total power or thrust is being capped because the model assumed uniform distribution of flow across the cross-section of channel. However, due to its advantages in computational time, the

0D model is capable of evaluating the impact of support structure as well as exploring a much wider range of different capping strategy. In the 2D model, the iteration for support structure is too expensive in terms of computational resources (each iteration would take 1-2 days and normally more than 100 iterations are required). Also due to the limitation in time and computational power only a very limited range of PTC strategies can be evaluated. In addition, the capping on the overall power or thrust is unrealistic because both flow and turbines are unevenly distributed, thus a more complex method which is able to control the capping at a single turbine scale is required. In this model the blockage ratio across the cross-section of a channel is fixed rather than turbine sizes (i.e. using smaller turbine in shallower water). Therefore the power or thrust per unit swept area of turbine are used as the indicator for capping. The model is able to control the capping on an element basis, which is the smallest possible scale for a finite element method model. This capping method will also resulted in a very different power and thrust profile to the ones generated by the 0D model because of the uneven distribution of flow, i.e. those parts having stronger flow tends to be capped earlier and more often and those having weaker flow may never been capped. Thus the comparison of the 2D model and the previous 0D model may not be representative because technically these two model are not equivalent in terms of the capping method. Nevertheless a comparison between the 0D and 2D models is made in Chapter 5.

In this model we assume there is no turbine placed in anywhere has a water depth less than 20 metres. This is due to the limitation in realistic implementation as well as the stability of model. The part that will be affected the most will be the bottom

sub-channel where nearly half of the channel has a water depth less than 20 metres according to our bathymetry database.

4.2.1 Turbine model

The model used in this chapter was built based on the DG-ADCIRC model and Serhadlıoğlu's (2014) modification. The DG-ADCIRC model approximates the flow using polynomial functions that can be modified to incorporate discontinuities between adjacent elements (Figure 4.2). The original DG solver Kubatko et al. (2006) is designed for modelling storm surge and tidal flows. The code was modified by Serhadlıoğlu (2014) to include tidal turbine by combining open channel actuator disc model into it. Such modification is done by calculating the power available to turbine on a edge and modifying the numerical flux accordingly.

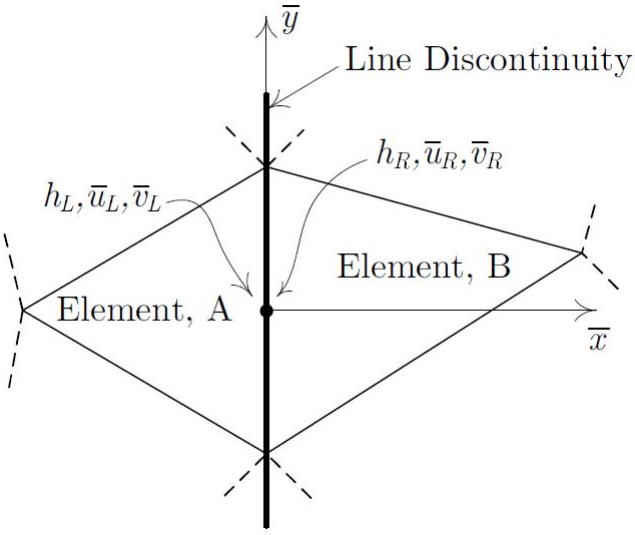

Figure 4.2: ocation of ux calculation for two elements either side of a line sink of momentum (Figure taken from Draper 2011)

There are generally two approaches to modelling tidal turbines in depth-averaged

flows. The first one is representing the additional thrust by placing turbines as additional bed friction coefficient in the governing equations (Blunden and Bahaj 2007, Karsten et al. 2008). Including an additional bed friction is mathematically straight forward and is easy to apply in the model. The second method represent turbine arrays by a line sink of momentum (Draper 2011) in the two-dimensional shallow water solver. This is able to distinguish the available power generated and the total extracted power from the tidal stream. This method assumes that tidal turbines are evenly distributed, the length of wake mixing zone is sufficiently small compared to the mesh size (Serhadlıoğlu 2014), and the change of flow through the domain is sufficiently slow so that it may be considered quasi-steady (Draper et al. 2010).

Serhadlıoğlu's (2014) model uses an open channel LMADT model (Draper 2011, Houlsby et al. 2008) to calculate the power extraction and momentum change across turbine arrays. Conventional LMADT theory is based on the assumption that the flow is incompressible (Bryden et al. 2007) and unconstrained which is not realistic for applications to tidal channels where the flow is constrained by the seabed and free surface. The open channel LMADT model (Houlsby et al. 2008) has extended conventional LMADT to account for the boundary constrain and changes in water depth when it pass through a turbine. In the model the flow experiences a discontinuous change in velocity and depth when passing through a turbine edge as power is removed by the turbine. This essentially assume that the local wake mixing is relatively short and can be modelled analytically as a discontinuous in the flow.

4.2.2 Capping algorithm

A more detailed explanation of the turbine model is given by Serhadlıoğlu (2014) and Draper (2011). The basic algorithm of the power and thrust capping, on an element edge basis, can be summarised roughly as below,

1. Upstream conditions from DG-ADCIRC SWE solver
2. Calculate blockage and α_4 of the current edge by averaging from the two adjacent nodes
3. Open channel actuator disc model to calculate an initial C_p, C_t and change in water depth $\triangle H$
4. Calculate available power, extracted power and turbine thrust per unit swept area
5. Check if the available power exceed the capping value P_{cap}, if so increase α_4
6. Check if the turbine thrust exceed the capping value T_{cap}, if so increase α_4
7. Check if solution converged, if so restore $\alpha_4$to its default value and continue, if not go back to step 3
8. Multiply power and thrust by the average depth and width of the current element to get local power and thrust
9. Summing up power and thrust of all turbine boundaries and output

7 days of analysis time is required to analyse half of a spring-neap cycle (see Figure 7 of Adcock et al. 2013), assuming that power and thrust etc. profiles are symmetric

in time. However the model will run for a few days longer than desired to allow for a spin-up before the model reach a steady state.

The capping algorithm can be presented more clearly by using a flowchart (Figure (4.3))

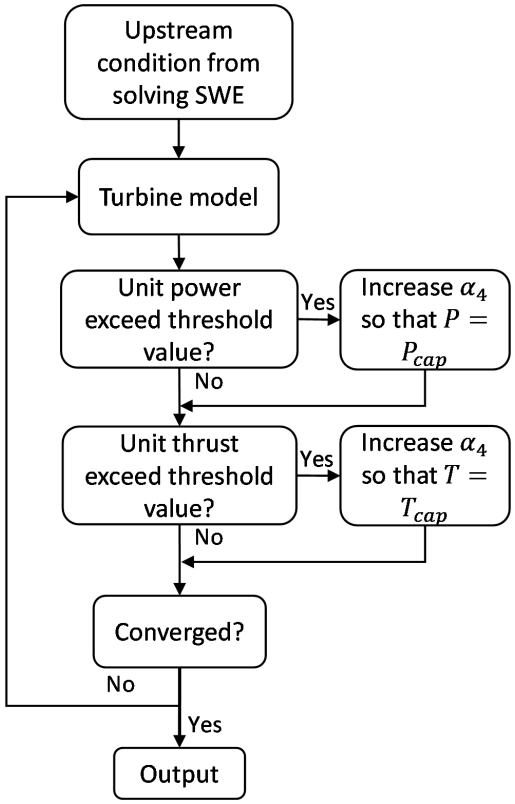

Figure 4.3: Flowchart of the PTC state algorithm

4.3 Results

4.3.1 Model validation

Before we start any further evaluation of capping, the model was first validated with field observation data. To facilitate this validation, the model was run for 3 days for

spin up prior to recording any results. Further time allowed for spinning up led to negligible changes in the results.

In order to validate the numerical model used in this work, a group of results obtained from the model, with different seabed drag coefficient (C_d, where drag is given by $F = \frac{1}{2}C_d\rho A_b u|u|$), were compared with field measurement obtained from seabed acoustic Doppler current profiler (ADCP) gauges deployed at three locations in the Pentland Firth. A more detailed explanation of the methodology and measurement of the field observation are given by Gardline Surveys (2001).

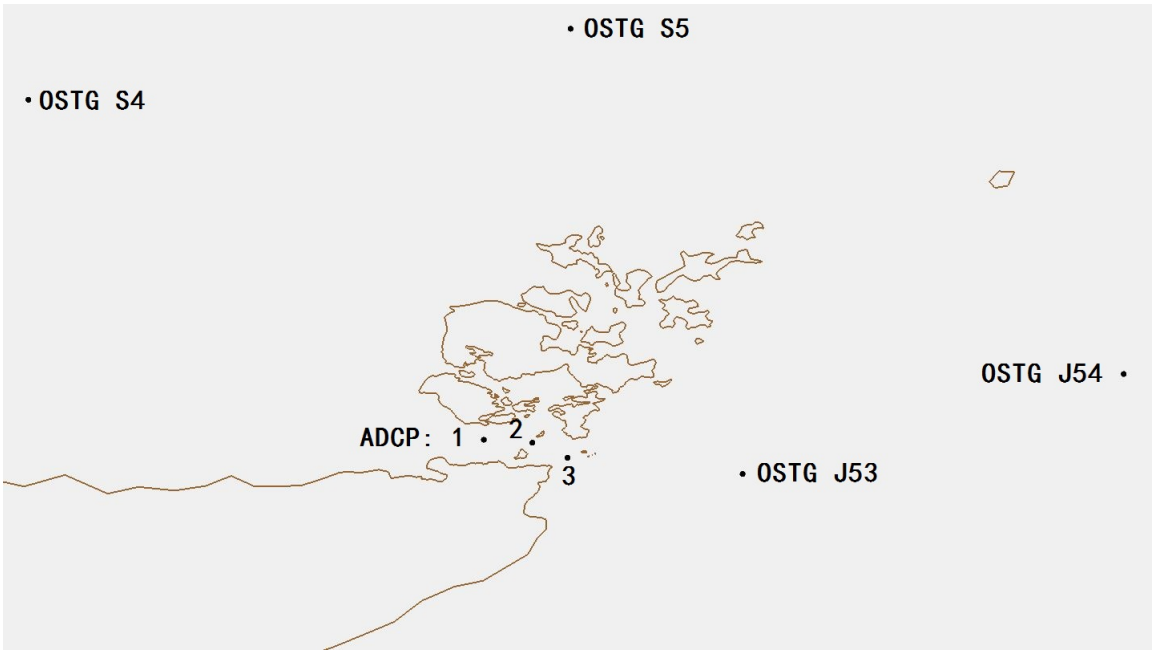

Figure 4.4: Map showing the locations of observation points

The locations of all observation points are shown in Figure (4.4), and their corresponding latitudes and longitudes are given in Table (4.1)

Current magnitude and phase obtained from harmonic analysis were used for comparison to field data. The observation were taken at three different depths: 11m, 43m and 75m. All three observation points have a average water depth of around

Table 4.1: Location of observation gauges

	Lat.	Long.
ADCP 1	58.726 N	3.236 W
ADCP 2	58.717 N	3.086 W
ADCP 3	58.67 N	2.976 W
OSTG S4	59.78 N	4.65 W
OSTG S5	60.00 N	2.967 W
OSTG J53	58.62 N	2.433 W
OSTG J54	58.93 N	1.25 W

80m, therefore the measurement at these three depths are believed to be a good representation of the vertical variation of data. The comparison was mainly focused on the ones at depth of 43m, given that the numerical data were obtained from a depth-averaged method. Tables (4.3.1) and (4.3) show the observed current magnitude and phase lag.

Table 4.2: Observed M_2 current magnitude and phase lag

	Current magnitude (cm/s)			Phase lag (°)		
Depth	$11m$	$43m$	$75m$	$11m$	$43m$	$75m$
ADCP 1	180.00	178.00	131.30	248.60	248.10	247.90
ADCP 2	264.30	249.70	153.60	242.70	242.50	242.40
ADCP 3	184.70	150.40	108.70	248.30	248.20	248.20

Table 4.3: Observed S_2 current magnitude and phase lag

	Current magnitude (cm/s)			Phase lag (°)		
Depth	$11m$	$43m$	$75m$	$11m$	$43m$	$75m$
ADCP 1	63.40	58.80	41.20	268.30	268.40	267.20
ADCP 2	89.50	84.10	51.20	268.60	268.70	268.70
ADCP 3	64.40	51.40	39.80	271.80	271.40	271.90

Tables (4.3.1) to (4.7) summarised the comparison of current magnitudes and phase lags of the East-West component only because that is the dominant flow direction in Pentland Firth. More detailed data for comparison will be given in Appendix I. Mean Square Error (MSE) is used here as an indicator of how well the numer-

ical data matches field data. Generally the results produced by models with higher seabed drag coefficients (C_d =0.004 to 0.0075) have better agreement. $C_d = 0.004$ has a better match in M_2 current magnitude. However, as stated by Adcock et al. (2013) agreement in phase lag would weight more than current magnitude in terms of model validation because it is less sensitive to measurement noise or bathymetric errors . $C_d = 0.0075$ has the best performance in terms of predicting the phase lag of S_2 component but it has much poorer agreement elsewhere. $C_d = 0.005$ has the best overall matching and as a results has been selected as the value of seabed drag coefficient for most of the later analysis.

The free surface elevations produced by the model were analysed using harmonic analysis by ADCIRC. Table 4.8 shows the comparison of M_2 water level amplitudes of the observed data given by Sinha and Pingree (1997) and the modeled results by the model with $C_d = 0.005$ (models with other drag coefficients have nearly identical results here). It shows a generally good agreement between the measured and modelled data. Although some amplitudes (e.g. OSTG J53) do not agree very well, the phases of all four locations show excellent agreement. As stated by Adcock et al. (2013) that agreement in phase is more important in modelling the tides, and that the mesh size around some of these points are quite course, which results in a higher error in the location. The general agreement between model and measurements is satisfactory given the approximations inherent in shallow water modelling.

Table 4.4: Numerical M_2 current magnitude

	Current magnitude (cm/s)				
C_d	$C_d = 0.0025$	$C_d = 0.0038$	$C_d = 0.004$	$C_d = 0.005$	$C_d = 0.0075$
ADCP 1	225.42	203.84	200.58	186.71	161.08
ADCP 2	272.27	245.59	243.33	228.36	199.47
ADCP 3	175.33	146.37	144.20	134.35	117.44
MSE*	1126.52	233.61	196.29	262.95	1298.57

* Mean square error is calculated based on numerical data and the observed data at depth of 43m

Table 4.5: Numerical M_2 phase lag

	Phase lag (°)				
C_d	$C_d = 0.0025$	$C_d = 0.0038$	$C_d = 0.004$	$C_d = 0.005$	$C_d = 0.0075$
ADCP 1	255.16	250.68	250.43	247.78	240.36
ADCP 2	248.99	244.36	244.44	242.89	238.37
ADCP 3	258.91	248.60	247.94	245.89	240.14
MSE	68.89	3.43	3.09	1.86	47.31

Table 4.6: Numerical S_2 current magnitude

	Current magnitude (cm/s)				
C_d	$C_d = 0.0025$	$C_d = 0.0038$	$C_d = 0.004$	$C_d = 0.005$	$C_d = 0.0075$
ADCP 1	89.19	79.29	77.33	70.36	58.67
ADCP 2	104.04	92.39	91.11	85.31	72.45
ADCP 3	60.91	57.73	56.68	51.32	42.61
MSE	470.53	176.21	140.13	45.03	71.00

Table 4.7: Numerical S_2 phase lag

	Phase lag (°)				
C_d	$C_d = 0.0025$	$C_d = 0.0038$	$C_d = 0.004$	$C_d = 0.005$	$C_d = 0.0075$
ADCP 1	279.46	277.12	277.58	276.64	269.81
ADCP 2	277.02	271.87	272.46	271.07	267.45
ADCP 3	287.60	275.15	274.80	273.81	269.27
MSE	151.33	33.38	36.66	26.44	2.70

Table 4.8: Comparison of M_2 water level amplitudes

	Observed		Modelled	
	Amplitude (m)	Phase (°)	Amplitude (m)	Phase (°)
OSTG S4	0.83	228	0.83	229
OSTG S5	0.69	252	0.75	254
OSTG J53	0.75	323	0.92	322
OSTG J54	0.66	323	0.72	321

4.3.2 Capping model verification

The modified model was first verified by considering power and thrust capping in an idealised channel with single tidal constituent — the M_2 tide which dominates at most candidate sites for energy extraction. PC TC and PTC have the same definition as in the previous chapters. The idealised channel used in this case has a dimension of $21km \times 7.7km \times 80m$ (see Figure 4.5), similar to the Pentland Firth channel which will be evaluated as the target site in the later section. The M_2 constituents used at both ends of this idealised channel are chosen from the corresponding location at Pentland Firth. Therefore, unlike the simplified case discussed in the previous chapter, the resulting power and thrust profiles show some asymmetry in direction. The capping strategy used here is capping based on power or thrust per unit swept area instead of capping the total power or trust.

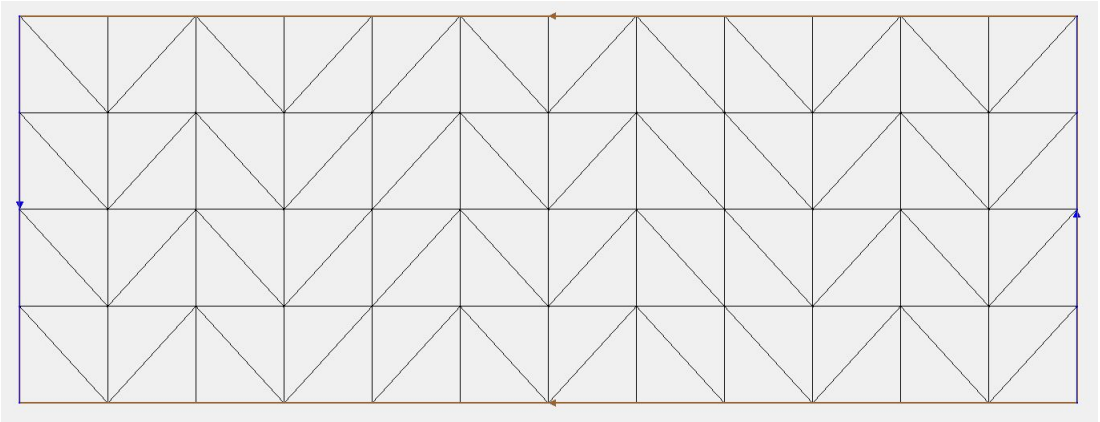

Figure 4.5: Mesh grid used in the idealised model, has a dimension of $21km \times 7.7km$ and depth of $80m$

The study was started by testing a few simplified examples before exploring power and thrust capping at the real site. Figure 4.6 to 4.8 presents the variations in power

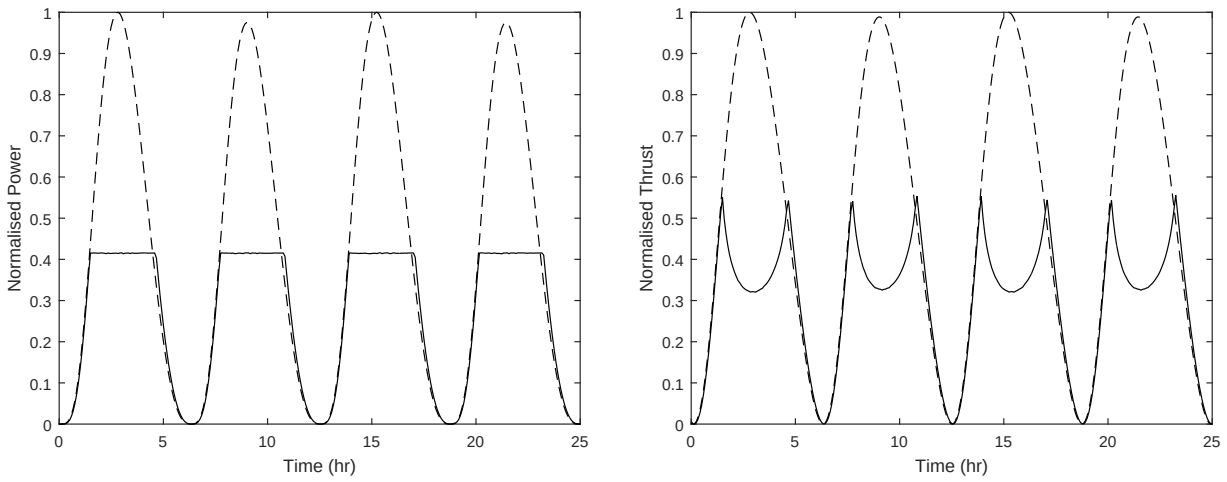

Figure 4.6: Power capped power and thrust profiles.
Rated power $P_{cap} = 2\text{kW/m}^2$; rated thrust $T_{cap} = 1.2\text{kN/m}^2$, $N = 1$, $B = 0.4$; default $\alpha_4 = 0.6$, dashed line for no capping and solid line for capping, similarly hereinafter for Figure (4.7) to (4.8)

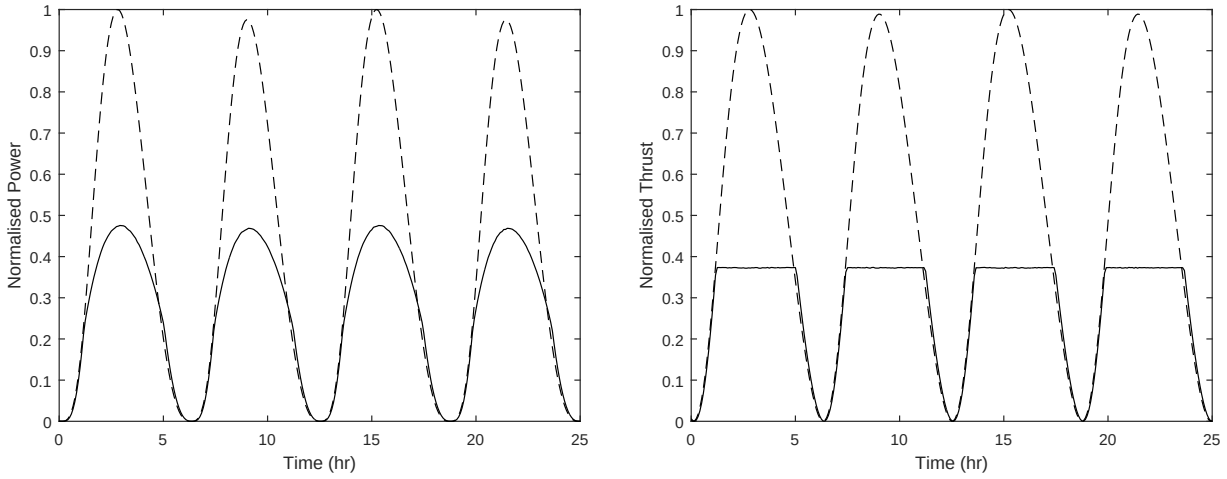

Figure 4.7: Thrust capped power and thrust

and thrust for models for a reference case with no capping, power capping only, thrust capping only, and combined power and thrust capping.

In the example shown in Figure 4.6 the power is capped at 2kW/m^2, around 40% of the uncapped peak value. A very similar reaction in power and thrust profiles to the ones from 0D models can be observed. The total power is capped and giving a

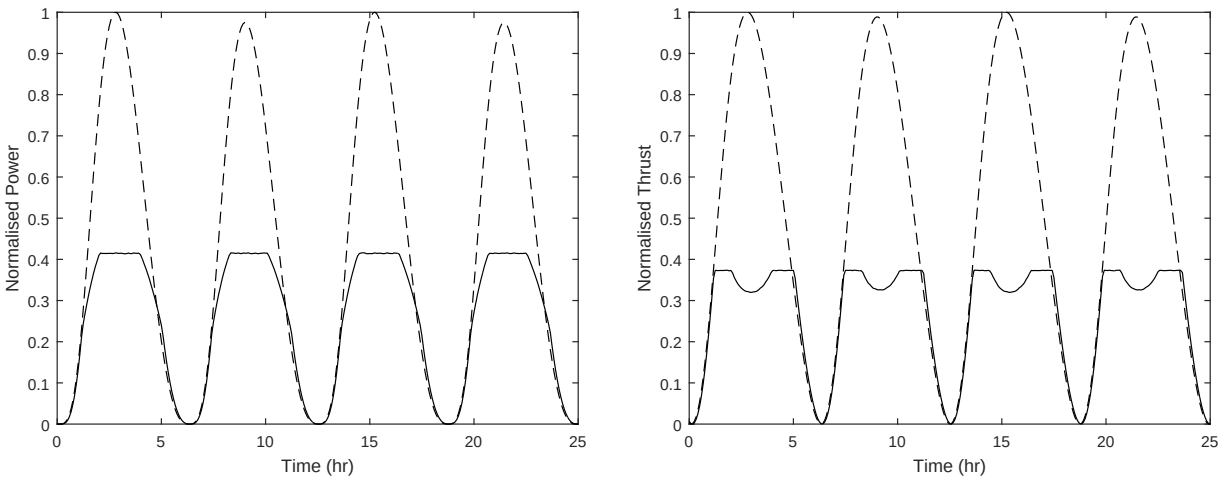

Figure 4.8: Combined power and thrust capped power and thrust

flat peak although all turbines are not necessarily synced in terms of capping. Thrust shows sharp peaks at the start and end of a capping state. In this simplified model flow velocity is nearly evenly distributed across the channel cross section. Once the flow is unevenly distributed (e.g. in a real site) it would be more complicated. Such case will be discussed in the later section.

Thrust capping also reduces the peak power in a similar way to what has been observed in the 0D model. Figure 4.7 shows how the power and thrust varies. Again using power capping alone does reduce the peak thrust, but there is still some sharp peak remains and the maximum is still considerably higher than when power and thrust capping are combined (as shown in Figure 4.8).

In summary, the power and thrust capping strategy that caps power or thrust per unit turbine swept area results in very similar effectiveness, when applied to a simplified channel, to the overall capping strategy used in the 0D model. A more complicated capping would be expected when applying this capping strategy to a real site (e.g. Pentland Firth).

4.3.3 Power and thrust variations due to capping

Most potential tidal energy sites exhibit a strong spring-neap tidal cycle as the M_2 and S_2 tidal constituents move in and out of phase. Therefore only M_2 and S_2 tidal constituents were considered here. Without some form of capping, tidal turbine farms will have an unreasonably low capacity factor (F_C). As stated in the previous chapter one goal of capping is to reach a similar or higher F_C than that of wind turbines. The designed rated power must be much lower than the peak power at spring tide.

A 2D mesh of Pentland Firth has been built for this model (Figure 4.9 and channel part enlarged in Figure 4.10). Those parts involving implementation of turbine arrays have been refined for a better performance of model. The previous chapter of 0D model has already evidenced the benefit of combined power and thrust capping. Therefore the combined capping will be the focus of this analysis. As has been stated before power and thrust are capped based on value per unit swept area, the power capping threshold value P_{cap} will be in kilo-watt per square metre (kW/m^2) and T_{cap} will be in kilo-Newton per square metre (kN/m^2). The examples used here has a $\alpha_4 = 0.5$ and $B = 0.4$ and has 3 rows of turbines in each of the sub-channels. Figure 4.11 and 4.12 shows a few example with $P_{cap} = 2, 4, 6kW/m^2$, $T_{cap} = 1.6, 2, 3kN/m^2$. The power capping values were chosen to be evenly distributed between 0 and the maximum uncapped power (exclusive). Thrust capping values were chosen based on the corresponding power-capped maximum thrust so that they are lower than the maximum PC thrust. Also the thrust capping values can not be too low otherwise it will effectively be only TC rather than a combined PTC. Figure 4.13 shows the

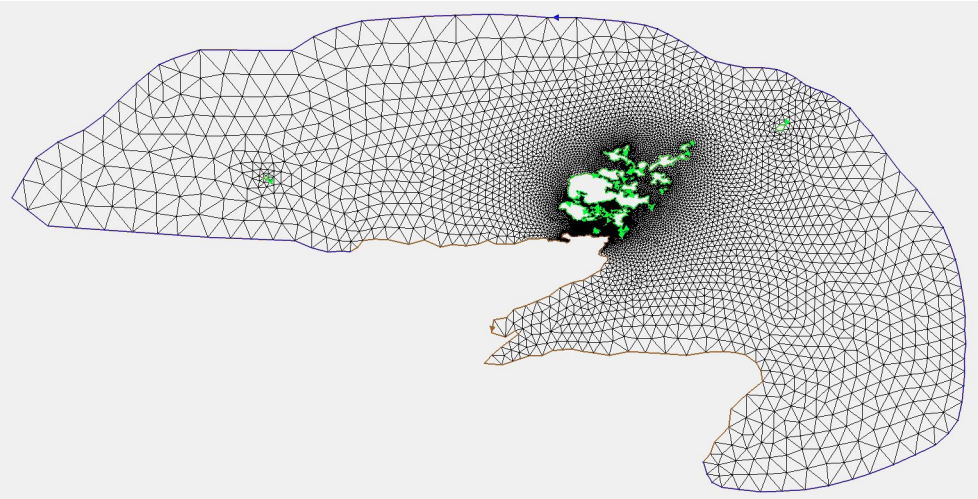

Figure 4.9: Mesh grid used in the Pentland Firth model

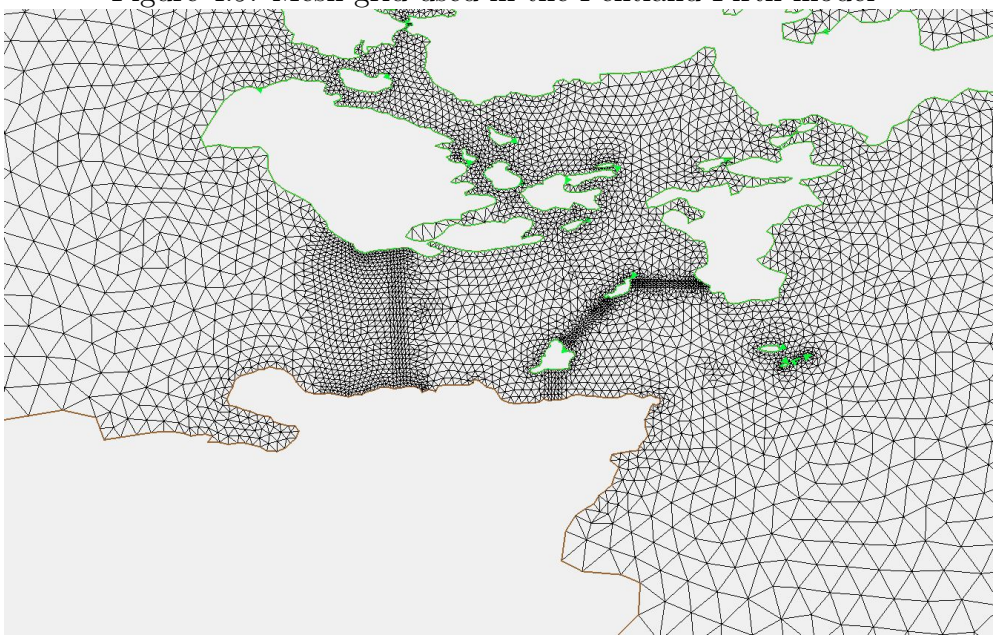

Figure 4.10: Mesh grid used in the Pentland Firth model

combined capping case with $P_{cap} = 2, 4, 6kW/m^2$ and $T_{cap} = 1.6, 2, 3kN/m^2$ correspondingly.

The power factor F_P is defined the same as before by Vogel (2014) as the ratio of capped power production to the power extracted by non-capping tidal farm. Figure (4.11) and (4.12) show only the power and thrust profile over half of a spring-neap

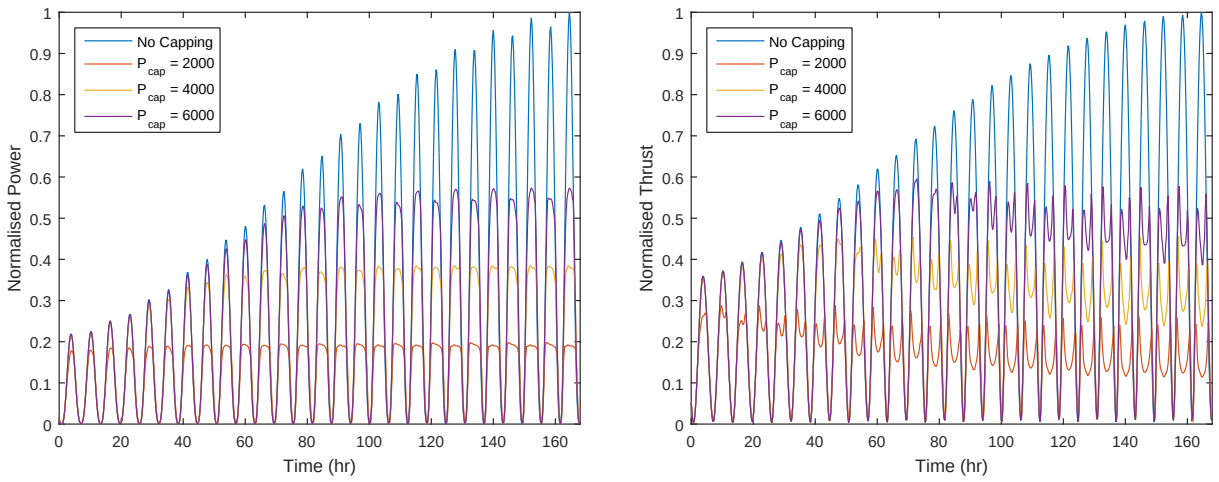

Figure 4.11: Normalised power and thrust with power capping

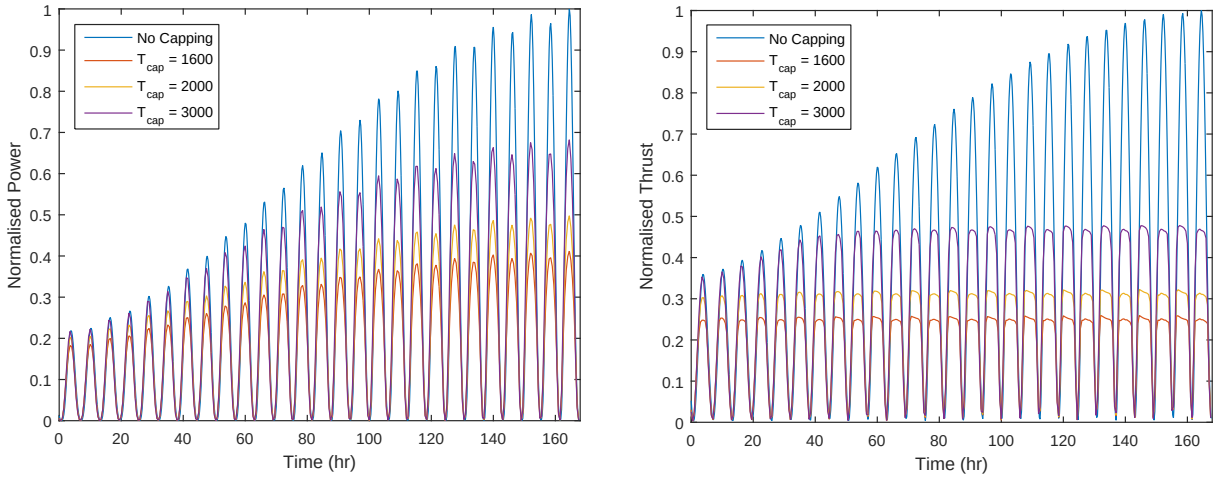

Figure 4.12: Normalised power and thrust with thrust capping

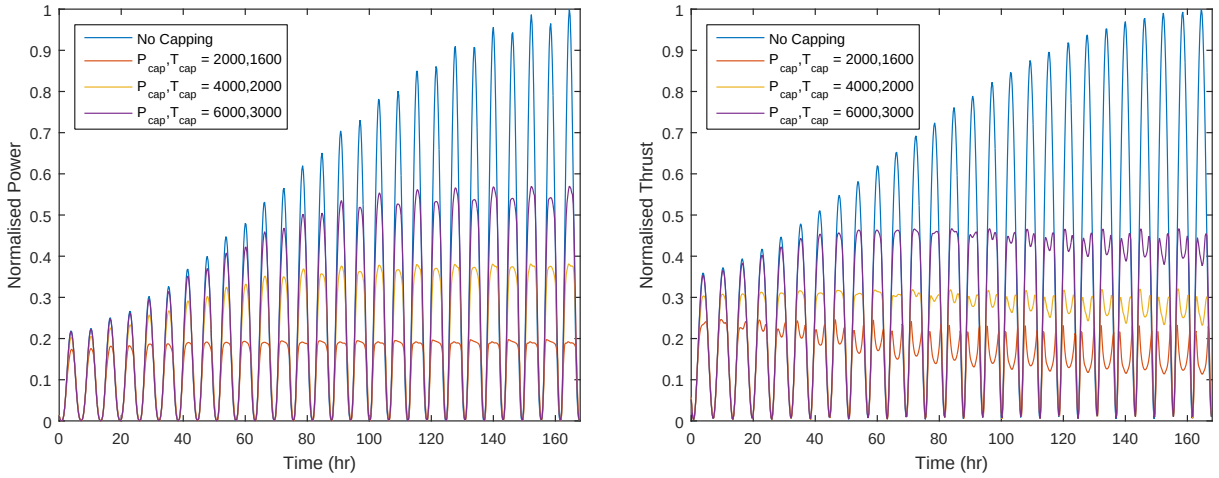

Figure 4.13: Normalised power and thrust with power and thrust capping

cycle because they are visually symmetric over time. The power and thrust profiles in both PC and TC cases are slightly different to those from a 0D simplified model – there is no "flat top" on the plots, especially at the stage where power or thrust is start to be capped. In a 0D simplified model power or thrust are only been capped once the overall value exceed the threshold, while in this 2D model capping started much earlier. This is because of the uneven distribution of flow across the channel cross section, which results in part of the turbines experiencing much higher flow than the channel's average one and hence results in an earlier capping at those turbines. The peaks of power and thrust are also different, especially the power-capped power which has a significant difference in the maximum. This difference in maximum is caused by the asymmetry of the Pentland Firth channel, in another word the difference of easting and westing flow. This difference in maximum has not been observed in the 0D model because of two reasons, the first being there is no difference in the flow going both direction in an idealised 0D channel, the second is that the overall power is capped at a fixed value regardless of flow direction. However the general patterns remain the same that PC leaves thrust with high sharp peaks, and TC leaves power only partially capped.

4.3.4 Exploration of power and thrust capping ratios

In this work a higher blockage case and a lower blockage case are considered. The higher blockage case has 3 rows of turbine in each of the three sub-channels with a uniform blockage of 0.4; the lower blockage case has only 1 row of turbine in each

sub-channel with blockage of 0.1 (consistent with the cases analysed by Adcock et al. (2013)). Analysis of combined power and thrust capping are applied to these two cases and each of them are discussed separately below.

4.3.4.1 High blockage case

Power production Tests of power and thrust capping of a higher blockage case is done in this section. the modelled power generation without any capping is as shown in Figure 4.14. As has mentioned in the previous chapter, combining power and thrust capping is likely to be more beneficial than operating power capping or thrust capping alone. In this model due to the fact that capping is based on power and thrust per unit turbine swept area, and that unlike the 0D model it is not possible to record the maximum power or thrust of each turbine, it is hard to define a reference power or thrust value that the capping value can be normalised to. For example, in the 0D model one can easily define a normalised rated power P^*_{cap} as, say 0.6 so that the peak power will be capped at 60% of the uncapped maximum; while in the 2D model each turbine has different size and capacity, and each element is not necessarily synced so that part of the turbine will be capped earlier and perhaps more often than others, resulting in a more complex capping operation and unclear definition of P^*_{cap}. Therefore, although it may lead to inconsistency with the 0D model, the power and thrust capping value will remain as dimensional value per unit swept area. The capacity factor F_C and power factor F_P have the same definition as in the 0D model chapter and the F_P is calculated according to the maximum power in Figure 4.14 (and Figure 4.21 in the later section).

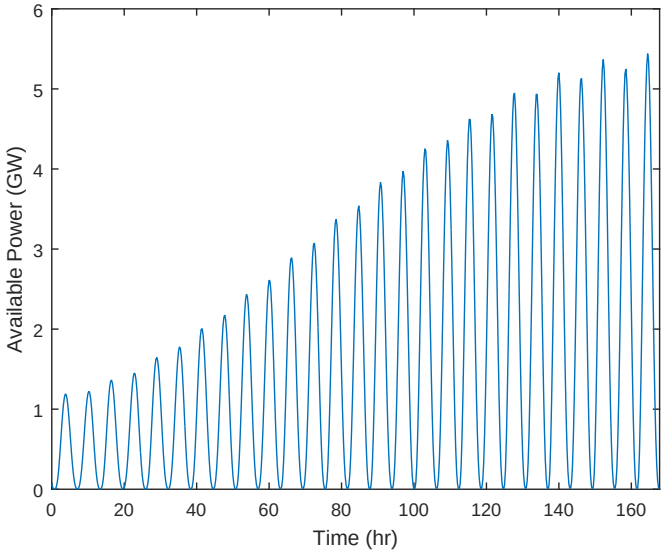

Figure 4.14: Modelled available power over half a spring-neap cycle

Figure 4.15 and 4.16 show how the F_C and F_P would change when different power and thrust capping combinations are used. The power production (Figure 4.15) shows a very similar pattern to the one obtained by 0D model although a different capping strategy was used.

Figure 4.15 again shows (in red circle) that an optimal capping zone exist where the benefits of power and thrust capping can be maximised while maintaining power production at an acceptable level, the corresponding area are circled out on Figure 4.16 as well. It is shown that the optimal T_{cap} is roughly linearly proportional to P_{cap}, in this case $T_{cap,optimal} = 0.5P_{cap}$. Figure 4.16 shows that an $F_C > 0.4$ would require P_{cap} to be lower than $6 \sim 6.5\text{kW/m}^2$ or T_{cap} to be lower than 2kN/m^2. Practical design of tidal farms will face the trade-off between F_C and F_P. A P_{cap} between 3 to 6kW/m^2 would likely to be an optimal range to operate. In this case there is barely any limitation to T_{cap} as F_C is not very sensitive to it. A $T_{cap} > 2\text{kN/m}^2$ would be

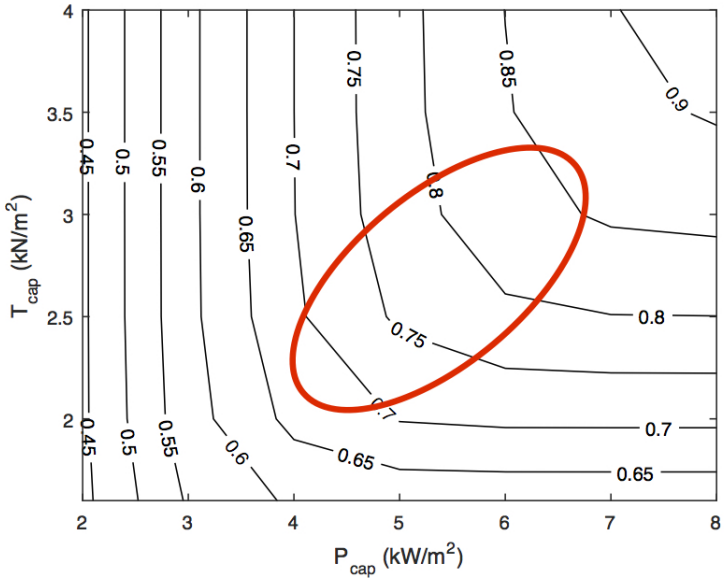

Figure 4.15: Contour plot of F_P with different power and thrust capping combination

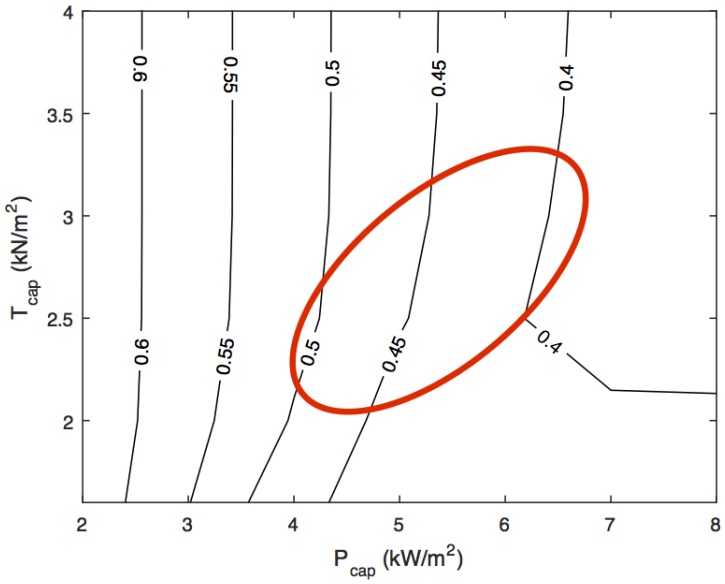

Figure 4.16: Contour plot of F_C with different power and thrust capping combination

enough to keep an optimal F_C, meaning an thrust loading reduction of up to 68%. Further decreasing would lead to drop in F_C as well as F_P.

Turbine thrust Figure 4.17 show how the maximum thrust that turbine apply to water flow, and receive from flow, would change at different capping settings. Due

to the difference in capping strategy, the thrust factor defined in the analysis of 0D idealised model is no long used here. Therefore the contour plot will be different from the one obtained by 0D models.

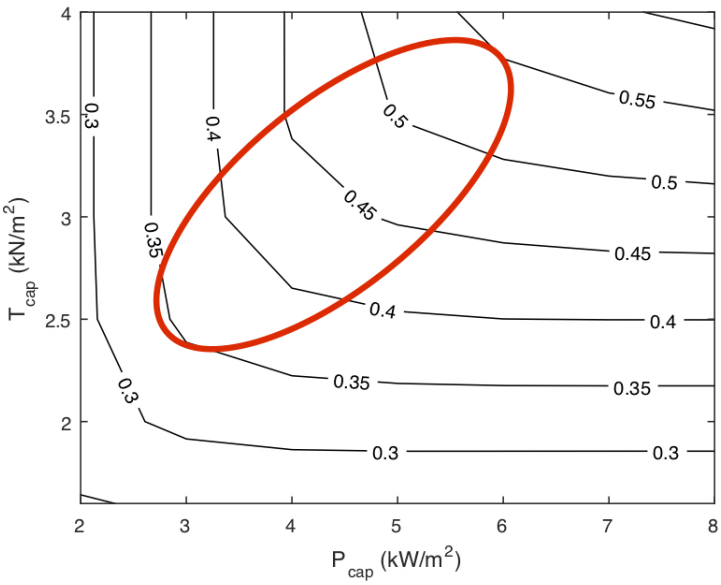

Figure 4.17: Normalised maximum thrust with different power and thrust capping combination

A similar pattern that peak thrust reduce in both direction as a stronger power or thrust capping is applied to the F_P plot is observed. The main difference is that peak thrust is less sensitive to P_{cap} than to T_{cap} as the "optimal zone" shifted left comparing to the F_P plot. There are two possible reasons causing this difference. The first reason is that power or thrust will naturally be more affected by the capping over itself – for example, power will be affected more by PC and thrust by TC simply because they are the parameters been capped. Another reason is that F_P is calculated based on power production over a spring-neap cycle, therefore it is less sensitive to the change in peak value, while in Figure 4.17 it is the peak thrust being considered.

It is important to note that although, according to definition, there is an optimal

capping zone in Figure 4.17, it is not the optimal region to operate. The optimal capping zone in F_P defines the combination of P_{cap} and T_{cap} that can maximise the benefits of capping given a limit to how much power can be given up. For thrust it is beneficial to reduce rather than maintaining it. Therefore the optimal capping zone in thrust plot is actually the least favoured zone. However, the optimal capping zone in F_P does not overlap with the one in thrust plot, meaning that operating PTC according to the F_P optimal zone is possible to optimise both power and thrust the same time. Also, the F_P optimal zone is below the one in thrust plot. This agree with the previous conclusion that introducing further TC to PC would bring benefits in reducing peak thrust with only little cost of power production.

Flowrate change The changes in flowrate ($\triangle Q$) in the Pentland Firth channels are more complicated than $\triangle Q$ in the 0D idealised channel, not only because of the simplification of 0D model, but also the complex inter-reactions of the three sub-channels. Here the $\triangle Q$ of the overall channel flowrate and the top, middle, bottom sub-channels with be analysed. The change of $\triangle Q$ according to different capping settings will be given in Figure 4.18. $\triangle Q$ here is defined as $\triangle Q = \frac{Q_{max,PTC}}{Q_{max,natural}} - 1$, hence a negative $\triangle Q$ stands for a decreasing in maximum flowrate.

The plot of overall $\triangle Q$ has the same pattern as predicted by the 0D idealised model, this again proves the effectiveness of idealised model in qualitative analysis. The middle sub-channel $\triangle Q$ is very similar to the overall one as it sits in the middle has the strongest flow among all three sub-channels. Both overall and middle $\triangle Q$ show that implementing tidal turbine will decrease the flowrate, and applying capping

can recover this change in flowrate. But the mechanism that sometimes applying TC actually leads to a higher change in flowrate remains unclear. For example the case with $P_{cap} = 6kW/m^2, T_{cap} = 3.5kN/m^2$ has a higher change in flowrate than the case with $P_{cap} = 6kW/m^2, T_{cap} = 4kN/m^2$. This is likely to be caused by the inter-reaction of the flow in three sub-channels that when extra thrust (i.e. turbines implemented) the "bypass" flow split from other sub-channels will join and increase the local flowrate. Because the middle sub-channel has the strongest flow among all three sub-channels, it is less affected than the other two.

The bottom sub-channel is slightly different to overall and middle sub-channel that the flowrate there is actually increased when a strong PC is applied. This can be better explained by the inter-reaction of three sub-channels. Because bottom sub-channel has a much lower flowrate than the middle one, it will be affect more by the split flow from middle sub-channel. When turbines are implemented and capped the flow split from the middle sub-channel will join and increase the top and bottom sub-channel flows. This explains the increasing in flowrate at a strong PC condition (left part of plot). Another possible reason is that as stated before the bottom sub-channel has turbine implemented only in part of it because part of the sub-channel has a very shallow water that is not suitable to place turbines. Those parts that do not have turbine implemented will, of course not be affected by any sort of capping.

The top sub-channel is the most complicated one because, unlike all other cases discussed here, its flowrate always increase where turbines are implemented instead of decrease. The maximum increase of flow occur at $P_{cap} = 5kW/m^2, T_{cap} = 4kN/m^2$,

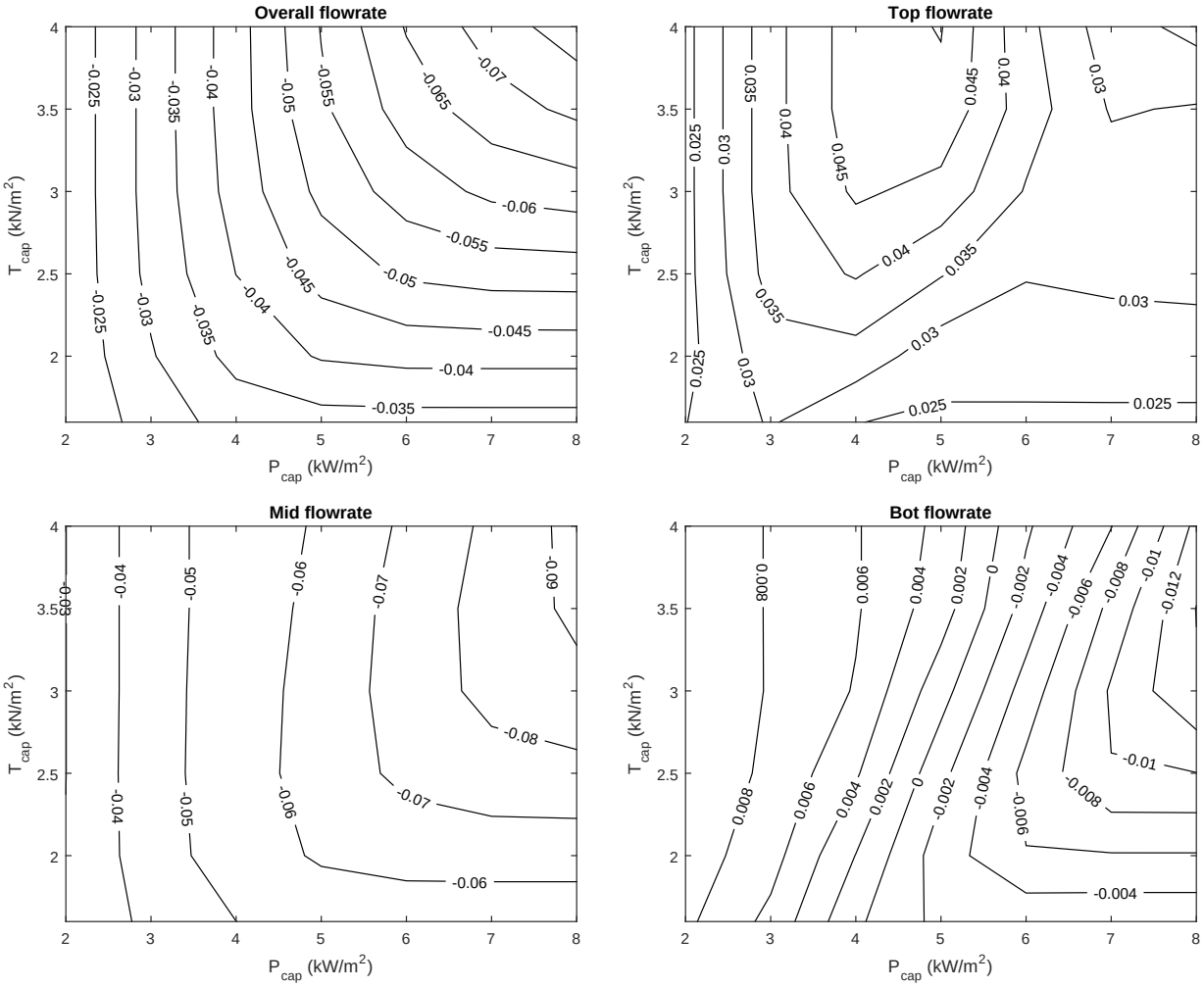

Figure 4.18: Contour plot of $\triangle Q$ with different power and thrust capping combination, each $\triangle Q$ is normalised according to the corresponding maximum natural flowrate without any turbine implemented

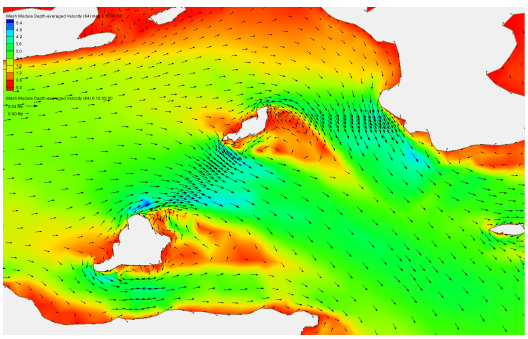

Figure 4.19: Flow patterns around the subchannels without turbines

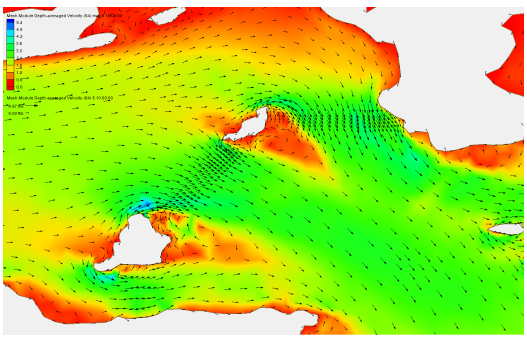

Figure 4.20: Flow patterns around the subchannels with turbines (high B case)

it is also higher than the case with $P_{cap} = 5kW/m^2$ and no TC although the later is not plotted on the graph. This analysis does seem to be different from Adcock et al. (2013). However they noted in their paper that the hydrodynamics of the top sub-channel predicted by the model was somewhat inconsistent with measurements, suggesting that it may have been poorly modelled in this coarser model. The complex behaviour of flowrate change can possibly be caused by the same reason as bottom sub-channel that the local flowrate is low and will be affected by split flow from middle sub-channel, and that the top sub-channel is facing North which results in a sharp turn of flow causing complex vortex (see Figures 4.19 and 4.20) after island Swona that may cause changes in the flow. However the mechanism behind this complex change in flow remains unclear. Therefore a precise conclusion could not be given due to the limiting tests have been done.

4.3.4.2 Low blockage case

A similar analysis to the power production, turbine thrust and change in flowrate of a low blockage case has been done with the only differences being number of turbine rows and blockage ratio. The low blockage case has 1 row of turbines in each of the 3 sub-channels and has a overall blockage ratio of 0.1.

Power production Tests of power and thrust capping of a lower blockage case is done in this section. the modelled power generation without any capping is as shown in Figure 4.21. Contour plots of F_P and F_C with different power and thrust capping settings of a low blockage case were given in Figures 4.22 and 4.23, all parameters

have the same definition as above. Due to the same reason stated above, the power and thrust capping value will remain as dimensional value per unit swept area.

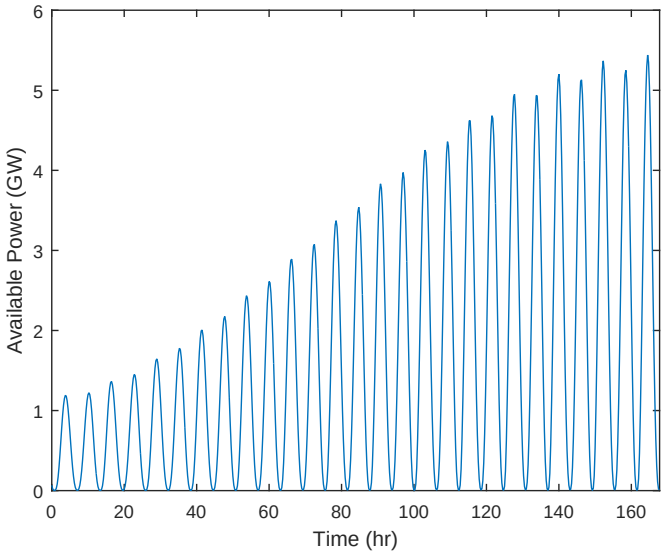

Figure 4.21: Modelled available power over half a spring-neap cycle

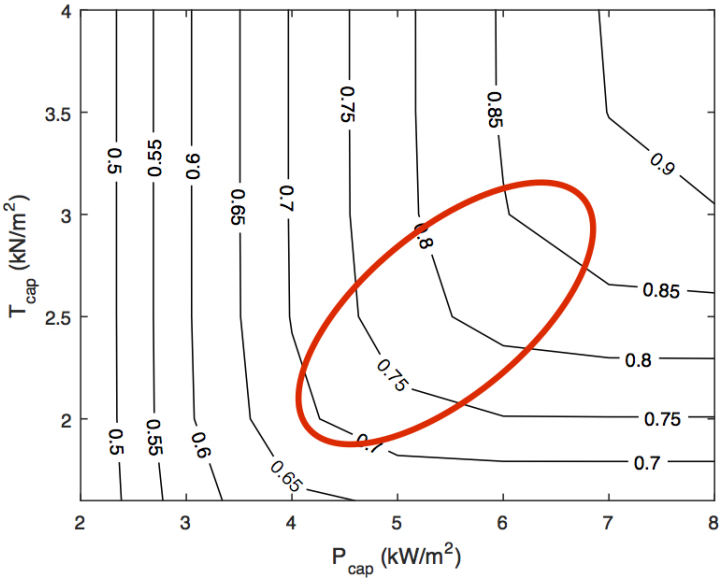

Figure 4.22: Contour plot of F_P with different power and thrust capping combination

According to Figures 4.22 and 4.23, the change in F_P and F_C in low blockage case

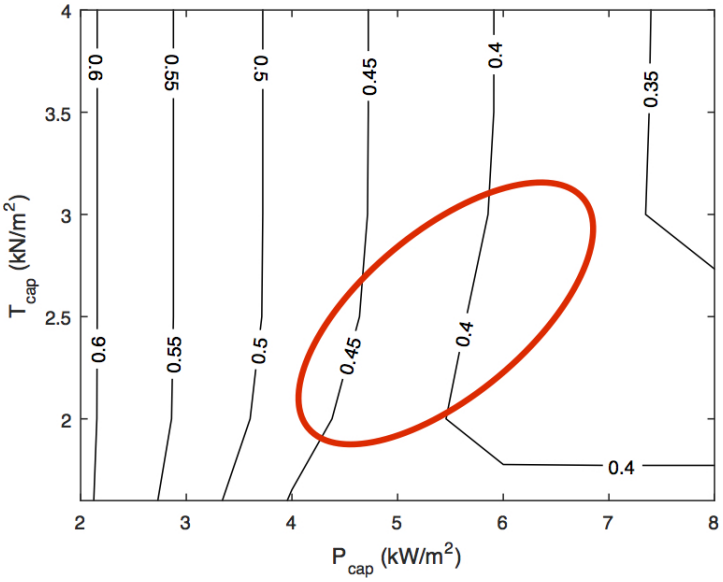

Figure 4.23: Contour plot of F_C with different power and thrust capping combination

are nearly identical to the ones in high blockage case, with the only difference being the values being scaled up slightly. The small difference in F_P and F_C is likely to be caused by the fact that in low blockage case turbines apply much less thrust to the flow.

Although it is not clear whether the plots of F_P and F_C will be nearly identical for all blockage and number of turbine rows settings at the same site, it is reasonably sensible to make such assumption that the same principle of optimal capping zone will apply to all cases so an optimal power and thrust capping obtained in one case can be applied to the other. Hence a comparison between these two cases can be made via a case study.

Turbine thrust Figure 4.24 shows how the maximum thrust would change when different power and thrust capping settings are applied. The axis are the same as

used in F_P and F_C plots that capping are based on power or thrust per unit swept area. Thrust is normalised to the non-capped maximum thrust.

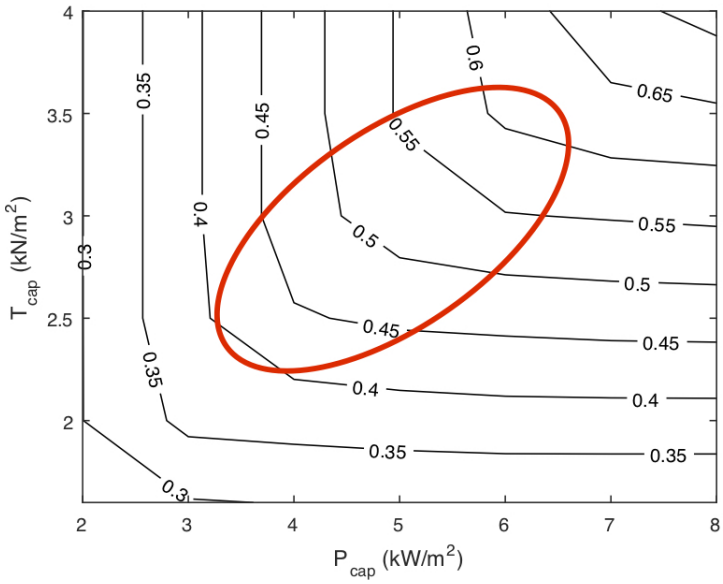

Figure 4.24: Normalised maximum thrust with different power and thrust capping combination

Comparing to Figure 4.17, Figure 4.24 has a "optimal capping zone" (red circled) at a lower position of the graph, but still higher than the F_P optimal zone. However it is important to note that, optimal capping zone is defined for power and is actually not the optimal setting for TC. Therefore an optimal capping for power and thrust can still be reached.

Flowrate change The change in flowrate is an important parameter indicating the environmental impact brought by implementing tidal turbines. This has been evaluated in the low blockage case and the results are plotted in Figure 4.25.

The overall $\triangle Q$ and middle sub-channel $\triangle Q$ are very similar to the high blockage

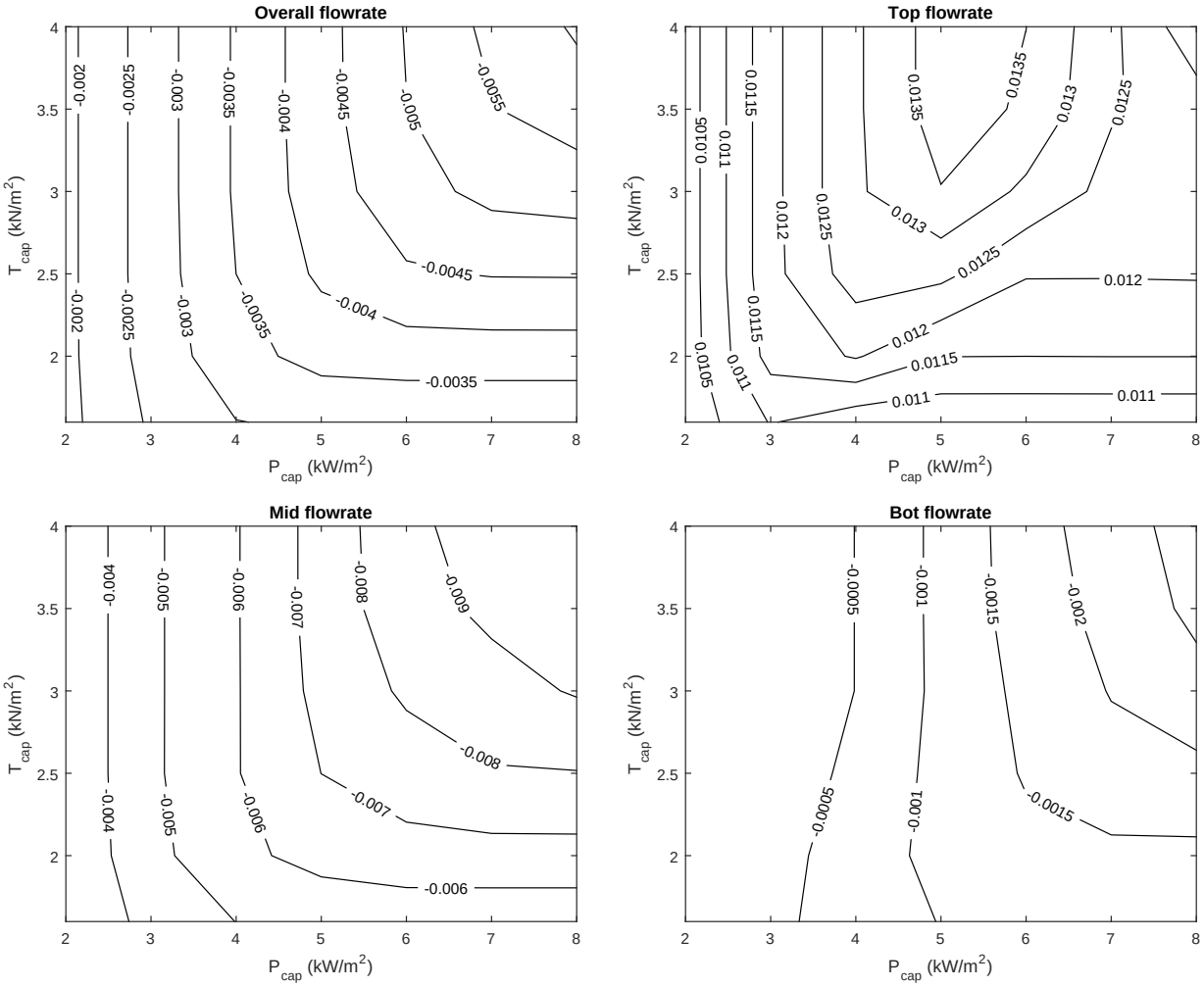

Figure 4.25: Contour plot of $\triangle Q$ with different power and thrust capping combination, each $\triangle Q$ is normalised according to the corresponding maximum natural flowrate without any turbine implemented

case and the one produced by idealised 0D model, but the value of $\triangle Q$ is less than 1/10 of that in high blockage case. This is as expected since low blockage case has only 1 row of turbines instead of 3, and blockage ratio is only 0.1 while high blockage case has a blockage ratio of 0.4. A much lower thrust applied by turbine arrays will indeed lead to a much lower change in flowrate.

The bottom sub-channel is slightly different to overall and middle sub-channel, however the general pattern is still similar – flowrate is decreased and more capping

will reduce this decrement. The difference in the bottom left part of bottom sub-channel $\triangle Q$ is likely to be caused by the same reasons causing the difference in bottom sub-channel flow in the high blockage case. First, it has much lower flow than the middle sub-channel, so flow split from the middle sub-channel will accelerate the top and bottom sub-channel flows. Second, as stated before the bottom sub-channel has turbine implemented only in part of it. Those parts that do not have turbine implemented will not be affected by capping.

The top sub-channel is the most complicated one because, very similar to the high blockage case, its flowrate increases where turbines are implemented instead of decrease. This can possibly be caused by the same reason as stated before that the local flowrate is low and will be affected by split flow from middle sub-channel.

4.4 Conclusion

This chapter has analysed power capping and thrust capping strategies in the Pentland Firth channel using a 2D Shallow Water Equations model. This analysis examined the conclusion from previous idealised 0D model chapter that adopting a capping strategy that prevents power or thrust exceeding a given value can be beneficial in improving capacity factor, reduce environmental impact and reduced requirements in support structure.

Although a different capping strategy was used to cap power or thrust per unit turbine swept area instead of the overall ones. The resulting F_P and F_C lead to the same conclusion that capping thrust in addition to power is more beneficial than

doing power capping alone. Both low and high blockage cases show an optimal capping zone in the F_P plots. Such optimal zone can be used as optimal capping settings to maximise the benefits of capping.

Flowrate change is much more complicated in a 2D model than in a idealised 0D model. The main reasons would be the complex geometry of Pentland Firth channel and the inter-reaction of flows in three sub-channels. The change of flowrate in bottom and top sub-channel are more complex. It is likely to be caused by the split flow from middle sub-channel where the flow is much stronger than the other two. Further efforts would be needed to be made in order to clarify the mechanism behind this complex change in flowrate. However, the general changes in flowrate follows the same principle that implementing turbines reduces the flow and capping recovers this reduction.

Thus it is shown that, consistent with the simple 0D model, a combined power and thrust capping strategy should be applied in tidal stream turbine farms. Although real site, with real turbines, will be much more complicated than the model used in this chapter, a 2D model is believed to be able to catch the principle effect of combined power and thrust capping in changing power production, reducing turbine thrust and reducing flowrate changes.

Although the best trade-off between different power and thrust capping strategies and total power production is still unclear, this work pointed out an optimal capping zone where the optimal settings for power and thrust capping should fall into. In real site application, making the trade off will be a balance between financial considerations and environmental impact. This work is aimed to proved a guidance in

power and thrust capping operation in order to maximise the benefits of capping (i.e. improving capacity factor and reduce environmental impacts etc.), and site specifically evaluate the effect of power and thrust capping in the Pentland Firth channel in terms of power production, turbine thrust and flowrate change.

Chapter 5

Comparison of Idealised 0D model and 2D SWEs model

5.1 Introduction

In Chapter 3 an idealised 0D model was used. Although certain degree of simplification will result in lower accuracy, the 0D model has the advantage of faster computation. The drag force produced by the presence of turbine support structures has been evaluated by using an iteration algorithm. However such iteration is impractical for the 2D model used in later chapter because it would require too much computational resources (months for a regular PC). The simplified model has been used to study power capping and thrust capping. Effort has been made to combine these two capping strategy together. The basic idea of power capping is to limit the peak power generated for economical concern over power generators. By applying power capping, the requirement in power generators size, which is mainly determined

by the maximum power required to be generated, can be reduced. Thrust capping that limits the maximum thrust over a tidal cycle was combined with power capping because both capping have the same operation principle that raising α_4 (or decreasing tip speed ratio) when power or thrust is higher than wanted. A few idealised channels under the affect of two dominant semi-diurnal tidal constituents, M_2 and S_2, were built for this study. The results given in Chapter 3 has shown that doing such combined capping rather than power capping only is beneficial in terms of both economic and environmental concerns. This 0D power and thrust capping model provided a fundamental understanding of combined capping.

Chapter 4 extended the study of power and thrust capping to a real candidate site for tidal power extraction, the Pentland Firth. The Pentland Firth is a well known tidal farm candidate site because of its fast tidal currents. In Chapter 3 one of the idealised cases is also based on Pentland Firth channel, although it is highly simplified. This "Pentland Firth" case will be used to make a comparison to the 2D model. The Pentland Firth consists of three sub-channels divided by islands Swona and Stroma. Therefore the analysis of parameters such as change in flowrate was done to each of these sub-channels as well as total overall flowrate. Similar to the 0D model, only M_2 and S_2 as the dominant tidal constituents were used in this model. Although efforts have been made to make the 2D model more consistent with the 0D one, the strategy of capping has to be changed because the overall capping used in idealised 0D model in impractical in real site due to the uneven distribution of flow across the cross section of channel. It has been explained in chapter 4 that the uneven distribution of flow causes part of the turbine to be capped earlier and maybe more

often. Thus a capping strategy based on power or thrust per unit turbine swept area was used to allow for individual capping in each part of turbines.

In this chapter a comparison of the idealised 0D model and 2D model is undertaken. The tidal constituents used in 2D model is consistent with the 0D models and make the comparison more representative. Although in the 2D model a different, but more realistic, method was used for power and thrust capping, a similar goal has been achieved that power and thrust were capped by a pre-determined fixed value. However, differences in the results of capping do exist and this has to be considered as the error brought by over-simplification of the idealised 0D model, since the main reason causing the variance in capping methods is that the overall capping method used in 0D model is impractical to be applied to a more complicated system. Another difference must be taken into consideration is that the 0D model did not consider the existence of islands or sub-channels in Pentland Firth, making it only representative in terms of the overall power, turbine thrust and flowrate. Therefore a comparison of these two model based on the channel overall power production, turbine total thrust and change in flowrate will be made.

5.2 Models

Channel model The channel model used in Chapter 3 is a 0D model, which simplified the tidal channel as a rectangular channel. In Chapter 4 a finite element method has been used to build the mesh of Pentland Firth (see Figure 5.1). Clearly the 2D model will produce a more realistic result than the 0D model because of advantages

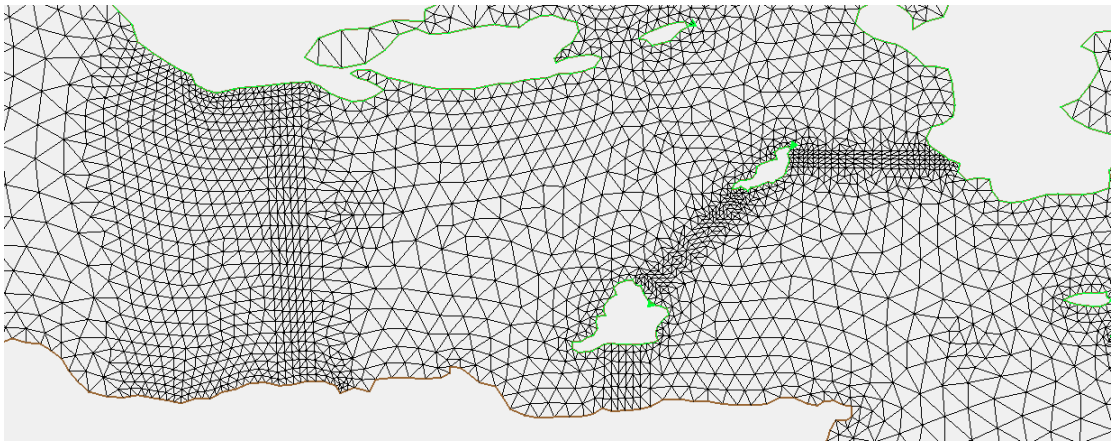

Figure 5.1: Mesh of the Pentland Firth (channel part only, figure showing a approximately $27km \times 20km$ area)

in catching the complex geography, considering the flow variation over two extra dimensions etc. However the purpose of a 0D model is not to accurately catch the dynamics of flow under power and thrust capping, instead, it is aiming to provide a conceptual understanding of the effects of power and thrust capping on power, thrust and flowrate of a tidal channel. Because of the advantages staged above, the 2D model will be used as a standard to verify the key findings in Chapter 3.

Turbine model The 0D model used in this study uses a constrained volume actuator disc theory (Vennell 2010, Garrett and Cummins 2007) as the model to simulate the power extraction by turbine arrays. It approximates the tidal turbine as a uniform circular plate resisting the passing flow. The 2D SWEs model uses a line sink of momentum to represent the power removal by tidal turbines. Such momentum sink uses a similar approach to the actuator disc theory to represent tidal turbines – the open channel LMADT model (Serhadlıoğlu 2014, Draper 2011, Houlsby et al. 2008). The open channel LMADT model (Houlsby et al. 2008) is able to consider the water

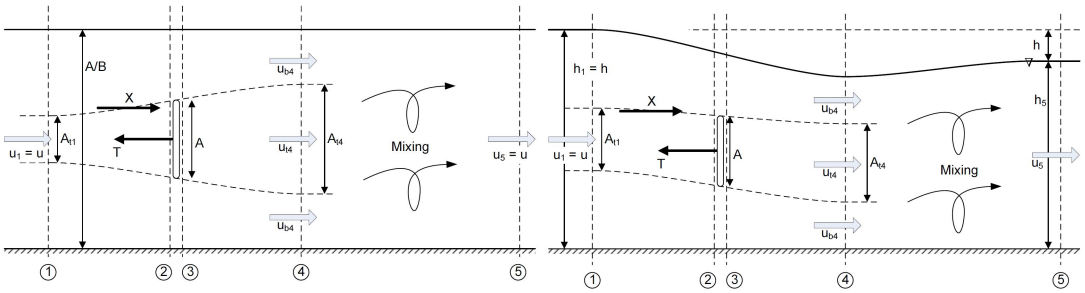

Figure 5.2: Comparison of the flow field (side view) of volume constrained LMADT (left) and open channel LMADT (right) (Draper 2011, Houlsby et al. 2008)

depth change across turbine arrays (see comparison in Figure 5.2), which is neglected in the 0D model.

5.3 Case Study

A rough comparison of change in F_P and F_C with $P^*_{cap}(P_{cap})$ and F_T combination were made in the results in Chapter 4. The similarity in the general pattern of F_P and F_C evident the effectiveness of a 0D model in estimating the impacts of power and thrust capping. However the power and thrust capping in both models use a different capping strategy and different parameters to indicate the degree of capping. In this section a few case studies were to be made based on the results generated by these two models. The results of the idealised "Pentland Firth" channel (channel 2 in Table 3.1 on page 69) used in the 0D model were to be compared to the 2D Pentland Firth channel model.

Due to the differences in parameters used to indicate the degree of capping in both models, a case study based on a same degree of capping cannot be made. However, in both chapters we have used two common parameters, F_P and F_C, as important

indicators of the benefits of capping. As stated before an $F_C > 0.5$ would be a reasonable task, and the same "optimal capping zone" applies in the F_P plots in both models. Therefore a case study was made based on the cases that satisfy the condition of $F_C > 0.5$ and optimal capping of power and thrust in both models.

Chapter 3 has included an analysis of sizes of support structures affected by power and thrust capping. However a similar analysis has not been done in the 2D model for two reasons. First, the iteration algorithm (see Figure 3.3 on page 58) used to calculate the size of support structure is not practical to be used in the 2D model due to significantly higher computational time. Second, support structures in real tidal turbine farms would not be affected only by the thrust applying on them, therefore providing the turbine thrust instead of calculating support structure size base on it is more sensible in this case.

According to Figure 3.15 and 3.16 on page 67, and Figures 4.15 and 4.16 on page 95, the $P^*_{cap} = 0.3$ and $F_T = 0.6$ high blockage case in 0D model and $P_{cap} = 4kW/m^2$ and $T_{cap} = 2kN/m^2$ high blockage case in 2D model were picked. The comparison results are presented in Figures 5.3 and 5.4 and Table 5.1.

Table 5.1: Comparison of modelled results

Case		F_C	F_P	$\bar{P}$/GW	T^*_{max}	T_{max}/GN	ΔQ_{max}
0D	No capping	0.28	1	1.48	1	2.93	27.1%
	PC	0.60	0.65	0.97	0.45	1.31	7.03%
	PTC	0.58	0.62	0.92	0.27	0.79	6.20%
2D	No capping	0.28	1	1.55	1	3.44	11.5%
	PC	0.52	0.70	1.08	0.46	1.57	4.29%
	PTC	0.50	0.66	1.03	0.32	1.10	3.66%

According to Figures 5.3 and 5.4 and Table 5.1, the 0D model and 2D model give

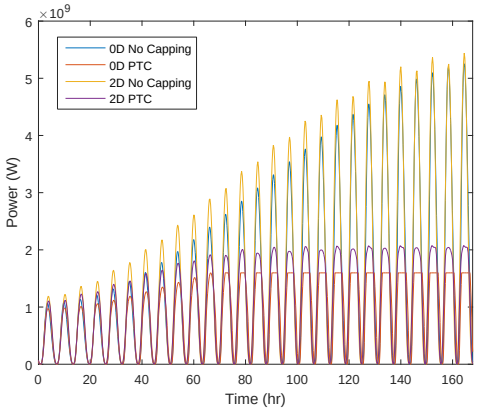

Figure 5.3: The uncapped and PTC power predicted by 0D and 2D models

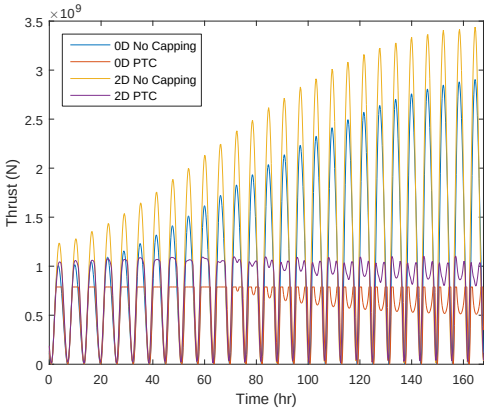

Figure 5.4: The uncapped and PTC turbine thrust predicted by 0D and 2D models

very good agreement in power and thrust. Although much larger difference appears in thrust than power, the performance of power and thrust capping in terms of thrust are very similar. In this case generally the 2D model produces higher power and larger thrust, partly because turbines are placed in the three sub-channels which has total length longer than the width of channel. Both models in Figure 5.3 give available power instead of extracted power because it gives a better representation of power produced by the turbines. The 0D model gives a much higher change in flowrate when it is not capped, however the ΔQ_{max} data from both models provides the same conclusion that applying power and thrust capping would significantly reduce the change in flowrate, although the details would be much more complicated in a real site (as shown in Section 4.3.4).

Regardless of the differences in capping operation and turbine arrangement, both models show a similar degree of capping to achieve an $F_C > 0.5$. The same reduction in the sharp peaks in thrust has been shown in Figure 5.4, meanwhile little difference

were made to F_C and F_P when combining TC into PC. This demonstrates the initial assumption of that introducing TC to PC is beneficial in reducing maximum thrust with only little cost of power production.

Given that the 0D model highly simplified the geometry, and that 2D model has a different operation of capping, this result demonstrates that such 0D model can provide a good first approximation of the performance of power and thrust capping in a tidal channel.

5.4 Conclusion

A comparison of the 0D idealised model used in Chapter 3 and the 2D SWEs model used in Chapter 4 has been made. This comparison is imperfect and can be improved because of several reasons. Differences exist in the strategy of capping, as mentioned previously, due to the fact that tidal turbines in real sites as well as in this 2D model are not synced. Also, definitions of parameters used to indicate the degree of capping are not consistent in these two models. However same parameters such as F_P and F_C were used to indicate the performance of capping, these parameters were used in the comparison to ensure similar cases in both models are being compared. An $F_C > 0.5$ was assumed based on the F_C data from wind turbine.

Both models haven shown a similar effect of power and thrust capping in terms of limiting the maximum power and thrust. Although the capped maximum power is different in these two models due to the difference in capping strategy, the thrust profiles show a high agreement in the way peak thrust being limited. Although an

estimation of support structure size was done using the 0D model, it has not been done by the 2D model due to significantly higher demand in computational power. A further study analysing the effect of reducing turbine thrust on support structure would be beneficial.

Although some differences exist, both models agreed that applying power and thrust capping would be beneficial in terms of reducing the changes brought by implementation of tidal turbines to the flow. This has the potential to reduce some environmental impacts relating the alteration of flow.

Chapter 6

Conclusions and Future Work

6.1 Conclusions

In this thesis two models, an idealised 0D model and a 2D Shallow Water Equations (SWEs) real site model, have been used to exam the effectiveness of combined power and thrust capping in a tidal turbine farm. The effects on power production, turbine thrust and environmental impacts have also been evaluated. This thesis has used power capping to limit the maximum power during peak tide in order to reduce the requirement in power generator, cabling and support structures. A similar capping method called thrust capping has been introduced to limit the maximum loading on the tidal turbines. Because of the fact that both capping strategy tune α_4 during peak tide to limit the power or thrust, and both sacrifice part of the power production when the load is high. The thrust capping has been combined with the previously mentioned power capping to maximise the benefit of doing capping. Both models considered here give similar results on the effectiveness of the different capping strategies.

In Chapter 3 a selection of idealised 0D channel models previously considered in the literature have been built to exam the leading-order effects of power and thrust capping. The models were firstly tested by a simplified case where the flow is formed by a single tidal constituent (M_2). Then a more realistic, although still highly simplified, case where evaluations were done over a sping-neap cycle in M_2 and S_2 channels. The models have been verified with Garrett and Cummins (2005), Vennell (2010). The change of available power as a function of different capping parameters in an idealised channel has been evaluated. A new algorithm has been designed to account for the power and thrust capping as well as the resulted change in supporting structures. An "optimal capping zone", which is defined as the part in a contour plot where the direction gradient is between 30° to 60° to the x-axis, has been used to describe the optimal combination of power and thrust capping that is able to maximise the benefit of capping according to different trade-off scenarios. Any point outside of the "optimal capping zone" can shift in either direction without a sharp drop in power production, meaning that more power or thrust capping show be applied. A general limitation of $F_C > 0.4$ has been used for the tidal turbines. Tests have been done in three idealised channels with different dimensions. Generally an $F_C = 0.5 \sim 0.6$ has been reach with the cost of losing 35% of power. Meanwhile the maximum thrust loading has been reduced by at least 70%, and the change in flowrate has been reduced by $70 \sim 80\%$. In summary, combining power and thrust capping can effectively reduce the maximum power, maximum thrust loading and change in flowrate.

In Chapter 4 a 2D SWEs model has been built with a modified DG-ADCIRC model, based on the Pentland Firth. In this chapter the results in Chapter 3 of power

and thrust capping were again examined in a more realistic model. A 2D model is used to simulate the tidal stream through three sub-channels at the Pentland Firth, based on the work by (Adcock et al. 2013). The mesh used in this model has a minimum mesh size of around 100 metres to closely match the island and land boundaries. A similar capping algorithm to the 0D capping model in Chapter 3 has been built with a few modifications. First, in this model the blockage ratio across the cross-section of a channel is fixed rather than turbine sizes. Second, the power or thrust per unit swept area of turbine are used as the capping indicator. This 2D model further considered the complex geometry and uneven distribution of flow and turbines in the site and hence the results are believed to be more reliable than the 0D model. 2 cases, one with lower blockage ratio and one with higher, have been evaluated and the results have been validated with field observation given by Gardline Surveys (2001). Flowrate change is much more complicated in the 2D model than in an idealised 0D model in Chapter 3. A precise conclusion cannot be made to the complex dynamics that cause this change. However, the general conclusion that applier stronger capping would lead to less change in flowrate still applies. Although a different capping strategy and different capping indicators are used, in the results a similar "optimal capping zone" to the one in Chapter 3 is observed, meaning that an optimal combined capping is achievable. This lead to the same conclusion that capping thrust in addition to power is more beneficial than doing power capping alone.

Chapter 5 carried out a case study comparing the 0D idealised model and the 2D SWEs model in Chapters 3 and 4. Although in the 2D model a different method was used for power and thrust capping, a similar capping of the overall power and thrust is

achieved. This comparison is challenging because of the inconsistency between these two models. The strategies of capping, as mentioned before, are different because tidal turbines in real sites are not synced, which has been caught by the 2D model but not the 0D one. Also, definitions of parameters are inconsistent in these two models because of the difference in capping methods. However several parameters such as F_P and F_C, which are used to indicate the performance of capping, remain the same in these two models. These parameters were used in this chapter to chose the cases to be compared. In terms of performance of capping (i.e. limiting the maximum power and thrust), both models haven shown a similar effect that the combined power and thrust capping can be optimised by operating within the "optimal capping zone". An estimation of support structure size has been done by the 0D model but not the 2D model due to significantly higher demand in computational power. In the case that such evaluation need to be done in the 2D model, a more optimised algorithm would be needed to shorten the computation time. Although these two models differ slightly in the capping results, it is agreed that implementing power and thrust capping would be beneficial in terms of improving capacity factor and reducing the change to the flow brought by extracting tidal energy.

6.2 Suggested Future Work

The idealised 0D model used in this thesis can be used to explore the power and thrust capping in any tidal channel site given that site can be roughly approximated by a rectangular channel. The performance of this model is great given how much

simplification has been made. However further improvements can still be made. For example in Chapter 3 the support structures were assumed to be hollow cylinder, of which the size is estimated as just be able to handle the maximum thrust loading. In real cases this assumption is not suitable because many other factors need to be considered in the design of tidal turbine support structures, such as extreme high speed, turbine failure etc. Also the algorithm used to calculate the size of support structure involves a complex iteration which would be computational expensive for more complicated cases (e.g. 2D models).

The 2D SWEs model evaluates power and thrust capping in the Pentland Firth. However this model can also be applied to non-channel sites. A different method that caps power and thrust based on the power and thrust per unit turbine swept area was used. This is valid assuming that all of the turbines have a fixed power to swept area ratio. However when the sizes of turbine varies and the flow across the turbine arrays is unevenly distributed, this assumption may not be valid. It has been mentioned in Chapter 4 that this model assume a fixed blockage ratio across the channel, in another word turbine sizes are varying. Therefore concerns could be raised against the method used for power and thrust capping here. Further study in finding a more realistic method to model power and thrust capping is therefore worth doing. A more realistic turbine models would also be helpful.

An important benefit assumed in this thesis is that limiting maximum power and thrust can save the capital cost by reducing the sizes of power generator and support structures. However a cost analysis of a tidal turbine farm would be required to quantify the economical benefits.

The complex change in flowrate observed in the modelled results of bottom and top sub-channels have not been fully understood. A possible explanation has been made that the flow split from the middle sub-channel will join and increase the top and bottom sub-channel flows when turbines are implemented and capped. Further study of the mechanism behind this change is necessary to fully understand the impact of power extraction and power and thrust capping on the flow.

In this project evaluation of the environmental impact brought by tidal power extraction has been attempted as well as evaluation of reducing the impact by applying power and thrust capping. The environmental impact is, however, hard to define and quantify. Therefore an assumption has been made in this work that the alteration of the local flow is the majority cause of the environmental impact. All of the environmental impact analysis were done by calculating the change in flowrate (mainly the magnitude but direction is also considered). The environmental impacts that are in direct relation to change in the local flowrate include pollutant dispersal and sediment transport etc. However no analysis of those impacts has been done in this work apart from the evaluation of change in flowrate. More detailed research is therefore suggested to understand these environmental impacts brought by extracting tidal energy, and the effect of power and thrust capping in terms of reducing these environmental impacts. And environmental impacts that are not related to the change in flow are not considered in this work and further study is need to understand such impacts.

References

Adcock, T. A. A. and Draper, S.: 2014a, Power extraction from tidal channels – Multiple tidal constituents, compound tides and overtides, *Renewable Energy* **63**, 797–806.

Adcock, T. A. A., Draper, S., Houlsby, G. T., Borthwick, A. G. L. and Serhadlıoğlu, S.: 2013, The available power from tidal stream turbines in the Pentland Firth, *Proceedings of the Royal Society of London A: Mathematical, Physical and Engineering Sciences* **469**(2157).

Adcock, T. A. A., Draper, S., Houlsby, G. T., Borthwick, A. G. L. and Serhadlıoğlu, S.: 2014, Tidal stream power in the Pentland Firth – long-term variability, multiple constituents and capacity factor, *Proceedings of the Institution of Mechanical Engineers, Part A: Journal of Power and Energy* **228**(8), 854–861.

Adcock, T. A. A., Draper, S. and Nishino, T.: 2015, Tidal power generation – A review of hydrodynamic modelling, *Proceedings of the Institution of Mechanical Engineers, Part A: Journal of Power and Energy* **229**(7), 755–771.

Adcock, T. and Draper, S.: 2014b, Different metrics for estimating the tidal stream energy resource, *1st PRiMaRE conference*, Plymouth, UK.

Ahmadian, R. and Falconer, R. A.: 2012, Assessment of array shape of tidal stream turbines on hydro-environmental impacts and power output, *Renewable Energy* **44**, 318–327.

Ahmadian, R., Falconer, R. and Bockelmann-Evans, B.: 2012, Far-field modelling of the hydro-environmental impact of tidal stream turbines, *Renewable Energy* **38**(1), 107–116.

Aizinger, V. and Dawson, C.: 2002, A discontinuous Galerkin method for two-dimensional flow and transport in shallow water, *Advances in Water Resources* **25**, 67–84.

Baston, S. and Harris, R. E.: 2011, Modelling the hydrodynamic characteristics of tidal flow in the pentland firth, *9th European Wave and Tidal Energy Conference*, Southampton, UK, p. 7.

Betz, A.: 1920, Das Maximum der theoretisch möglichen Ausnutzung des Windes durch Windmotoren, *Gesamte Turbinenwesen* **26**, 307–309.

Blanchfield, J., Garrett, C., Rowe, A. and Wild, P.: 2008, Tidal stream power resource assessment for Masset Sound, Haida Gwaii, *Proceedings of the Institution of Mechanical Engineers, Part A: Journal of Power and Energy* **222**(5), 485–492.

Blunden, L. S. and Bahaj, A. S.: 2007, Tidal energy resource assessment for tidal

stream generators, *Proceedings of the Institution of Mechanical Engineers, Part A: Journal of Power and Energy* **221**, 137–146.

Bonar, P. A. J.: 2017, *Toward best practice in the design of tidal turbine arrays*, PhD thesis, The University of Edinburgh.

Bonar, P. A. J., Bryden, I. G. and Borthwick, A. G. L.: 2015, Social and ecological impacts of marine energy development, *Renewable and Sustainable Energy Reviews* **47**, 486–495.

Boyle, N. G.: 2017, Astronomy Know How.
URL: *http://www.astronomyknowhow.com*

Bryden, I. G., Couch, S. J., Owen, A. and Melville, G.: 2007, Tidal current resource assessment, *Proceedings of the Institution of Mechanical Engineers, Part A: Journal of Power and Energy* **221**, 125–135.

Burton, T., Sharpe, D., Jenkins, N. and Bossanyi, E.: 2001, *Wind Energy Handbook*, John Wiley & Sons, Ltd, West Sussex.

Chippada, S., Dawson, C. N., Martinez, M. and Wheeler, M. F.: 1998, A Godunov-type finite volume method for the system of shallow water equations, *Computer Methods in Applied Mechanics and Engineering* **151**, 105–129.

Copping, A., Hanna, L., Whiting, J., Geerlofs, S., Grear, M., Blake, K., Coffey, A., Massaua, M.and Brown-Saracino, J. and Battey, H.: 2013, Environmental Effects of Marine Energy Development around the World: Annex IV Final Report,

Technical report, IEA Ocean Energy Systems Initiative, Pacific Northwest National Laboratory, Richland, WA, USA.

DECC: 2011, UK Renewable Energy Roadmap, *Technical report*, Department of Energy and Climate Change.

Draper, S.: 2011, *Tidal Stream Energy Extraction in Coastal Basins*, PhD thesis, Department of Engineering Science, University of Oxford.

Draper, S., Adcock, T. A. A., Borthwick, A. G. L. and Houlsby, G. T.: 2014, Estimate of the tidal stream power resource of the Pentland Firth, *Renewable Energy* .

Draper, S., Houlsby, G. T., Oldfield, M. L. G. and Borthwick, A. G. L.: 2010, Modelling tidal energy extraction in a depth-averaged coastal domain, *IET Renewable Power Generation* .

Draper, S., Nishino, T., Adcock, T. A. A. and Taylor, P. H.: 2016, Performance of an ideal turbine in an inviscid shear flow, *Journal of Fluid Mechanics* **796**, 86–112.

Easton, M. C., Woolf, D. K. and Bowyer, P. A.: 2012, The dynamics of an energetic tidal channel, the Pentland Firth, Scotland, *Continental Shelf Research* **48**, 50 – 60.

URL: *http://www.sciencedirect.com/science/article/pii/S0278434312002233*

European Parliament: 2009, Directive 2009/28/EC of the European Parliament and of the Council of 23 April 2009 on the promotion of the use of energy from renewable sources and amending and subsequently repealing directive.

Falconer, R. A.: 1993, *An introduction to nearly-horizontal flows. Coastal, Estuarial, and Harbour Engineer's Handbook*, E. & F. N. Spon Ltd, London.

Fraenkel, P. L.: 2002, Power from Marine Currents, *Proceedings of the Institution of Mechanical Engineers, Part A: Journal of Power and Energy* **216**, 1–14.

Gardline Surveys: 2001, Pentland Firth tidal stream observations, *Technical report*, Gardline Surveys.

Garrett, C. and Cummins, P.: 2005, The Power Potential Of Tidal Currents In Channels, *Proceedings of the Royal Society A* **461**, 2563–2572.

Garrett, C. and Cummins, P.: 2007, The efficiency of a turbine in a tidal channel, *Journal of Fluid Mechanics* **588**, 243–251.

Hau, E. and Renouard, H. V.: 2006, *Wind Turbines: Fundamentals, Technologies, Application, Economics*, Berlin: Springer-Verlag.

Hou, F., Bao, X., Li, B. and Liu, Q.: 2015, The assessment of extractable tidal energy and the effect of tidal energy turbine deployment on the hydrodynamics in Zhoushan, *Acta Oceanologica Sinica* **34**(5), 86–91.

Houlsby, G. T., Draper, S. and Oldfield, M. L. G.: 2008, Application of Linear Momentum Actuator Disc Theory to Open Channel Flow, *Technical report*, Department of Engineering Science, University of Oxford.

Jeffrey, H., Jay, B. and Winskel, M.: 2013, Accelerating the development of marine

energy: Exploring the prospects, benefits and challenges., *Technological Forecasting and Social Change* **80**(7), 1306–1316.

Joukowsky, N. E.: 1920, Windmill of the NEJ type, *Transactions of the Central Institute for Aero-hydrodynamics of Moscow* .

Karsten, R. H., McMillan, J. M., Lickley, M. J. and Haynes, R. D.: 2008, Assessment of tidal current energy in the Minas Passage, Bay of Fundy, *Proceedings of the Institution of Mechanical Engineers, Part A: Journal of Power and Energy* **225**, 493–507.

Kubatko, E. J., Westerink, J. J. and Dawson, C.: 2006, *hp* discontinuous Galerkin methods for advection dominated problems in shallow water flow, *Computer Methods in Applied Mechanics and Engineering* **196**, 437–451.

Lanchester, F. W.: 1915, A contribution to the theory of propulsion and the screw propeller, *Transactions of the Institution of Naval Architects LVII: 98e116* .

Le Provost, C., Lyard, F., Molines, J. M., Genco, M. L. and Rabilloud, F.: 1998, A hydrodynamic ocean tide model improved by assimilating a satellite altimeter-derived data set, *Journal of Geophysical Research* **103**(C3), 5513–5529.

Leishman, J. G.: 2006, *Principles of Helicopter Aerodynamics*, UK: Cambridge Aerospace Series, Cambridge, Cambridge University Press.

MacKay, D. J. C.: 2009, *Sustainable Energy: Without the Hot Air*, UIT Cambridge Ltd.

Martin-Short, R., Hill, J., Kramer, S., Avdis, A., Allison, P. and Piggott, M.: 2015, Tidal resource extraction in the Pentland Firth, UK: Potential impacts on flow regime and sediment transport in the Inner Sound of Stroma, *Renewable Energy* **76**, 596 – 607.

URL: *http://www.sciencedirect.com/science/article/pii/S0960148114008106*

McAdam, R.: 2011, *Studies into the Technical Feasibility of the Transverse Horizontal Axis Water Turbine*, PhD thesis, Department of Engineering Science, University of Oxford.

McAdam, R. A., Houlsby, G. T., Oldfield, M. L. G. and McCulloch, M. D.: 2009, Experimental testing of the transverse horizontal axis water turbine, *European Wave and Tidal Energy Conference*, pp. 360–365.

Muchal, S. and Willden, R. H. J.: 2014, Impact of support structures on turbine farm power, *3rd Oxford Tidal Energy Workshop*.

Murray, R. O. and Gallego, A.: 2017, A modelling study of the tidal stream resource of the Pentland Firth, Scotland, *Renewable Energy* **102**, 326–340.

Neill, S. P., Litt, E. J., Couch, S. J. and Davies, A. G.: 2009, The impact of tidal stream turbines on large-scale sediment dynamics, *Renewable Energy* **34**(12), 2803–2812.

Nishino, T. and Willden, R. H. J.: 2012, The efficiency of an array of tidal turbines partially blocking a wide channel, *Journal of Fluid Mechanics* **708**, 596–606.

O'Rourke, F., Boyle, F. and Reynolds, A.: 2010, Tidal Energy Update 2009, *Applied Energy* **87**(2), 398–409.

Peterson, M.: 2008, Tidal Turbine Cost Estimation Research, *Technical report*, University of Maine Orono.

Platzman, G. W.: 1991, *Tidal Evidence for Ocean Normal Modes*, John Wiley & Sons, Ltd, New York.

Pugh, D. T.: 1996, *Tides, Surges and Mean Sea-Level*, John Wiley & Sons, Ltd.

Rankine, W. J.: 1865, Transactions, *Institute of Naval Architects* **6**(13).

Salter, S. H. and Taylor, J. R. M.: 2007, Vertical-axis tidal-current generators and the Pentland Firth, *Proceedings of the Institution of Mechanical Engineers, Part A: Journal of Power and Energy* **221**(2), 181–199.

Schluntz, J.: 2014, *Tidal Turbine Array Modelling*, PhD thesis, University of Oxford.

Serhadlıoğlu, S.: 2014, *Tidal Stream Resource Assessment of the Anglesey Skerries and the Bristol Channel*, PhD thesis, Department of Engineering Science, University of Oxford.

Serhadlıoğlu, S., Adcock, T. A. A., Houlsby, G. T., Draper, S. and Borthwick, A. G. L.: 2013, Tidal Stream Energy Resource Assessment of the Anglesey Skerries, *International Journal of Marine Energy* pp. 98–111.

Shields, A., M., Dillon, L. J., Woolf, D. K. and Ford, A. T.: 2009, Strategic priorities

for assessing ecological impacts of marine renewable energy devices in the Pentland Firth (Scotland, UK), *Marine Policy* **33**, 635–642.

Shields, M. A., Woolf, D. K., Grist, E. P., Kerr, S. A., Jackson, A., Harris, R. E., Bell, M. C., Beharie, R., Want, A., Osalusi, E., Gibb, S. W. and Side, J.: 2011, Marine renewable energy: The ecological implications of altering the hydrodynamics of the marine environment, *Ocean & Coastal Management* **54**(1), 2–9.

Sinha, B. and Pingree, R. G.: 1997, The principal lunar semidiurnal tide and its harmonics: baseline solutions for M2 and M4 constituents on the northwest European continental shelf, *Continental Shelf Research* **17**, 1321–1365.

Tan, W. Y.: 1992, *Shallow-water hydrodynamics*, Vol. 55 of *Elsevier Oceanography Series*, Amsterdam: Elsevier.

Vennell, R.: 1998, Observations of the Phase of Tidal Currents along a Strait, *Journal of Physical Oceanography* **28**(8), 1570–1577.

Vennell, R.: 2010, Tuning turbines in a tidal channel, *Journal of Fluid Mechanics* **663**, 253–267.

Vennell, R.: 2011, Estimating the power potential of tidal currents and the impact of power extraction on flow speeds, *Renewable Energy* **36**, 3558–3565.

Vennell, R.: 2012, The energetics of large tidal turbine arrays, *Renewable Energy* **48**(C), 210–219.

Vennell, R.: 2013, Exceeding the Betz limit with tidal turbines, *Renewable Energy* **55**, 277–285.

Vennell, R. and Adcock, T. A. A.: 2014, Energy storage inherent in large tidal turbine farms, *Proceedings Mathematical, Physical, and Engineering Sciences / The Royal Society* **470**.

Vennell, R., Funke, S., Draper, S., C., S. and Divett, T.: 2015, Designing large arrays of tidal turbines: A synthesis and review, *Renewable and Sustainable Energy Reviews* **41**, 454–472.

Vogel, C.: 2014, *Theoretical Limits to Tidal Stream Energy Extraction*, PhD thesis, Department of Engineering Science, University of Oxford.

Vogel, C., Willden, R. and Houlsby, G.: 2014, The Power Potential of a Tidal Turbine Array with Turbine Power Capping, *Proceedings of the 2nd Asian Wave and Tidal Energy Conference (AWTEC), Tokyo, Japan*, pp. 31–32.

Warren, C. R., Lumsden, C., O' Dowd, S. and Birnie, R. V.: 2005, 'Green OnGreen': public perceptions of wind power in Scotland and Ireland, *Journal of Environmental Planning and Management* **48**, 853–875.

WaveNet: 2003, Technical summary report: overview of the work of the European thematic network on wave energy, *Technical report*, WaveNet.

Whelan, J. I., Graham, J. M. R. and Peiro, J.: 2009, A free-surface and blockage correction for tidal turbines, *Journal of Fluid Mechanics* **624**, 281–291.

Whelan, J. I., Thomson, J., Graham, J. M. R. and Peiro, J.: 2007, Modelling of free surface proximity and wave induced velocities around a horizontal axis tidal stream turbine, *Proceeding of 7th European wave and tidal energy conference, Porto, Portugal*.

White, F. M.: 2009, *Fluid Mechanics*, McGraw Hill.

Witt, M. J., Sheehan, E. V., Bearhop, S., Broderick, A. C., Conley, D. C., Cotterell, S. P., Crow, E., Grecian, W. J., Halsband, C., Hodgson, D. J., Hosegood, P., Inger, R., Miller, P. I., Sims, D. W., Thompson, R. C., Vanstaen, K., Votier, S. C., Attrill, M. J. and Godley, B. J.: 2012, Assessing wave energy effects on biodiversity: the wave hub experience, *Philosophical Transactions of the Royal Society of London A: Mathematical, Physical and Engineering Sciences* **370**, 502–529.

Xia, J., Falconer, R. A. and Lin, B.: 2010, Numerical model assessment of tidal stream energy resources in the Severn Esturary, UK, *Proceedings of the Institution of Mechanical Engineers Part A: Journal of Power and Energy* **224**(7), 969–983.

Zhang, Y., Lin, Z. and Liu, Q.: 2014, Marine renewable energy in China: Current status and perspectives, *Water Science and Engineering* (3), 288–305.

Appendix A

Appendix I: Model Validation Data

The model validation has been done by comparing the current magnitude (in cm/s) and phase lag (in °) of M_2 and S_2 components. Both data has been divided into East-West and South-North direction.

Table A.1: Observed data at ADCP 1

		Easting		Northing	
	Depth	Magnitude	Phase lag	Magnitude	Phase lag
M_2	$11m$	180.00	248.60	12.20	165.40
	$43m$	178.00	248.10	7.20	229.40
	$75m$	131.30	247.90	14.00	267.00
S_2	$11m$	63.40	268.30	6.60	221.40
	$43m$	58.80	268.40	6.70	220.40
	$75m$	41.20	267.20	5.80	236.20

Table A.2: Observed data at ADCP 2

		Easting		Northing	
	Depth	Magnitude	Phase lag	Magnitude	Phase lag
M_2	$11m$	264.30	242.70	106.20	69.50
	$43m$	249.70	242.50	100.10	67.50
	$75m$	153.60	242.40	56.00	65.70
S_2	$11m$	89.50	268.60	35.70	93.70
	$43m$	84.10	268.70	34.70	93.20
	$75m$	51.20	268.70	19.60	92.70

Table A.3: Observed data at ADCP 3

		Easting		Northing	
	Depth	Magnitude	Phase lag	Magnitude	Phase lag
M_2	$11m$	184.70	248.30	185.70	74.10
	$43m$	150.40	248.20	148.60	73.10
	$75m$	108.70	248.20	100.90	73.20
S_2	$11m$	64.40	271.80	61.60	99.40
	$43m$	51.40	271.40	46.20	99.30
	$75m$	39.80	271.90	31.00	94.80

Table A.4: Numerical data with $C_d = 0.0025$

		Easting		Northing	
	Location	Magnitude	Phase lag	Magnitude	Phase lag
M_2	ADCP 1	225.42	255.16	4.10	186.83
	ADCP 2	272.27	248.99	117.43	78.46
	ADCP 3	175.33	258.91	192.57	80.71
S_2	ADCP 1	89.19	279.46	11.03	192.56
	ADCP 2	104.04	277.02	44.79	105.56
	ADCP 3	60.91	287.60	73.94	109.70

Table A.5: Numerical data with $C_d = 0.0038$

		Easting		Northing	
	Location	Magnitude	Phase lag	Magnitude	Phase lag
M_2	ADCP 1	203.84	250.68	9.63	253.29
	ADCP 2	245.59	244.36	92.47	70.49
	ADCP 3	146.37	248.60	163.97	75.32
S_2	ADCP 1	79.29	277.12	7.15	225.64
	ADCP 2	92.39	271.87	37.56	98.75
	ADCP 3	57.73	275.15	64.81	102.47

Table A.6: Numerical data with $C_d = 0.004$

		Easting		Northing	
	Location	Magnitude	Phase lag	Magnitude	Phase lag
M_2	ADCP 1	200.58	250.43	10.87	263.18
	ADCP 2	243.33	244.44	90.28	69.37
	ADCP 3	144.20	247.94	162.30	75.27
S_2	ADCP 1	77.33	277.58	6.08	235.37
	ADCP 2	91.11	272.46	36.71	96.70
	ADCP 3	56.68	274.80	63.50	102.67

Table A.7: Numerical data with $C_d = 0.005$

		Easting		Northing	
	Location	Magnitude	Phase lag	Magnitude	Phase lag
M_2	ADCP 1	186.71	247.78	15.25	267.00
	ADCP 2	228.36	242.89	87.28	65.51
	ADCP 3	134.35	245.89	151.87	72.73
S_2	ADCP 1	70.36	276.64	5.77	265.91
	ADCP 2	85.31	271.07	33.07	93.41
	ADCP 3	51.32	273.81	57.52	100.51

Table A.8: Numerical data with $C_d = 0.0075$

		Easting		Northing	
	Location	Magnitude	Phase lag	Magnitude	Phase lag
M_2	ADCP 1	161.08	240.36	16.52	257.17
	ADCP 2	199.47	238.37	82.09	60.53
	ADCP 3	117.44	240.14	131.32	66.66
S_2	ADCP 1	58.67	269.81	6.15	277.68
	ADCP 2	72.45	267.45	29.59	88.98
	ADCP 3	42.61	269.27	47.91	95.50